UCSF

UC San Francisco Electronic Theses and Dissertations

Title

The mechanism and stereochemistry of dehydrogenase activity with modified pyridine coenzymes

Permalink

https://escholarship.org/uc/item/360714vb

Author

Marschner, Thomas M.

Publication Date

1988

Peer reviewed|Thesis/dissertation

The Mechanism and Stereochemistry of Dehydrogenase
Activity with Modified Pyridine Coenzymes

by

Thomas M. Marschner

B.S. (University of Wisconsin - Parkside) 1979

DISSERTATION

Submitted in partial satisfaction of the requirements for the degree of

DOCTOR OF PHILOSOPHY

in

Pharmaceutical Chemistry

in the

GRADUATE DIVISION

of the

UNIVERSITY OF CALIFORNIA

San Francisco

To my parents

Acknowledgements

Robert Smith and his cohorts reminded me that things could be (much, much) worse and for that I am grateful.

I would like to thank my family for their encouragement and support during my graduate education.

The Mechanism and Stereochemistry of Dehydrogenase Activity with Modified Pyridine Coenzymes

Abstract

Thomas M. Marschner

Glyceraldehyde-3-phosphate dehydrogenase, G3PDH, which normally catalyzes the oxidative phosphorylation of D-glyceraldehyde-3-phosphate also catalyzes a modification of β-NADH forming β-6-hydroxy-1,4,5,6-tetrahydronicotinamide adenine dinucleotide, (6HTN)AD. This product is the result of the addition of water across the 5,6 double bond of β-NADH. The enzymatic hydration reaction requires the presence of a polybasic anion such as phosphate, pyrophosphate or citrate and the rate of reaction increases as the pH is lowered. Investigations into the stereochemistry of the hydration reaction reveals that both the protonation step at C5 and the subsequent hydroxylation step at C6 occur stereospecifically with a *cis* hydration of the 5,6 double bond. The polybasic anion appears to serve as a general acid catalyst in the initial protonation step with the anion binding in or near the inorganic phosphate binding site. Citrate bridges the active site with terminal carboxyl groups binding in the inorganic phosphate binding site and the glyceraldehyde-3-phosphate anion binding site. Investigations into the anion dependence of the reaction rate shows the presence of positive cooperativity in the binding of the anion as indicated by sigmoidal binding/activity curves. These results suggest that the anion may induce conformational changes upon binding to the enzyme similar to the changes observed for binding of β-NAD$^+$.

The synthesis and enzymatic characterization of a new pyridine coenzyme analog containing a nicotinamide arabinotide moiety has been carried out. The redox potentials are -339 mV for β-araNAD$^+$ and -319 mV for

α-NAD$^+$ and the λ_{max} is 346 nm and 338 nm for β-araNADH and α-araNADH, respectively. Anomerization of the reduced analogs leads to a 5:1 ratio of α-araNADH to β-araNADH at 90° C. These results establish that the relative configuration of the 2' hydroxyl to the base is the primary determinant for the configuration-dependent changes in λ_{max}, redox potential of the pyridine nucleotides and the preferred anomeric configuration of the reduced coenzymes. Comparison of the ^{1}H NMR and ^{31}P NMR spectral data of the analogs with those for the ribo-coenzymes are reported and the conformational analysis discussed. The coenzyme properties of the arabino analogs have been evaluated with yeast and horse liver alcohol dehyrogenases. Both the α- and β-anomers are found to serve as coenzymes and the stereochemistry of hydride transfer is identical for both anomers.

Table of Contents

List of Tables

List of Figures

Section II. Synthesis, Characterization and Enzymatic Properties of α- and β-Nicotinamide Arabinoside Adenine Dinucleotides.

Section III. Isotope-Induced Nonequivalence in a Symmetrical Molecule: Measurement of the ^{31}P-^{31}P Geminal Coupling Constant in Pyrophosphate.

Section I. The Kinetics and Mechanism of Yeast Glyceraldehyde-3-phosphate Dehydrogenase-catalyzed Hydration of β-NADH.

Introduction

D-Glyceraldehyde-3-phosphate dehydrogenase (D-glyceraldehyde-3-phosphate:NAD+ oxidoreductase, phosphorylating, E.C. 1.2.1.12), G3PDH[1], is an enzyme common to both the glycolytic and gluconeogenic pathways. Its role in glycolysis makes it a key enzyme in the major pathway for carbohydrate metabolism in most organisms. It occurs widely in nature and has been isolated from at least 26 different sources including several bacterial sources (Harris and Waters, 1975). G3PDH compromises approximately 20% of the total soluble protein in yeast and up to 10% of the total soluble protein in muscle (Krebs et al., 1953; Cori et al., 1945). The reaction catalyzed by G3PDH is the reversible oxidative phosphorylation of D-glyceraldehyde-3-phosphate to D-1,3-diphosphoglycerate with the concomitant reduction of the cofactor β-NAD+ to β-NADH (Figure I.1). The reaction pathway (Segal and Boyer, 1953) consists of a series of reactions beginning with formation of a thiohemiacetal intermediate resulting from attack of Cys-149 on D-glyceraldehyde-3-phosphate. Direct

---

[1]Abbreviations used: G3PDH, D-glyceraldehyde-3-phosphate dehydrogenase; NAD+, β-nicotinamide adenine dinucleotide; NADH, β-nicotinamide adenine dinucleotide, reduced form; (6HTN)AD, β-6-hydroxy-1,4,5,6-tetrahydro-nicotinamide adenine dinucleotide; DEAE, diethylaminoethyl; DTT, dithiothreitol; Tris, tris(hydroxymethyl) aminomethane; PIPES, piperazine-N,N'-bis[2-ethanesulfonic acid]; MMTS, methylmethane thiosulfonate; (cTHN)AD, α-$O^{2'}$-cyclotetrahydronicotinamide adenine dinucleotide; EDTA, ethylenediamine tetraacetic acid; GAP, D-glyceraldehyde-3-phosphate; TED, Tris, EDTA, DTT buffer; FID, free induction decay.
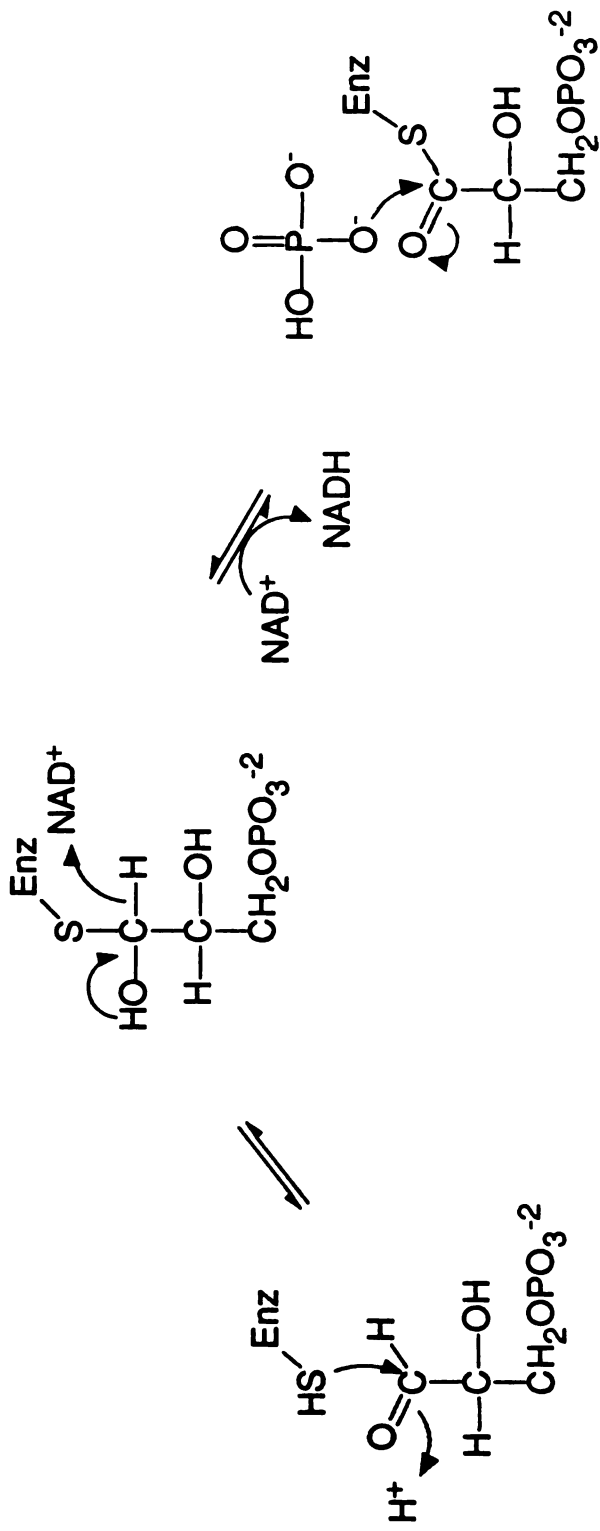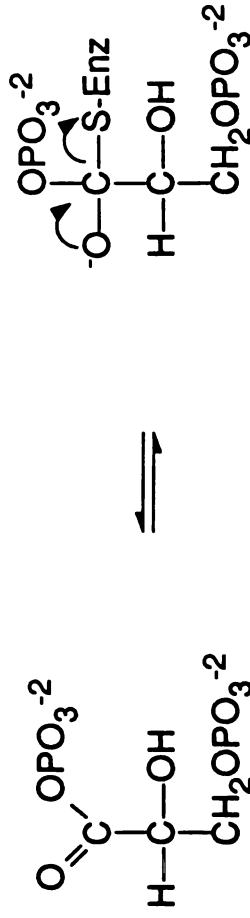
Figure I.1. The mechanism of oxidative phosphorylation catalyzed by glyceraldehyde-3-phosphate dehydrogenase.

3

hydride transfer from the thiohemiacetal to C4 of the nicotinamide ring follows with formation of a covalent thioester enzyme intermediate. This transfer of hydride occurs stereospecifically to the *si*-face[2] of the nicotinamide ring (Levy and Vennesland, 1957; Cornforth et al, 1962). Attack of the thioester intermediate by bound inorganic phosphate follows with release of the product 1,3-diphosphoglycerate.

The enzyme is a tetramer consisting of four identical polypeptide chains with a subunit molecular weight of 35000 daltons (Jaenicke et al., 1968; Harris and Perham, 1965). The amino acid sequences of the yeast (Jones and Harris, 1972), pig muscle (Harris and Pernham, 1965) and lobster muscle (Davidson et al., 1967) enzymes, among others, have been determined and show a surprisingly high degree of identity. The structures of G3PDH from several different sources have also been determined by X-ray crystallography. The crystal structure of the lobster enzyme reveals an asymmetry in the quaternary structure of the tetramer, and it was found that the tetramer was actually composed of a dimer of subunit dimers (Moras et al., 1975). Some of the largest differences in electron density between the structurally unique subunits occur in the vicinity of the active site. The active site is located near the region of intersubunit contact and this may be the reason for the highly cooperative nature (both positive and negative) of substrate binding observed for this

---

[2]The *si* and *re* designations will be used in place of the older A- and B-face notation for designating stereochemistry at the sp^2 chiral centers of β-NAD+ and β-NADH. For chemistry at C4, C5 and C6 of the nicotinamide ring of β-NAD+ and β-NADH the *re* designation corresponds to the A-face and the *si* designation corresponds to the B-face.

enzyme (Harris and Waters, 1965 and references therein).

G3PDH is also known to catalyze several other reactions besides substrate level oxidative phosphorylation. These activities include acyl transfer (Harting and Velick, 1954; Oesper, 1954), ester (Park et al., 1961) and acyl phosphate hydrolysis (Harting, 1954) and thiol ester hydrolysis (Wolff and Black, 1959) (Figure I.2). These activities have all been shown to be a consequence of an active thiol group on the enzyme (Cys-149) and are inhibited by thiol-modifying reagents such as iodoacetate.

Another reaction catalyzed by G3PDH, first reported in 1954 (Rafter et al., 1954), involves a modification of the pyridine nucleotide cofactor β-NADH resulting in the loss of its characteristic 340 nm absorbance. Both rabbit muscle and yeast G3PDH have been found to catalyze this reaction (Chaykin et al., 1956). The modified pyridine coenzyme was first referred to as NADHX and later was identified by Oppenheimer and Kaplan (1974b) to be β-6-hydroxy-1,4,5,6-tetrahydronicotinamide adenine dinucleotide, (6HTN)AD (Figure I.3). This product is the result of the addition of water across the 5,6 double bond of the dihydronicotinamide ring of β-NADH and has also been shown to be an intermediate in the nonenzymatic breakdown of reduced pyridine nucleotides in acid (Oppenheimer and Kaplan, 1974a; Miksik and Brown, 1978). G3PDH-catalyzed hydration of β-NADH requires the presence of a polybasic anion and phosphate, pyrophosphate, citrate and arsenate have been shown to be effective in promoting the reaction (Rafter et al., 1954; Hilvers et al., 1966). The rate of β–NADH hydration is highly pH-dependent and increases as the pH is lowered. It has been postulated that the most likely role of the polybasic anion in the reaction is to serve as a general acid catalyst in the initial protonation reaction (Oppenheimer and Kaplan, 1974b). This is consistent with the

5

$$CH_3\overset{O}{\underset{||}{C}}-OPO_3^{-2} + H^{32}PO_4^{-2} \rightleftharpoons CH_3\overset{O}{\underset{||}{C}}-O^{32}PO_3^{-2} + HPO_4^{-2}$$

$$CH_3\overset{O}{\underset{||}{C}}-OPO_3^{-2} + HAsO_4^{-2} \rightleftharpoons CH_3\overset{O}{\underset{||}{C}}-OAsO_3^{-2} + HPO_4^{-2}$$

Acetyl Phosphate

$$\downarrow$$

$$CH_3COO^- + HAsO_4^{-2}$$
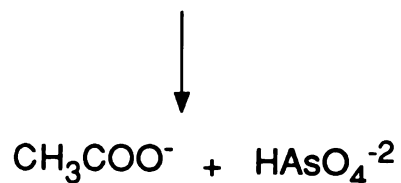
Acyl Transferase Activity

$$CH_3\overset{O}{\underset{||}{C}}-OPO_3^{-2} \longrightarrow CH_3COO^- + HPO_4^{-2}$$

Phosphatase Activity

$$CH_3\overset{O}{\underset{||}{C}}O-\!\!\!\!\bigcirc\!\!\!\!-NO_2 \longrightarrow CH_3COO^- + HO-\!\!\!\!\bigcirc\!\!\!\!-NO_2$$
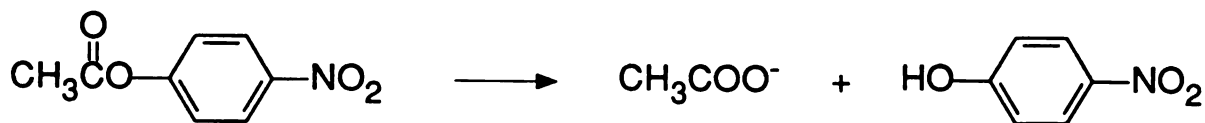
p-Nitrophenyl acetate

Esterase Activity

Figure I.2.   Other reactions catalyzed by glyceraldehyde-3-phosphate dehydrogenase.

observed pH dependence of the reaction rate. General acid catalysis has been demonstrated in the breakdown of reduced pyridine nucleotides (Johnson and Tuazon, 1977). Figure I.4 shows the proposed mechanism for the enzymatically catalyzed hydration of β-NADH based on the requirement for this anion. Catalysis occurs with initial protonation at C5 of the dihydronicotinamide ring with formation of a positively charged iminium ion intermediate. Subsequent attack by water at C6 leads to formation of product. As shown in Figure I.4, general acid catalysis is likely to be involved in the initial protonation step.
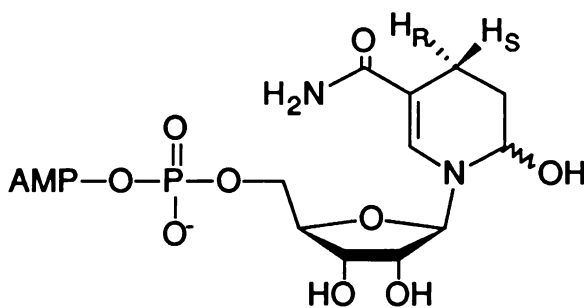
FIGURE I.3.   The structure of β-6-hydroxy-1,4,5,6-tetrahydro-
              nicotinamide adenine dinucleotide, (6HTN)AD.

Hilvers et al. (1966) reported that the rate of the enzymatic hydration reaction was accelerated by acetylating the enzyme with acetyl phosphate. Acetylation of the enzyme occurs at Cys-149 forming the same intermediate that is implicated in the acyl transfer and ester hydrolysis activities mentioned above. In the presence of β-NADH, the acetylated enzyme is susceptible to reduction by β-NADH analogous to the reverse 'half-reaction' of Figure I.1. Bound NADH is therefore able to undergo either hydration to (6HTN)AD or oxidation to NAD+. The relative rates of these two competing reactions are pH and anion-dependent with the hydration reaction becoming the predominant pathway below pH 6 (Hilvers et al., 1966).

7
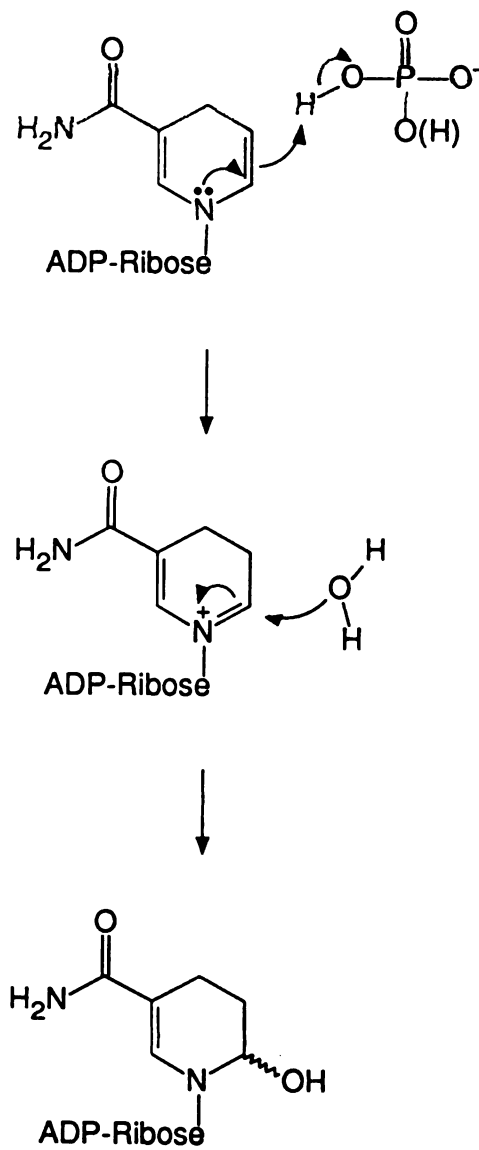
Figure I.4. Proposed mechanism for β-NADH hydration.

8

In an investigation of the mechanism of β-NADH hydration catalyzed by G3PDH, Oppenheimer and Kaplan (1974b) carried out stereochemical studies on the enzymatic hydration reaction. Deuterium labeling studies indicated a lack of stereospecificity in the initial protonation at C5 of the dihydronicotinamide ring. They suggested that the enzymatic group promoting the protonation reaction, be it the polybasic anion or an acidic residue on the enzyme, was symmetrically positioned relative to the plane of the dihydronicotinamide ring and thus capable of protonating either the re- or si - face.

Oppenheimer and Kaplan also observed a lack of stereospecificity in the hydroxylation reaction which led them to suggest the following for the hydroxylation step: (i) Partial, but not total, stereospecificity in the attack of water on the nicotinamide cation intermediate due to the partial blocking of the si face of the ring by protein active site residues. (ii) G3PDH catalyzed only the initial protonation reaction and the actual product released by the enzyme was the cationic nicotinamide intermediate. This intermediate would then react with water outside of the active site and yield products dependent on the conformation of the dinucleotide in solution. (iii) The polybasic anion itself reacted with the cationic nicotinamide intermediate, and it was the complex that was released into solution. This complex then underwent nonenzymatic hydrolysis outside of the active site with re-formation of the intermediate cationic nicotinamide which reacted with water as in (ii) above.

The lack of stereospecificity for an enzymatic hydration reaction of this type is quite unusual (Rose, 1972). There are several well-studied enzymatic hydration reactions which show complete stereospecificity for addition of water to a double bond (Figure I.5). For example, aconitase, an enzyme in the citric acid cycle, catalyzes the reversible interconversion of citrate and isocitrate via

9

I. Hydration Reactions exhibiting trans stereochemistry

A. Aconitase
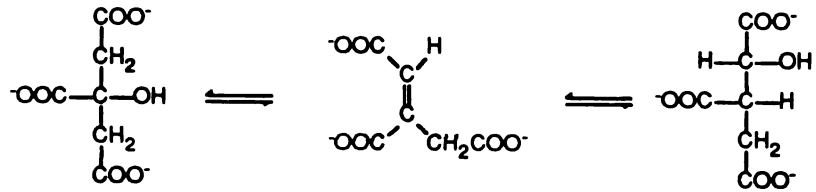
B. Fumarase
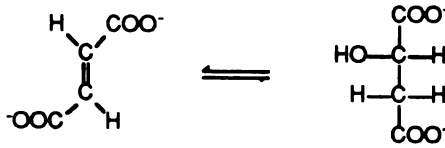
C. Enolase

II. Hydration reactions exhibiting cis stereochemistry

A. Enoyl CoA hydratase (crotonase)

$$R = C_4 - C_{16}$$
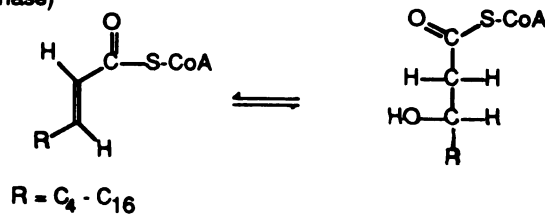
B. Dehydroshikimate dehydratase
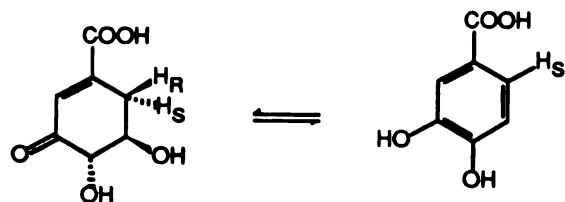
C. Methylglutaconyl-CoA Hydratase
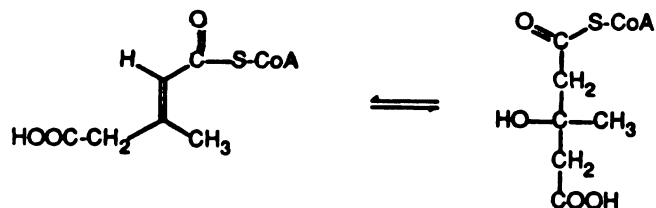
Figure I.5. Other enzymatic reactions involving addition of water across a double bond.

10

the intermediary *cis*-aconitate. Catalysis occurs with an initial *trans* elimination of water followed by *trans* addition of water to the *cis*-aconitate intermediate (Alworth, 1972). Fumarase, another enzyme in the citric acid cycle, catalyzes the *trans* addition of water to fumarate forming *S*-malate (Gawron and Fondy, 1954). Likewise, the interconversion of D-2-phosphoglycerate and phosphoenolpyruvate catalyzed by enolase occurs via a reaction exhibiting *trans* stereochemistry (Tiepel et al., 1968; Cohn et al., 1970).

Examples of *cis* hydrations (or *syn* eliminations) in enzyme catalyzed reactions are generally rare (Figure I.5). Enoyl-CoA hydrase (crotonase) is an enzyme involved in fatty acid oxidations and utilizes the α,β-unsaturated acyl-CoA produced by acyl-CoA dehydrogenases. This enzyme has been shown to carry out the *cis* hydration of the 2-enoyl-acyl-CoA ester substrate forming β-hydroxy acyl CoA (Willadsen and Eggerer, 1975). Other examples of *cis* dehydrations include dehydroshikimate dehydrase (Hanson and Rose, 1963) and methylglutaconyl-CoA hydrase (Messner et al., 1975). The participation of an acidic hydrogen alpha to a carbonyl on the substrate is a common feature of all these *cis* hydrations and a rationale for their stereochemistry has been suggested (Rose, 1970).

The metabolic role of (6HTN)AD and the significance of the hydration reaction are as yet unknown. There is a report in the literature of the isolation of an ATP-requiring enzyme from yeast which catalyzes the conversion of (6HTN)AD to NADH (Griffiths and Chaplain, 1962) It has, however, not been characterized and its role in cellular metabolism is unknown. With intracellular concentrations of β-NADH and phosphate of ~0.05 mM and ~2 mM, respectively (Long, 1961; Fersht, 1977) a significant portion of bound NADH may indeed undergo hydration forming (6HTN)AD by this mechanism. The high intracellular concentration of the enzyme itself (~1 mM) also suggests that the hydration

11

reaction may be catalyzed at a metabolically significant rate. Also, it is important to note that a large proportion of G3PDH in the cell exists as the acyl-enzyme with D-3-phosphoglycerate (Bloch et al., 1971) which may be important in light of the increased hydration activity brought about by acetylation.

We report here the results of deuterium labeling experiments carried out to further investigate the initial protonation step in the mechanism for the hydration reaction. Also, kinetic studies utilizing an HPLC separation of the reaction products were performed to probe the stereoselectivity (if any) for the subsequent hydroxylation step. Experiments were carried out to characterize the steady-state kinetics of the hydration reaction and to investigate the binding of both the dinucleotide and the anion. Modification of the enzyme with methylmethane thiosulfonate (MMTS) was carried out to investigate the involvement of Cys-149 in substrate binding and its role in catalysis.

Experimental

Materials. Fresh baker's yeast (*Saccharomyces cerevisiae*) was purchased locally from Boudin Bakery. Ammonium sulfate was from BRL and was ultrapure grade. Toluene was AR grade and was from Baker. Tris, Bis-Tris and PIPES buffers, EDTA, DTT and methylmethane thiosulfonate were from Sigma as were β-NAD$^+$, DL-glyceraldehyde-3-phosphate diethyl acetal (monobarium salt) and disodium pyrophosphate. DEAE-Sepharose CL-6B and Sephadex G-200 were obtained from Pharmacia. Sodium arsenate and citric acid were obtained from Mallinckrodt. Triethylamine was purchased from Aldrich and HPLC grade methanol was from Baker. All reagents were used without further purification. PD-10 disposable gel filtration columns containing prepacked Sephadex G-25M were purchased from Pharmacia and Centricon-30 ultrafiltration devices were from Amicon. Chelex-100 resin was obtained from Bio-Rad and regenerated according to the manufacturer's instructions before use. Doubly distilled, deionized water was used throughout. Triethylammonium bicarbonate buffer was prepared by bubbling CO_2 through an aqueous solution of triethylamine to the appropriate pH. Triethylammonium phosphate buffer was prepared by titration of an H_3PO_4 solution with triethylamine to the appropriate pH.

G3PDH Isolation and Purification.

The isolation and purification of G3PDH from baker's yeast were carried out using modifications of various published procedures (Butler and Jones, 1970; Byers, 1981).

Methods. Protein concentrations were measured spectrophotometrically at 280

nm using the literature value for the extinction coefficient ($^{1\%}E_{280}$ = 8.6) (Kirschner et al., 1966). Enzyme activity assays were done spectrophotometrically using a Hitachi 100-80 spectrophotometer interfaced to an Apple II computer. The assays were conducted at constant temperature (25 °C) in 1 mL cuvettes placed in a Peltier-controlled cell holder. The activity of G3PDH throughout the purification procedure was assayed using the usual reaction catalyzed by the enzyme, *i.e.* oxidative phosphorylation of D-glyceraldehyde-3-phosphate with concomitant reduction of β-NAD$^+$ to β-NADH (Worthington Enzyme Manual, 1972). Arsenate is used in place of phosphate in this assay since the product of the reaction, 1-arseno-3-phosphoglyceric acid, rapidly undergoes ester hydrolysis thereby eliminating any product inhibition. The rate of reaction was measured by monitoring the increase in absorbance at 340 nm due to formation of β-NADH. DL-Glyceraldehyde-3-phosphate (GAP) was prepared from the barium salt of the diethyl acetal using Dowex 50 (H$^+$ form) according to the instructions supplied by Sigma. The concentration of the stock D-GAP solution was measured using an endpoint assay adding sufficient enzyme such that the reaction was essentially complete in ~10 minutes. The D-GAP concentration was determined by measuring the total change in absorbance at 340 nm due to NADH formation using an extinction coefficient of 6220 M^{-1} cm^{-1} (Horecker and Kornberg, 1948). The stock D-GAP solution was stored frozen (-70 °C).

The enzyme assay mixture consisted of the reagents, volumes, concentrations and order of addition shown in Table I.1. The first four reagents were added to a 1 mL cuvette and allowed to equilibrate to temperature (25 °C). The reaction was started by addition of D-GAP and the change in absorbance was monitored at 340 nm. The rate of reaction (slope) was calculated by least squares analysis of the time scan data.

14

Table I.1.   Assay mixture for activity determination of G3PDH

Addition Order	Volume (μL)	Reagent
1	760.5	15 mM sodium pyrophosphate, 30 mM Na_2HAsO_4, pH 8.5
2	100.0	DTT (30 mM in assay buffer)
3	100.0	β-NAD+ (2.5 mM in assay buffer)
4	5.0	G3PDH
5	34.5	D-GAP (14.5 mM in H_2O)

Toluene lysis. To five pounds of crumbled fresh bakers yeast in a 4 L beaker was added 1.1 L of toluene. The beaker was placed in a 45 °C water bath and the mixture was incubated with occasional stirring until the yeast had liquified (*ca.* 70 minutes). The water bath was removed and the mixture was allowed to stand at room temperature for three hours. Next, 2.1 L of cold (4 °C) distilled water was added and the mixture was cooled to 0 °C in an ice bath with occasional stirring. The mixture was then transferred to a 6 L Erlenmeyer flask and allowed to stand overnight in the refrigerator after which a fat layer formed on the top of the mixture. The fat layer was removed by suction through a glass pipet connected to a water aspirator. The bottom 'aqueous' layer was centrifuged at 9500 *g* for 30 min using 500 mL centrifuge bottles. The yellow supernatant was used in the following ammonium sulfate precipitation step.

Ammonium sulfate precipitation. All the following steps in the enzyme purification were carried out at 4 °C unless otherwise noted. Ammonium sulfate (808.5 g, 0 to 50 % saturation) was added slowly with stirring to the yellow supernatant and allowed to stir for 1 hour. The solution was then centrifuged at

10000 *g* for 15 min and the supernatant was decanted off. Ammonium sulfate (585.9 g, 50 to 80% saturation) was added and the solution was allowed to stir overnight at 4 °C. The solution was then centrifuged at 10000 *g* for 30 min and the supernatant was discarded. The pellets were dissolved in 100 mL total of 10 mM Tris buffer, pH 8.1 containing 1 mM EDTA and 0.3 mM DTT ('TED' buffer). The solution was filtered through a small plug of glass wool to remove a small amount of lipid and insoluble material. The protein solution was adjusted to pH 8.1 with 10% NH_3 (aq.).

DEAE-Sepharose CL-6B chromatography. The crude G3PDH solution from above was desalted by dialysis. The protein solution was placed in dialysis sacs and dialyzed against 6 L of TED buffer for 12 hours. The buffer was replaced (6 L), and the dialysis was continued for another 12 hours. At this point the procedure described for the anion exchange chromatography was carried out on only a portion of the dialyzed crude G3PDH sample to avoid overloading the column. The procedure was then repeated on the remaining protein solution with similar results.

DEAE-Sepharose CL-6B was prepared by washing with 2 L each of 1 M sodium acetate, pH 3, then 0.5 M NaOH, and, finally, 1 M sodium acetate, pH3 on a sintered glass filter. The gel was then washed with 2 L TED buffer. The gel was packed in a 5 x 25 cm column and washed with 2 L of TED buffer. The crude desalted G3PDH sample (250 mL) was applied to the column and eluted with a 0 to 0.4 M NaCl gradient (1.5 x 1.5 L) in TED buffer. Fractions (20 mL) were assayed for protein spectrophotometrically using the absorbance at 280 nm. G3PDH activity was measured using the activity assay described above. Figure I.6 shows the elution profile for this column. Fractions 48-52 were pooled, and the enzyme was precipitated by saturating the solution with

ammonium sulfate (761 g/L).

Sephadex G-200 Chromatography. Sephadex G-200 was swollen according to the manufacturer's instructions and a 2.6 x 95 cm column was packed under a pressure head of 16 cm H_2O using a Mariott flask. The column was washed with 1 L TED buffer at a flow rate of *ca.* 10 mL/hr. The ammonium sulfate suspension from above was centrifuged (30 min., 10000 *g*), and the supernatant was decanted. The precipitate was redissolved in 25 mL of TED buffer, and the solution was centrifuged to remove a small amount of insoluble material (15 min, 16000 *g*). The volume of the supernatant was 30 mL of which 15 mL was applied to the G-200 column. The column was eluted with TED buffer under a pressure head of 16 cm H_2O with a flow rate of *ca.* 10 mL/hr. Fractions (150 drop, 4.35 mL) were collected and assayed for protein (absorbance at 280 nm) and G3PDH activity. The elution profile for this column is shown in Figure I.7. Fractions 58-74 were pooled and the G3PDH was precipitated by saturating the solution with ammonium sulfate (761 g/L). The remaining DEAE sample from above (15 mL) was also chromatographed in this manner with similar results. The G3PDH was precipitated and the pure protein from both G-200 runs was pooled.
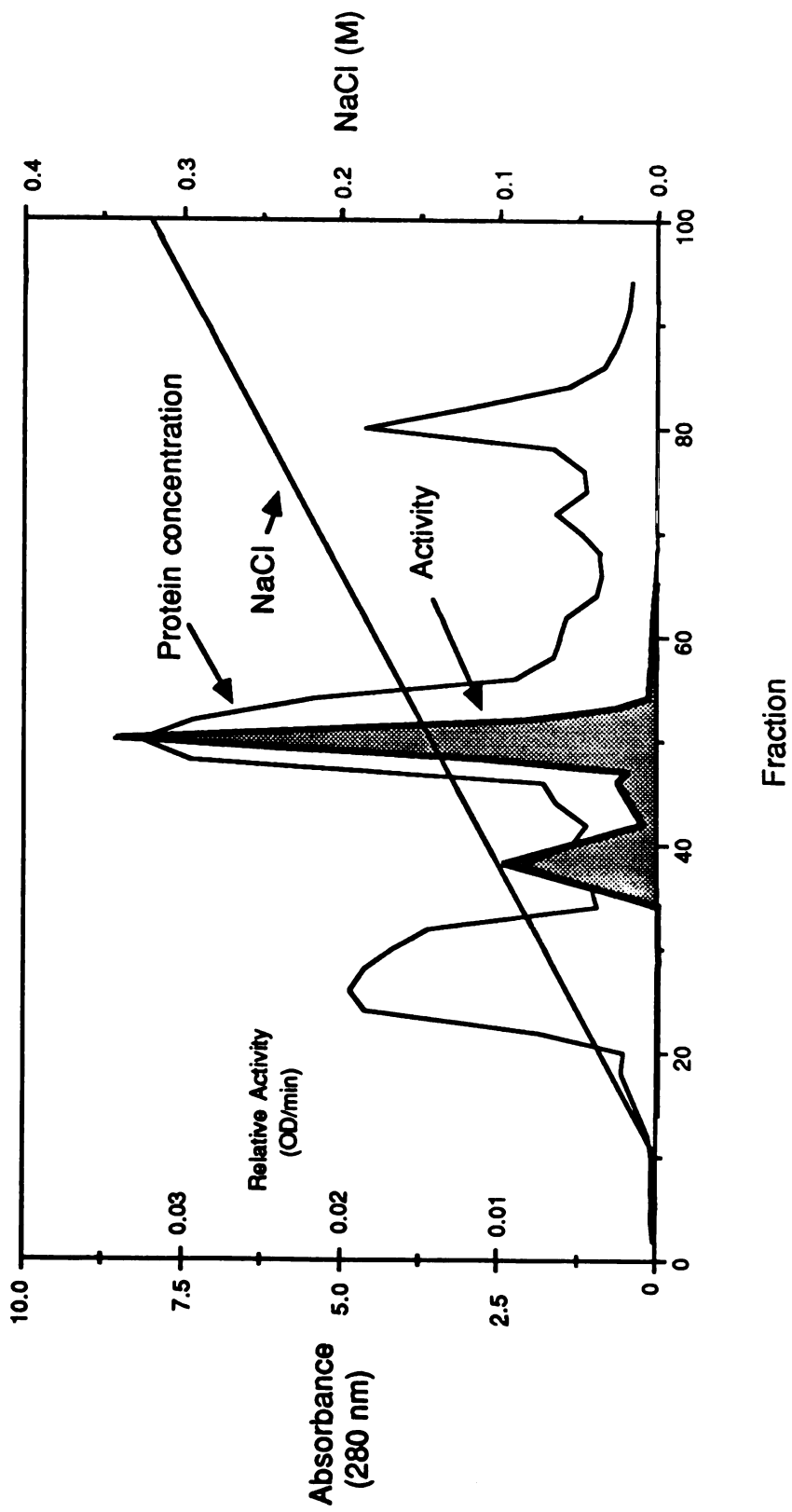
Figure I.6. Elution profile for purification of G3PDH on DEAE-Sepharose CL-4B.
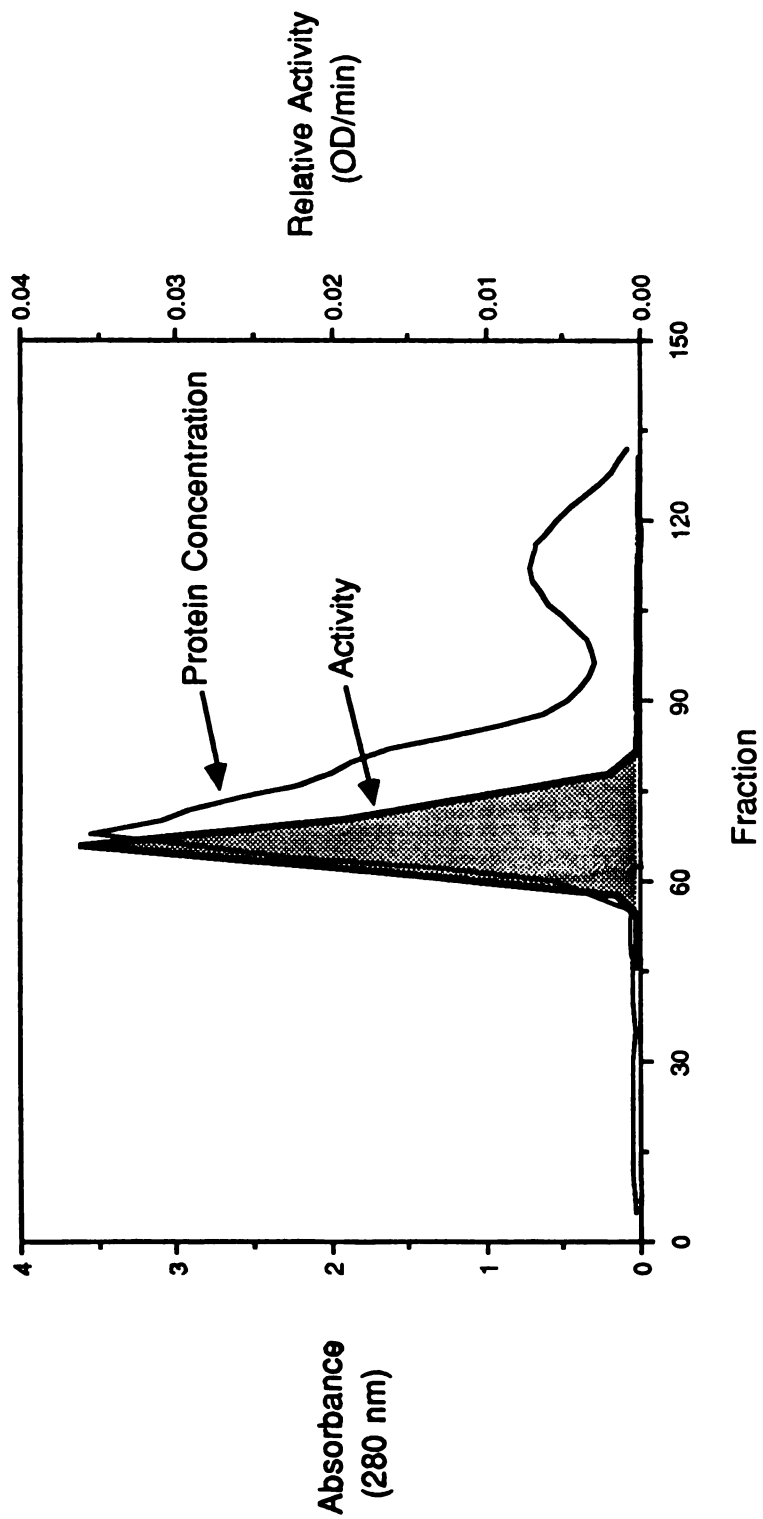
Figure I.7.   Elution profile for purification of G3PDH on Sephadex G-200.

19

Crystallization of G3PDH. The precipitated G3PDH from above was dissolved in *ca.* 15 mL of TED buffer and centrifuged (15 min, 10000 *g*) to remove a small amount of insoluble material. The precipitate was discarded and G3PDH was crystallized out of the supernatant by dropwise addition of a saturated ammonium sulfate solution (adjusted to pH 8.1 with Tris base) until the solution appeared opalescent. The solution was allowed to stand overnight at 4 °C. Several drops of saturated ammonium sulfate was added each day for the next several days to ensure complete precipitation of the enzyme. The crystalline suspension of G3PDH was stored at 4 °C. The crystallized enzyme was shown to be homogeneous by polyacrylamide gel electrophoresis as well as by ion-exchange chromatography on a Pharmacia HR5/5 Mono-Q ion exchange FPLC column.

Kinetics of G3PDH-catalyzed β–NADH Hydration

Methods.

Initial rate kinetic assays for the hydration activity of G3PDH (or thiomethylated-G3PDH) were carried out using a Hewlett Packard 8452A diode array spectrophotometer interfaced to a Hewlett Packard 89500 Chemstation computer. Reactions were carried out at 30 °C using a thermostatted cell holder in a total volume of 0.4 mL. Semi-micro black masked cuvettes with a path length of 1 cm were used. The rates of reaction were determined from the increase in absorbance at 292 nm using either a linear regression analysis of the data or by fitting the data to a quadratic of the form $^{340}A = at^2 + bt + c$ where b is the calculated initial rate of reaction. These fits were done using software provided with the Chemstation computer. A wavelength of 292 nm was used because at this wavelength, the absorbance of β-NADH is lower than that at
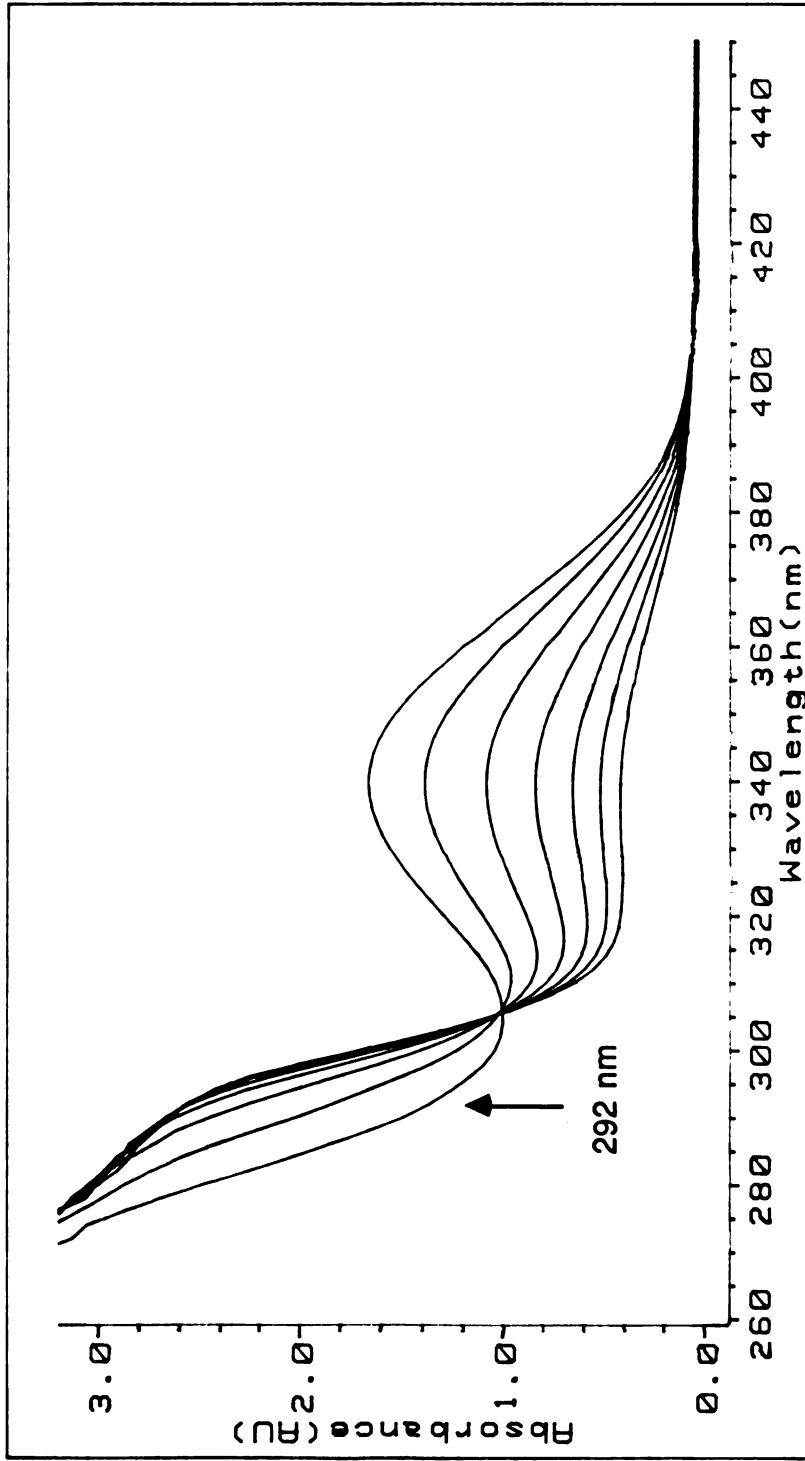
Figure I.8. Time dependence of the UV spectrum of the G3PDH-catalyzed hydration reaction mixture. Spectra were acquired every 5 minutes. The enzyme concentration was 0.5 mg/mL.

21

340 nm thus permitting higher intial concentrations of β-NADH to be used. As shown in Figure I.8 the total change in absorbance at 292 nm is roughly the same as that at 340 nm (although opposite in sign) so there is no significant loss in sensitivity. In fact, there is actually an increase in sensitivity due to the decrease in noise in going from a starting absorbance of ~2 OD at 340 nm to < 1 OD at 292 nm. Reactions were carried out in 50 mM Bis-Tris buffer for reactions run at pH 6.0 and in 50 mM PIPES buffer for reactions run at pH 7.2. Native G3PDH was prepared by first centrifuging the ammonium sulfate suspension and dissolving the precipitate in 10 mM Tris buffer, pH 8.1. Residual sulfate, a potential inhibitor of G3PDH, was removed by gel filtration and concentrated as described below for the thiomethylation procedure. The ionic strength of the reaction mixtures were maintained at 1.5 M using KCl except for reactions at very high concentrations of the polybasic anion (i.e > 0.5 M). In these cases, the ionic strength was not controlled. The pH of each sample was checked before enzyme addition and adjusted if necessary. The contribution to the ionic strength by the polybasic anion was determined by calculating the concentration of each of the ions at the pH of the reaction mixture. All other ionizations with pK_a values ≥ 2 pH units above the pH of the reaction mixture were ignored. For example, for phosphate (pK_a = 7.2) the concentrations of $H_2PO_4^{-1}$ and HPO_4^{-2} were calculated at pH 6.0 and their ionic strength contributions were added to give the total ionic strength due to phosphate. The third ionization (yielding PO_4^{-3}) was ignored since its concentration is extremely small at pH 6.0 (pK_a = 12.4). The concentrations of stock β-NADH and enzyme solutions were determined spectrophotometrically at 340 nm and 280 nm, respectively. Stock enzyme solutions were stored at 0 °C. The assay mixtures were allowed to equilibrate to temperature for *ca.* 5 min and the reactions were initiated by the addition of enzyme. The enzyme

concentration used in the assays was 0.5 mg/mL (14.3 μM active sites). The pD values for those reactions run in deuterated buffer were determined using the standard electrode correction for deuterium (pD = meter reading + 0.4) (Glasoe and Long, 1960).

Data Analysis. At high concentrations of enzyme, the formation of the enzyme-substrate complex (ES) significantly alters the concentration of free substrate in solution. Under these conditions the simple equation which describes the hyperbolic rate profile for an enzymatic reaction exhibiting Michaelis-Menten kinetics is no longer valid. For this reason, the data for the hydration reaction were fit to an equation which takes the high enzyme concentration into account (Segel, 1975).

$$\frac{v}{^{app}V_{max}} = \frac{(E + S + \,^{app}K_m) - \sqrt{(E + S + \,^{app}K_m)^2 - 4ES}}{2E}$$

The data were fit to this equation using nonlinear regression analysis using the algorithm of Cleland (1967) (See Appendix 1 for a description of the algorithm used in the regression analyses). An enzyme active site concentration of 14.3 μM was entered for E and the equation was solved for both V_{max} and K_m. In these fits, the varied substrate was β-NADH and the 'fixed' substrate was the polybasic anion.

Data for citrate binding were fit using nonlinear regression analysis to the equation:

23

$$v = \frac{V_{max} + S^n}{K' + S^n}$$

where V_{max} is the maximal velocity, K' is a constant comprised of the intrinsic dissociation constants and the interaction factors and n, in the limiting case, is the number of subunits. If the degree of interaction is not very high, n will not correspond to the number of sites. Any value of $n > 1$ indicates positive cooperativity. The linear form of this equation is the Hill equation:

$$\log\left(\frac{v}{V_{max} - v}\right) = n \log(S) - \log K'$$

The slope of this plot gives the parameter n. Most cooperative binding data is plotted in this form. If an accurate value of V_{max} can not be easily determined then the data must be fit in a nonlinear fashion as described above.

Equilibration kinetics of (6HTN)AD

The rates of equilibration of the (6HTN)AD epimers were investigated by first isolating (nearly) pure (6S-HTN)AD by reverse phase HPLC. (6R,S-HTN)AD was prepared on a preparative scale from 5 mg β-NADH at pH 6.0 in 2.0 mL of 0.5 M pyrophosphate buffer containing 0.5 mg/mL native G3PDH. The reaction mixture also contained 1 mM DTT. The reaction was monitored at 340 nm and after the absorbance had dropped to <10% of its initial value the reaction was quenched by addition of K_2CO_3 to pH 10. The sample was applied to a reverse phase HPLC column and chromatographed as described

24

below for the hydroxylation stereochemistry experiments. NH_3 (10 % aq) was added to the peak fraction to pH ~10 thereby preventing significant epimerization from occurring. The HPLC sample (*ca.* 1 mg (6S-HTN)AD; ~80% pure S epimer) was used directly in the equilibrium kinetics experiments without concentration, lyophilization or other manipulations.

(6S-HTN)AD, the low population epimer, was used to investigate the equilibration since the observed changes in concentration as equilibrium was reached would be greatest in the 6S → 6R direction. The equilibration reaction was carried out in pyrophosphate buffer, pH 6.0 and the temperature was maintained at 30° C with a water bath. The ionic strength was maintained at 1.5 M using KCl. The ionic strength contribution of pyrophosphate in the samples was calculated as described above for the enzyme kinetics experiments. The reaction volume was 2.5 mL, and the initial concentration of (6HTN)AD was approximately 0.1 mM. Aliquots (200 µL) were removed at the appropriate time intervals and quenched in 0.3 mL of 0.5 M K_2CO_3. Samples were stored at 0° C until they were chromatographed. To determine the general acid rate constants for the equilibration reaction, the reaction was carried out at pyrophosphate concentrations of 0.1, 0.2 and 0.3 M. The reaction at pH 7.2 was carried out in 0.1 M pyrophosphate buffer. It is important to note here that there is a very significant concentration effect (and a less significant ionic strength effect) on the pH of the pyrophosphate solutions as well as the other anions used in this study. For example, dilution of a 0.2 M pyrophosphate solution to 0.1 M resulted in a pH change of *ca.* +0.4 units. For this reason, the pH of all the samples were adjusted after sample preparation (but before addition of the (6S-HTN)AD).

HPLC was carried out as described below for the hydroxylation stereochemistry experiments. The peaks were integrated and their relative

intensities were calculated. The data for the experiments at pH 6.0 were fit to Equation 2a solving for $(k_1 + k_{-1})$, A_0 and A^{eq} and the individual rate constants were calculated employing the relation in Equation 2b.

$$\frac{A_t - A^{eq}}{[A]_0 - A^{eq}} = e^{-(k_1 + k_{-1})} \quad (2a) \qquad \frac{A^{eq}}{B^{eq}} = \frac{k_1}{k_{-1}} \quad (2b)$$

Stereochemistry of hydroxylation

The stereochemistry (stereoselectivity) of the hydroxylation reaction at C6 of the cationic iminium ion intermediate in the enzyme catalyzed reaction was investigated by examining the time course of product formation. Since the epimers of (6HTN)AD are in relatively rapid thermodynamic equilibrium at the pH values used in these studies, isolation of the product mixture alone results in the recovery of a mixture of diastereomers in ratios near that of the equilibrium mixture. This is a result of epimerization at the C6 position of the tetrahydronicotinamide ring and therefore does not allow the determination of the hydroxylation stereochemistry by simple product analysis. An HPLC system was developed to separate the products of this reaction and also to allow the monitoring of the time course of the reaction.

The hydration reaction was carried out in 50 mM PIPES buffer containing 100 mM pyrophosphate, pH 7.2. β-NADH and G3PDH were added to final concentrations of 2 mM and 0.5 mg/mL, respectively. The reaction volume was 3 mL and the reaction was carried out at 30 °C in a water bath. Aliquots (0.1 mL) were withdrawn at the appropriate time points and the reaction was quenched by diluting the aliquot into 0.4 mL of 75 mM K_2CO_3 (pH ~10) containing 40 μM 3',5'-cAMP as an internal standard. These samples were

26

stored frozen (-70 °C) until they could by assayed. The ionic strength was adjusted to 1.5 M with KCl.

The time course of the hydration reaction was monitored by reverse phase HPLC on a Microsorb Dynamax® C-18 column (5 μm, 0.46 x 25 cm). The column was eluted with 0.1 M triethylammonium phosphate buffer, pH 7.5 using a 10 to 14% methanol gradient over 28 minutes. The flow rate was 1.0 mL/min. A Beckman Model 420 gradient controller was used, and the column was monitored at 265 nm using a Kratos SF769 variable wavelength detector. A Hewlett Packard 1090 liquid chromatograph equipped with a diode array detector and interfaced to a Hewlett Packard Chemstation computer was used for some of the studies. The sample size was 0.4 mL and the detector was set to 2 absorbance units full scale (AUFS). Peak areas were measured for the (6HTN)AD diastereomers and normalized to the area of the internal standard peak (retention time = 27 min). The peak areas were also corrected for (6HTN)AD formed by the nonenzymatic hydration reaction

The stereochemistry of the nonenzymatic hydration reaction was carried out in an similar manner. Identical reaction conditions were used except that buffer was substituted for enzyme.

Stereochemistry of protonation

The stereochemistry of the protonation of the C5 position of the dihydronicotinamide ring was investigated by ^{1}H NMR of the (6HTN)AD reaction products using a dideuterium labeled-β-NADH. $[4-^2H_2]$-β-NADD$_{RS}$, labeled with two deuterium atoms at the N4 position of the dihydronicotinamide ring, was prepared according to the method of Oppenheimer and Kaplan (1974b) and was purified by HPLC using the conditions described above for the

purification of (6HTN)AD. Enzyme catalyzed hydration of this deuterium labeled NADH was carried out in deuterated buffer (50 mM PIPES, 100 mM pyrophosphate, pD 7.2) at 30 °C. $NADD_{AB}$ (0.7 μmole) was dissolved in buffer and to this was added 0.5 mg of G3PDH (previously exchanged into deuterated buffer by ultrafiltration) in a total volume of 1.0 mL. The extent of reaction was monitored spectrophotometrically at 340 nm. After the reaction had proceeded to approximately 90% completion (*ca.* 5 hours), the reaction was quenched by addition of solid K_2CO_3 to a final pH of 10. The (6HTN)AD epimers were purified by HPLC on a Microsorb C-18 reverse phase column using the conditions described above. The peaks corresponding to the two epimers were collected as one fraction. The quenched reaction mixture was lyophilized, and the residue was dissolved in 1 mL of water. The sample was then filtered (0.2 μm) and injected on the column (3 x 400 μL) . Peak fractions were collected using a Pharmacia Frac-100 connected to the detector output signal. Solid K_2CO_3 was added to the (6HTN)AD fraction to pH ~10. The sample was then lyophilized and redissolved in 2 mL of 0.1 M ammonium bicarbonate, pH 8.0 and applied to a Baker-10 SPE™ octadecyl extraction column which had been previously washed with methanol (3 mL) followed by buffer (3 mL). The column was then rinsed with 1 mL of ammonium bicarbonate and the 6HTNAD was then eluted by washing the column with ammonium bicarbonate:methanol (2:1). Approximately 80% of the (6HTN)AD was recovered in the ammonium bicarbonate:methanol wash. The remaining 20% was not retained by the column and was found in the initial ammonium bicarbonate wash. The column was washed with buffer (3 mL), and the washings from the previous sample application were applied and eluted as before. Total recovery of desalted 6HTNAD was >95% using this procedure. The (6HTN)AD fractions were pooled and a 1.1 equivalents of NaOH was added (0.1 M) to provide the proper

28

counterion. The sample was lyophilized to dryness and residual ammonium bicarbonate was removed by additional lyophilizations from water.

The stereochemistry of the nonenzymatic reaction was investigated by incubating β-NADD$_{AB}$ in the identical buffer as described above. The reaction was allowed to proceed overnight after which >90% of the NADD$_{RS}$ had reacted. HPLC showed, however, that very little (6HTN)AD remained and that the major reaction product was cTHNAD[3]. Since cyclization of (6HTN)AD to form cTHNAD does not involve any further chemistry at C5 of the tetrahydronicotinamide ring, any stereospecificity of protonation would remain intact during subsequent anomerization at C1' and dehydration (Oppenheimer and Kaplan, 1974a). Thus, cTHNAD can itself be used to determine the presence of stereoselectivity for protonation at the C5 position. The cTHNAD was isolated and purified by reverse phase HPLC as described above for (6HTN)AD.

NMR Spectroscopy

^{1}H NMR spectroscopy of the various (6THN)AD and cTHNAD samples was carried out at 500 MHz using a General Electric GN-500 instrument with an

---

[3]Note that cTHNAD itself is formed as a mixture of epimers due to the asymmetric center generated at C6 of the tetrahydronicotinamide ring. The two epimers are formed in a 9:1 ratio (Oppenheimer, 1987) with the 6R compound predominating. They are separable by HPLC (Figure I.7) and the 6R epimer was isolated and used for the NMR studies.

internal deuterium lock. Generally, samples were passed through a small (~ 1 mL) column of Chelex-100 to remove any paramagnetic metal ions before lyophilization. NMR samples were lyophilized twice from 99.8% D_2O and then dissolved in 100.0% D_2O to a final volume of 0.35 mL. The samples contained 50 μM EGTA to suppress paramagnetic broadening and 5 mm NMR tubes were used. The probe temperature was maintained at 25° C. The spectral width was ± 3000 Hz and quadrature phase detection was employed. The pulse width was set to correspond to a 45° tip angle and no post-acquisition delay was used. The free induction decays were acquired using a 16 bit digitizer and stored in 16K data points. The FID was apodized with a single exponential before fourier transformation resulting in a line broadening of 0.2 Hz. Chemical shifts were measured relative to internal 3-(trimethylsilyl)propionic-[2,2,3,3-$^2H_4$]acid (TSP).

Thiomethylation of Cys-149 of G3PDH

Thiomethylation of the G3PDH active site residue Cys-149 was carried out using a modification of the procedure described by Smith et al. (1975). Crystallized G3PDH was centrifuged, and the precipitate dissolved in 0.5 mL of 10 mM Tris buffer, pH 8.1. The enzyme was reduced by incubation with 1 mM DTT for 30 min at 0 °C. DTT was then removed by passage through a Pharmacia PD-10 disposable desalting column equilibrated in Tris buffer (bed volume = 9.1 mL, void volume = 2.5 mL). The sample (0.5 mL) was applied to the column and the column was washed with 1.0 mL aliquots of Tris buffer. One mL fractions were collected. The enzyme appeared in the 2.5 to 5.0 mL fractions with >95% recovery. The column was then re-equilibrated by washing with at least 2 column volumes (*ca.* 20 mL) of Tris buffer. The enzyme fractions were pooled, and the protein concentration was measured

spectrophotometrically. Next, a 100-fold molar excess of methyl methane-thiosulfonate was added from a stock solution of 0.2 M prepared in water and the solution was allowed to incubate for 30 minutes at 0 °C. The protein was then concentrated to ≤0.5 mL using a Centricon-30 ultrafiltration device (30K Dalton cutoff). The ultrafiltration device was spun at 5000 rpm for 45 min at 4 °C in a Sorvall SS-34 rotor fitted with adapters. Next, the excess MMTS was removed on a PD-10 desalting column using the same procedure as described above for removal of DTT. The fractions containing protein were pooled and concentrated to a final volume of *ca.* 0.5 mL by ultrafiltration again using a Centricon-30 ultrafiltration device. Assays of this modified enzyme in the absence of reducing agent (*e.g.* DTT) showed no oxidative phosphorylation activity indicating complete inactivation brought about by quantitative blocking of the active site cysteine. The enzyme showed full activity, however, when assayed in the presence of reducing agent.

Results

HPLC Separation of (6HTN)AD Diastereomers

An HPLC separation of the acid breakdown and G3PDH-catalyzed hydration products of β-NADH has been reported by Miksic and Brown (1978). Attempts at achieving baseline separation of the reaction products using their conditions were not successful and required a modification of the chromatographic conditions. Figure I.9 shows a typical chromatogram obtained by HPLC of the G3PDH-catalyzed hydration mixture using a triethylammonium phosphate-methanol mobile phase. This separation shows improved resolution of the (6HTN)AD diastereomers over the procedure of Miksic and Brown and is amenable to both analytical and preparative separations. Up to 2 mg of material has been successfully chromatographed with negligible loss of resolution. The elution order of the reaction products is unchanged from the previously reported procedure as indicated by relative peak heights and UV spectroscopy of the individual components.

Identification of the peaks in the chromatogram was carried out by Miksic and Brown using authentic samples of (6HTN)AD and the primary acid degradation products of β-NADH, α-$O^{2'}$-6A,B-cyclotetrahydronicotinamide adenine dinucleotide, (cTHN)AD. They reported the identification of peaks **3** and **4** as α- and β-(6HTN)AD. Isolation of these peaks and investigation by ^{1}H NMR reveals that, in fact, the peaks correspond to the epimers of (6HTN)AD rather than the α- and β-anomers. The presence of epimers is a result of the generation of an asymmetric center at the C6 position of the dihydronicotinamide ring in the product (Figure I.10). The α anomers of (6HTN)AD were not detected. Williams et al. (1976) carried out ^{13}C NMR studies of (6HTN)AD prepared using the procedure of Oppenheimer and
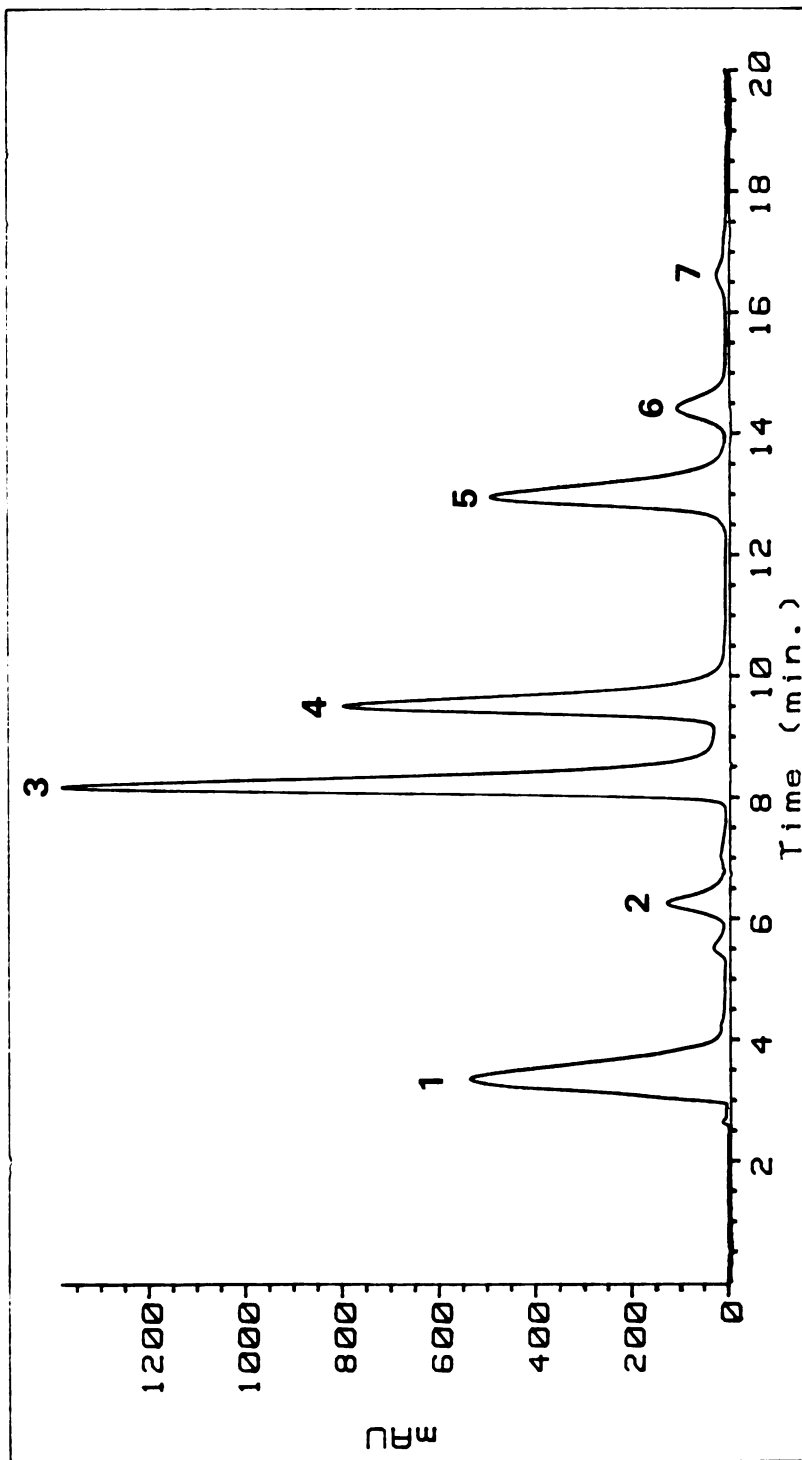
Figure I.9. HPLC separation of the hydration reaction products. Peak assignments are described in the text.

Kaplan (1974b) and also found only the β-anomer. Two sets of ^{13}C resonances were observed, however, in a ratio that corresponded to that observed in the ^{1}H NMR spectrum of a mixture of (6HTN)AD epimers. Figure I.11 shows the normalized UV spectra of peaks **3** and **4** showing a slight (*ca.* 2 nm) red shift in the 280 nm shoulder of the 6R epimer.

(6R-HTN)AD   (6S-HTN)AD
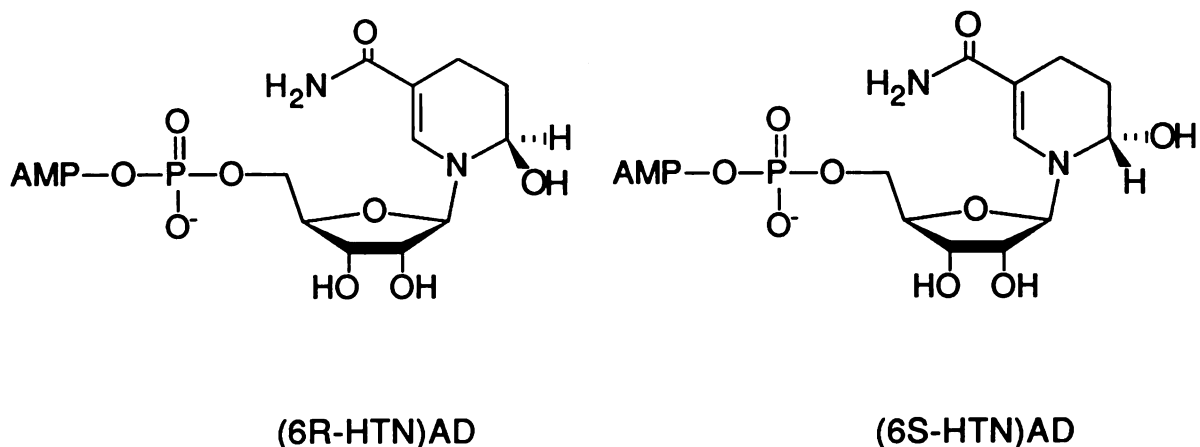
Figure I.10.   Anomers of (6HTN)AD generated by formation of a chiral center at C6 of the tetrahydronicotinamide ring.

Isolation and ^{1}H NMR of an equilibrium mixture of epimers can be used to assign the two (6HTN)AD peaks (peaks **3** and **4** in Figure I.9) to their respective component of the (6HTN)AD epimeric pair. In an equilibrium mixture of epimers, Oppenheimer and Kaplan (1974b) observed a ratio of 65% of the 6S-epimer (*re*-face hydroxyl) and 35% of the 6R-epimer (*si*-face hydroxyl). This is also the ratio observed in the HPLC separation of the (6HTN)AD diastereomers (Figure I.9). Assuming that there are no large differences in the UV spectrum of the diastereomers (*i.e.,* extinction coefficient at 265 nm), peaks
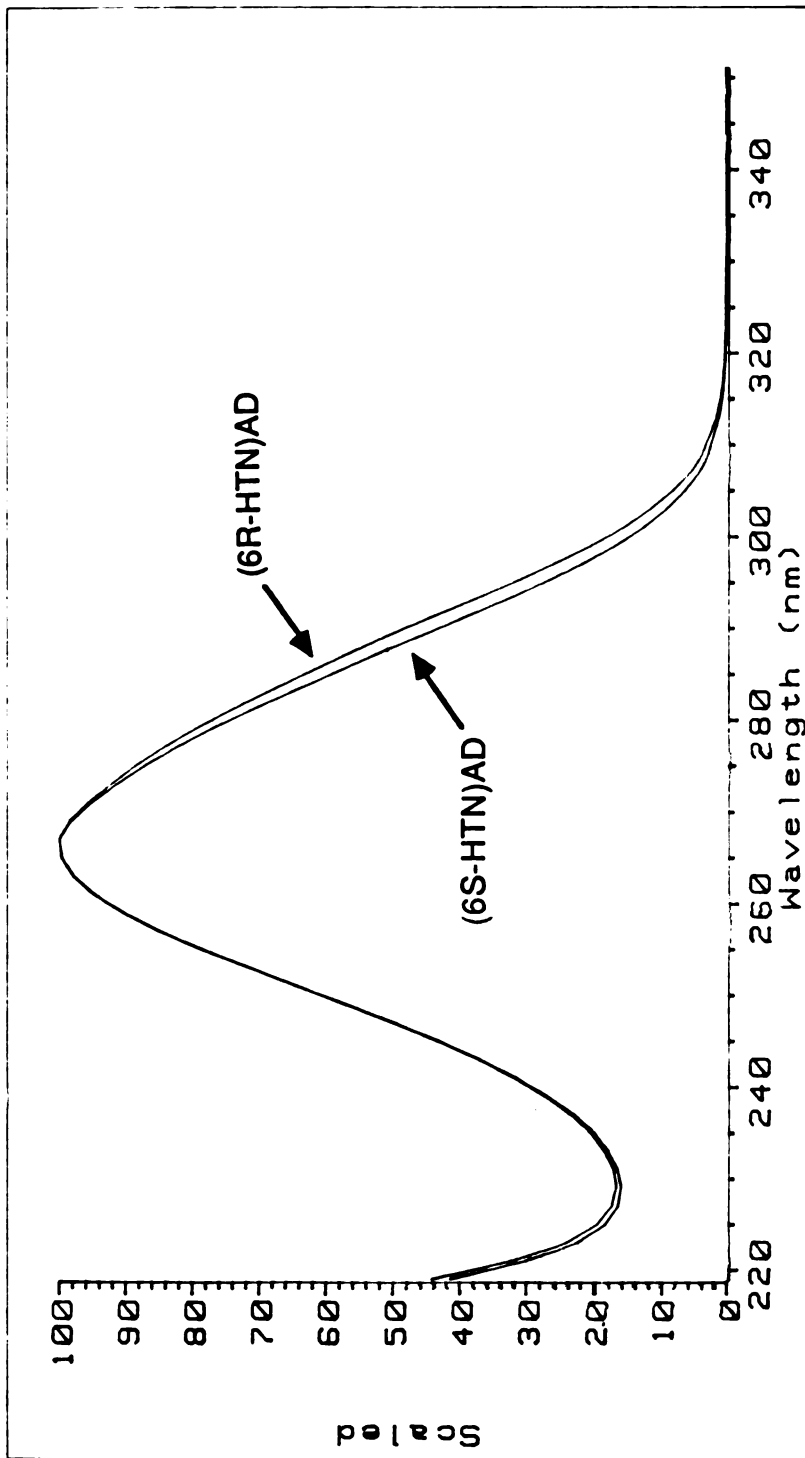
Figure I.11. UV spectra of (6R-HTN)AD and (6S-HTN)AD. Spectra were acquired directly during the HPLC elution using a diode array detector.

3 and **4** can be assigned to β-(6S-HTN)AD and β-(6R-HTN)AD, respectively.

Table I.2 shows a summary of the compounds isolated by this HPLC technique and their retention times.

Table I.2. Identification, retention times and structures of HPLC component peaks.

Peak Number	Retention time (min)	Product
1	3.3	G3PDH
2	6.2	ADP-Ribose[a]
3	8.1	β-(6S-HTN)AD
4	9.5	β-(6R-HTN)AD
5	12.9	β-NADH
6	14.4	α-$O^{2'}$-6R-THN AD
7	16.6	α-$O^{2'}$-6S-THN AD

[a]Miksic and Brown (1979) observed this peak as a 'secondary acid product' and identified it as AMP. We find, however, that this peak has the same retention time as authentic ADP-Ribose and is the more likely product since the pyrophosphate linkage is relatively stable under the reaction conditions.

Stereochemistry of Protonation of the G3PDH-catalyzed Hydration Reaction

In contrast to the deuterium labeling studies of Oppenheimer and Kaplan (1974b), we observed the stereospecific incorporation of deuterium at C5 of the dihydronicotinamide ring in the G3PDH-catalyzed hydration of β-NADH. Figure I.12 shows a portion of the ^1H NMR spectrum of the C5 proton resonances of the diastereomeric mixture of (6HTN)AD prepared from β-NADD$_{AB}$ in D_2O and isolated by reverse phase HPLC. The assignments of the resonances in the proton NMR spectra of the diastereomers have been published (Oppenheimer and Kaplan, 1974b). Based on the relative intensities of the resonances, the upfield resonance is assigned to the axial C-5 proton (*re*-face proton) in the 6R diastereomer (*si*-face hydroxyl) and the downfield resonance is assigned to the

(5R,6S)-[4-²H₂, 5-²H]-(6HTN)AD
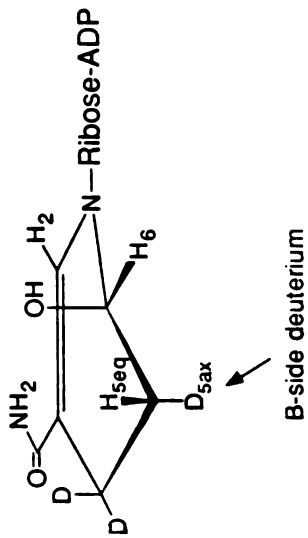
(5R,6R)-[4-²H₂, 5-²H]-(6HTN)AD
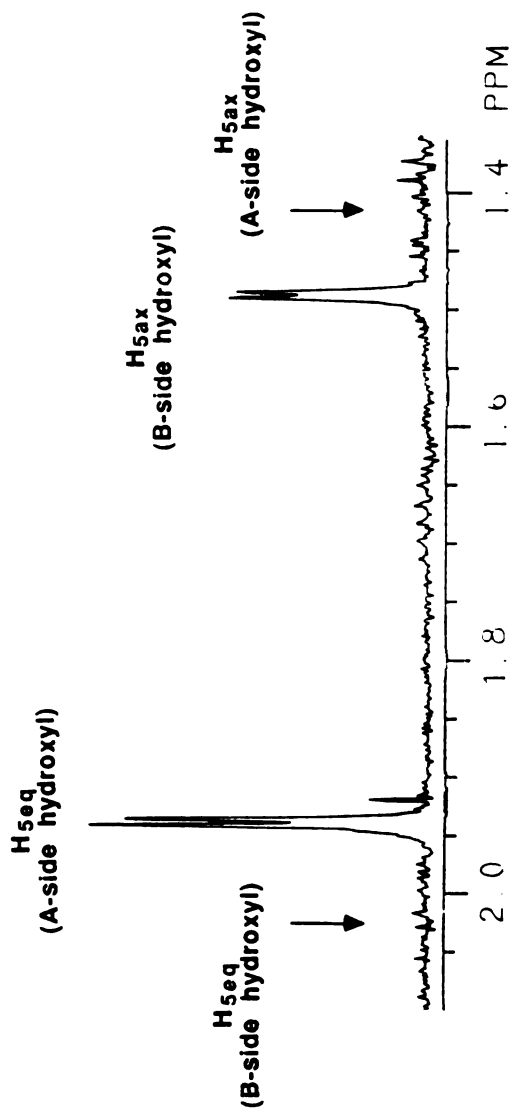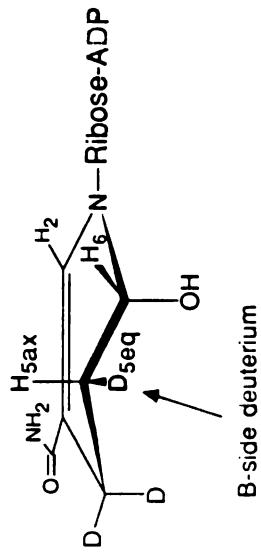
Figure I.12. ¹H NMR spectrum of the C5 protons of (R,S-6HTN)AD prepared enzymatically from β-NADD$_{AB}$ in D₂O. Also shown are the positions of the additional C5 resonances that would appear if deuteration had occurred randomly at C5.

equitorial C-5 proton (*re*-face proton) in the 6S diastereomer (*re*-face hydroxyl). The only coupling constant observed is the J_{5-6} coupling constant of 2.5 Hz. The absence of resonances corresponding to the *si*-face protons in the diastereomeric product mixture (at 1.42 and 2.05 ppm for (6S-HTN)AD and (6R-HTN)AD, respectively) shows, therefore, that only one deuterium is incorporated at C5 in the enzymatic hydration reaction and that deuteration occurs stereospecifically to the *si*-face of the dihydronicotinamide ring.

Stereochemistry of Protonation of the Nonenzymatic Hydration Reaction

The destruction of β-NADH in acid and concentrated buffer solutions is well known. The reaction proceeds via two pathways, in one of which the initial reaction is hydration of the 5,6 double bond of the dihydronicotinamide ring analogous to the enzymatic hydration reaction (Figure I.13) (Oppenheimer and Kaplan, 1974a). Anomerization at C1' of the nicotinamide ribose follows with formation of α-(6HTN)AD. Subsequent dehydration results in the so-called 'acid product', cTHNAD (Oppenheimer and Kaplan, 1974a). In the alternate pathway, β-NADH first undergoes anomerization at C1' of the ribose followed by hydration of the 5,6 double bond again resulting in the formation of α-(6HTN)AD. Since the protonation reaction is rate-limiting (Johnson and Tuason, 1978), nonenzymatic deuteration at C5 is expected to result in the incorporation of only one deuterium in the product. Since subsequent anomerization and dehydration does not involve any further chemistry at C5, the stereochemistry of the remaining proton at C5 will reflect the stereochemistry of the nonenzymatic protonation reaction. Thus, for the nonenzymatic reaction we isolated the major component of the cTHNAD formed (6R-α-$O^{2'}$-cTHNAD) and Figure I.14 shows the ^{1}H NMR spectrum of the C5 axial and equitorial protons of this compound. Assignments of the resonances
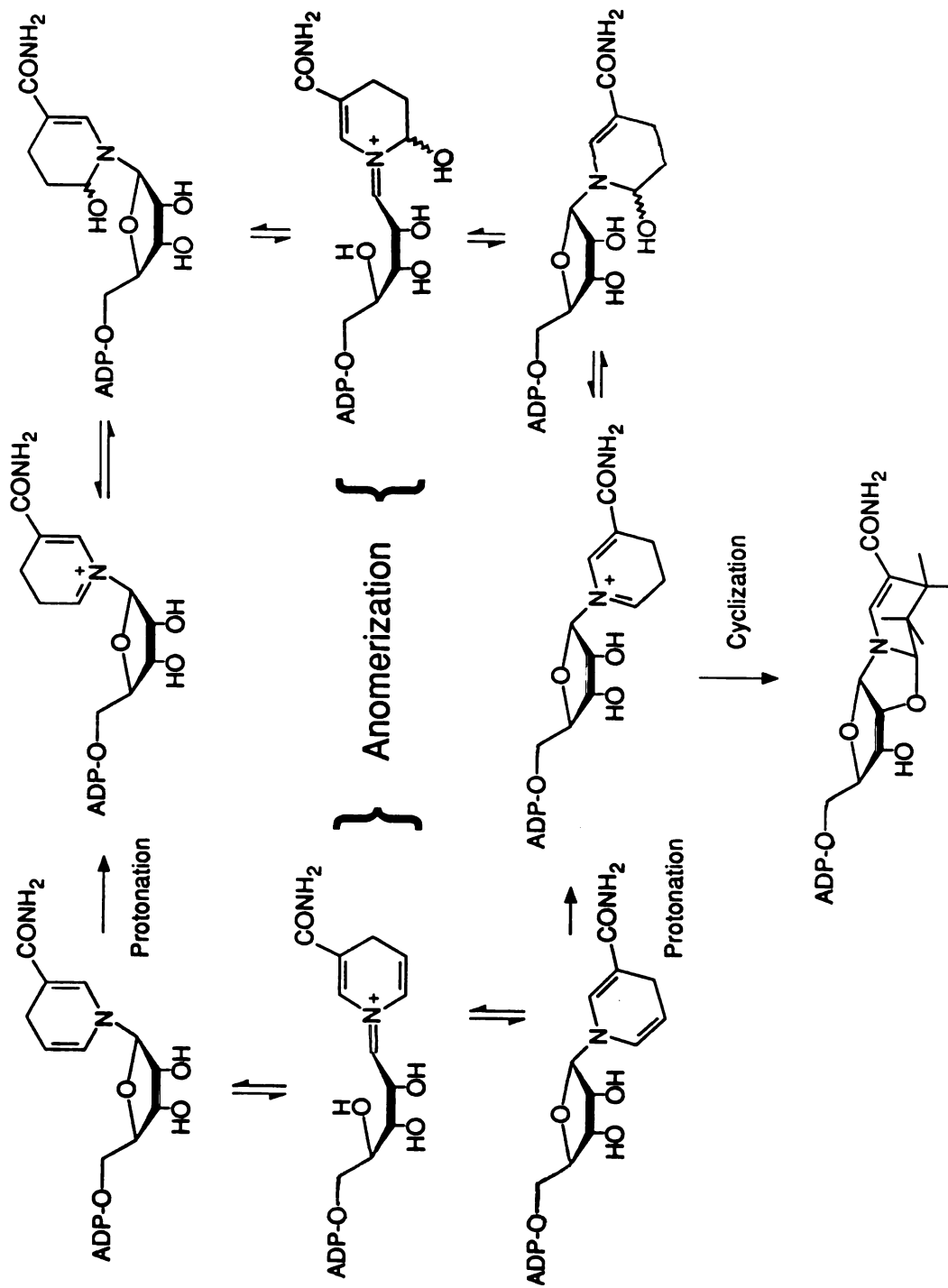
Figure I.13. The mechanism of the acid breakdown of β-NADH. Two different pathways result in the formation of the same product. Only the 6S epimer of the product is shown. The 6R epimer accounts for only ~10% of the total (from Oppenheimer and Kaplan, 1974a).
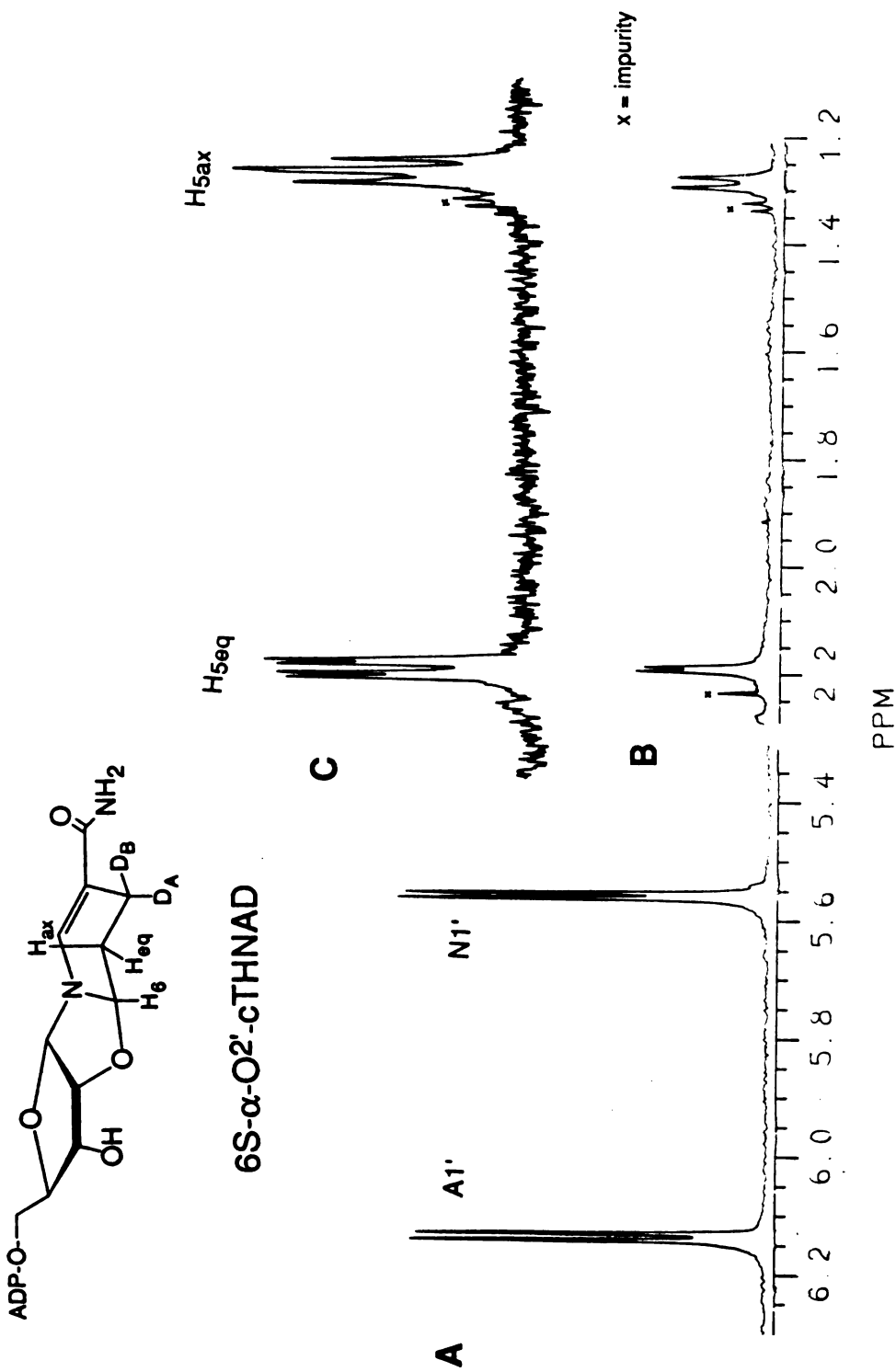
Figure 1.14. A portion of the ¹H NMR spectrum of 6S-cTHNAD derived from the nonenzymatic breakdown of β-NADD$_{RS}$ in 0.1 M pyrophosphate/D$_2$O, pD 6.0. The presence of resonances corresponding to both an axial and equatorial proton (spectrum B) shows that deuteration occurs randomly at C5 of the dihydronicotinamide ring. Integration of these resonances relative to the anomeric resonances (spectrum A) indicates that only one deuterium is incorporated at C5 suggesting that protonation is rate-limiting. Spectrum C is the same product obtained in H$_2$O. The geminal coupling between the C5 axial and C5 equatorial protons in this compound is readily observed.

in this compound have been previously reported (Oppenheimer and Kaplan, 1974a). The bottom spectrum in Figure I.14 shows resonances for both an axial C5 proton at 1.28 ppm and an equatorial C5 proton at 2.19 ppm. Both of these resonances integrate to one half of a proton relative to the anomeric C1' protons at 5.56 and 6.14 ppm. This demonstrates that the nonenzymatic hydration reaction shows no stereoselectivity for protonation of the dihydronicotinamide ring of β-NADH, *i.e.*, protonation at C5 occurs equally to both the *re*-face and *si*-face of the dihydronicotinamide ring. The top spectrum in Figure I.14 shows the corresponding spectrum of the product of the nonenzymatic reaction of β-NADD$_{AB}$ in unlabeled buffer (H_2O). Note that in this spectrum there is an additional coupling constant due to the geminal $J_{5ax\text{-}5eq}$ coupling (-11.5 Hz).

Acid catalyzed epimerization of (6HTN)AD

Miksic and Brown (1978) reported the separation and nonenzymatic equilibration of (6HTN)AD although, as mentioned above, they incorrectly identified the two compounds as α- and β-(6HTN)AD. The actual components at equilibrium are the epimeric pair (6R-HTN)AD and (6S-HTN)AD. We chose to investigate the effect of pH and buffer concentration on the rates of epimerization of (6HTN)AD. Figure I.15 shows the relative concentrations of the two epimers over time after dilution of a solution of predominantly (6S-HTN)AD (the thermodynamically less stable of the two epimers) into 0.1 M pyrophosphate buffer, pH 6.0. At pH 6.0, the epimers reach thermodynamic equilibrium in approximately 30 minutes. The data for this plot were fit to a simple first order equilibration and the K_{eq} for the epimerization was calculated to be 1.59. This corresponds to a free energy difference of 0.3 kcal/mol for the two epimers. Also shown in Figure I.15 is the epimerization reaction in 0.1 M

41
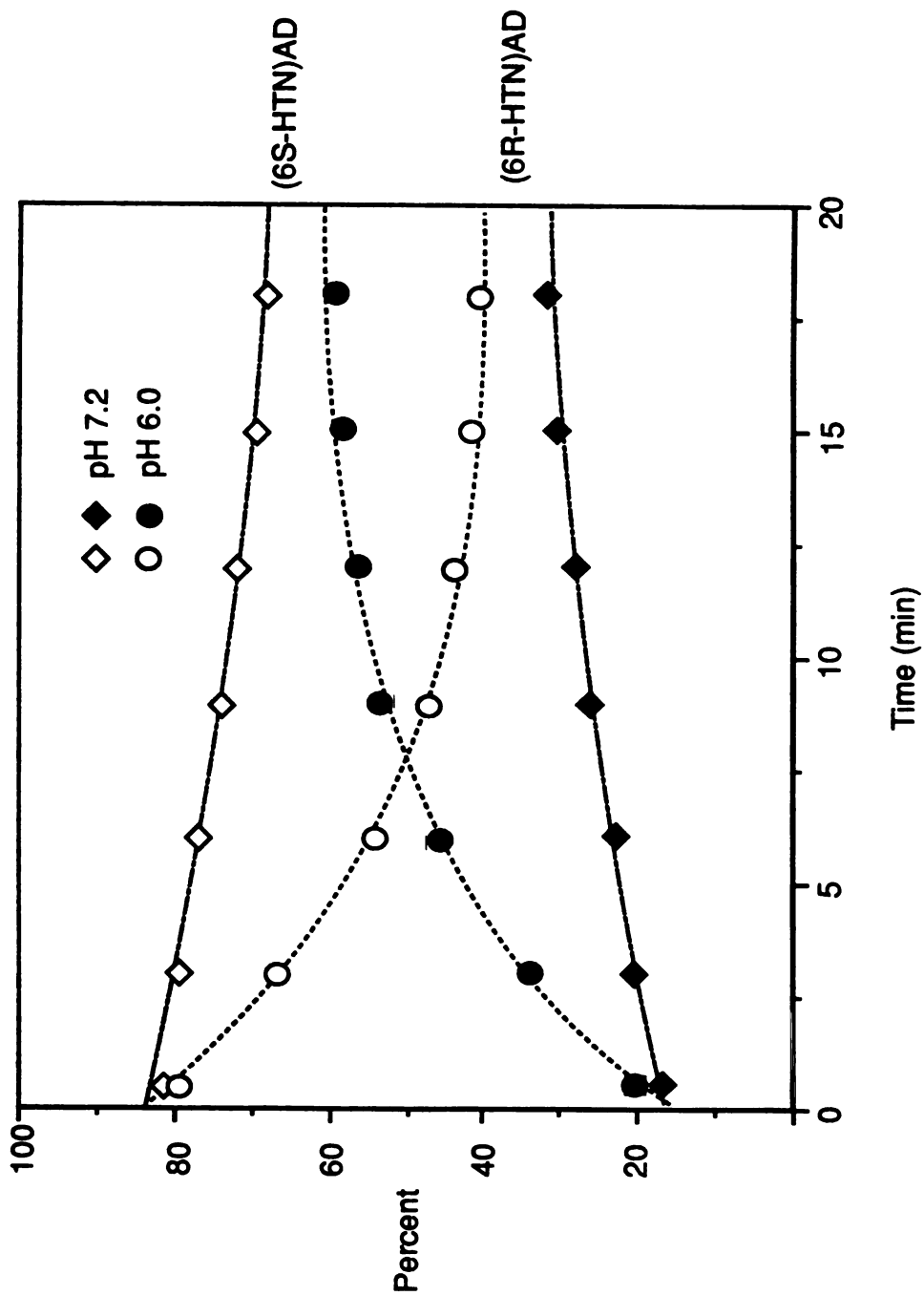
Figure I.15. The time course of (6S-HTN)AD epimerization at pH 6.0 and pH 7.2.

pyrophosphate buffer, pH 7.2. At pH 7.2 the rate of epimerization is considerably slower and the profile appears nearly linear over the time course studied. The equilibration reaction at pH 6.0 was repeated at 0.2 and 0.3 M pyrophosphate and the data from these experiments are shown in Figure I.16. A plot of the k_{obs} vs. buffer concentration shows a non-zero slope as well as a non-zero y-intercept implicating both general and specific acid catalysis in the epimerization reaction. Thus, the large pH effect on the rate of equilibration (Figure I.15) is due to both the decrease in hydronium ion concentration (H_3O^+) and the decrease in the concentration of the protonated form of the buffer involved in general acid catalysis. In this particular case the buffer catalyzing the epimerization reaction in the pH range 6-7 is $H_2P_2O_7^{-2}$ ($pK_3 = 6.60$). Figure I.17 shows the mechanism for general- and specific-acid catalyzed epimerization. It is noteworthy that a similar reaction, the anomerization of reduced pyridine nucleotides, shows only specific acid catalysis (Oppenheimer and Kaplan, 1975). The mechanisms for both reactions are similar in that they both involve the protonation of the oxygen of a carbinolamine with subsequent formation of an iminium ion intermediate.

Stereochemistry of hydroxylation

Oppenheimer and Kaplan reported the isolation of a mixture of epimers of (6HTN)AD from the hydration reaction catalyzed by G3PDH and proposed that the hydroxylation reaction was nonspecific for reasons mentioned above. As shown above (Figure I.15), the epimers of (6HTN)AD reach thermodynamic equilibrium in about 30 minutes at pH 6.0. Simple isolation of the reaction products will give essentially an equilibrium mixture of epimers regardless of the stereochemistry of the enzymatic hydration reaction. Also, we have found

43
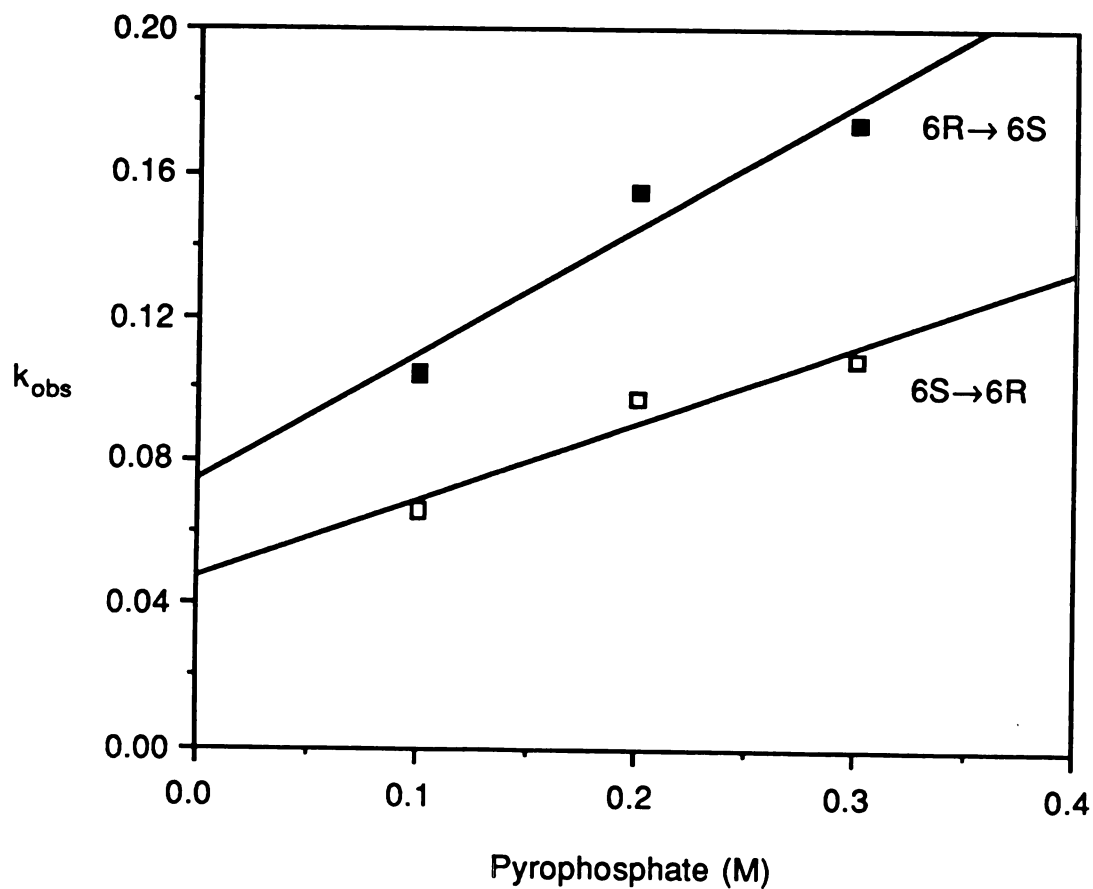
Figure I.16. Buffer dependence of the reaction rate of (6HTN)AD epimerization. The nonzero y-intercept implicates specific acid catalysis as well.

General acid catalysis: R = e.g. phosphate
Specific acid catalysis: R = H_2O
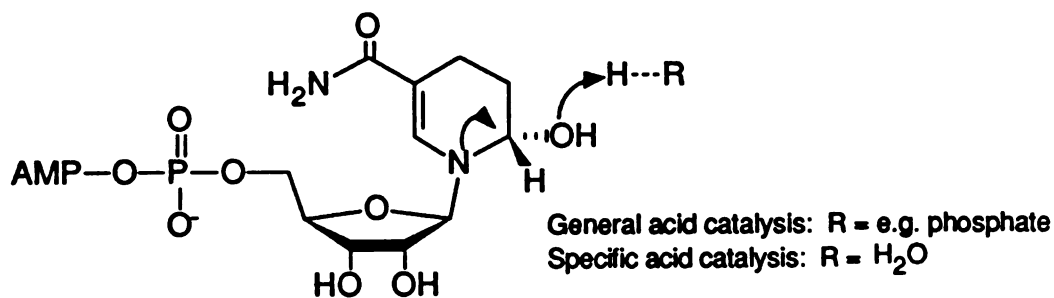
(6R-HTN)AD
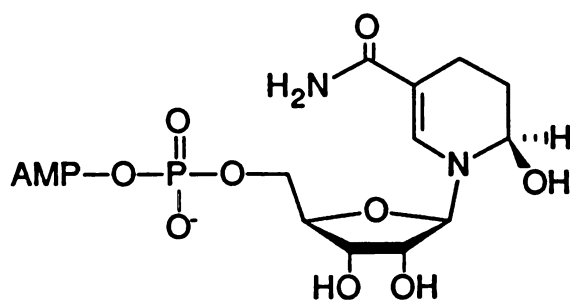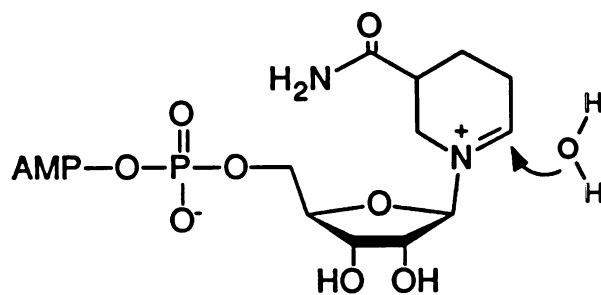
(6S-HTN)AD

Figure I.17. Mechanism of epimerization of (6HTN)AD showing both general- and specific-acid catalysis.

45

that the HPLC-separated diastereomers are quite unstable and rapidly reach equilibrium during lyophilization and workup even with careful attention to pH and temperature.

Because of this instability, we chose instead to monitor the concentration of the two epimers in the reaction mixture over time. The reaction was initiated by the addition of enzyme, and aliquots of the reaction mixture were withdrawn at the appropriate time-intervals and quenched by raising the pH to 10. These samples were then chromatographed and the relative amounts of the (6HTN)AD diastereomers measured. Figure I.18 shows the time course of the G3PDH-catalyzed hydration reaction at pH 7.2 (corrected for the nonenzymatic hydration reaction). Also shown in Figure I.18 is the time course for the nonenzymatic reaction. These data reveal that there is indeed a stereochemical preference for the hydroxylation reaction and that hydroxylation occurs on the si-face of the nicotinamide ring with a stereoselectivity of at least 90%. The nonenzymatic reaction, however, shows no observable stereoselectivity in the hydroxylation reaction since both diastereomers appear at equilibrium over the entire course of the reaction (as determined by analysis of the HPLC chromatograms).

Michaelis-Menten kinetics of G3PDH -catalyzed β-NADH Hydration

NADH binding to native G3PDH

The steady-state kinetics for the hydration reaction catalyzed by native G3PDH show saturation kinetics for binding of β-NADH and a Lineweaver-Burk plot is shown in Figure I.19a. The K_M was calculated by nonlinear regression using an equation which takes the high enzyme concentration (14.3 μM) into account. At 0.5 M phosphate the K_M for β-NADH was calculated to be 270 μM.

46
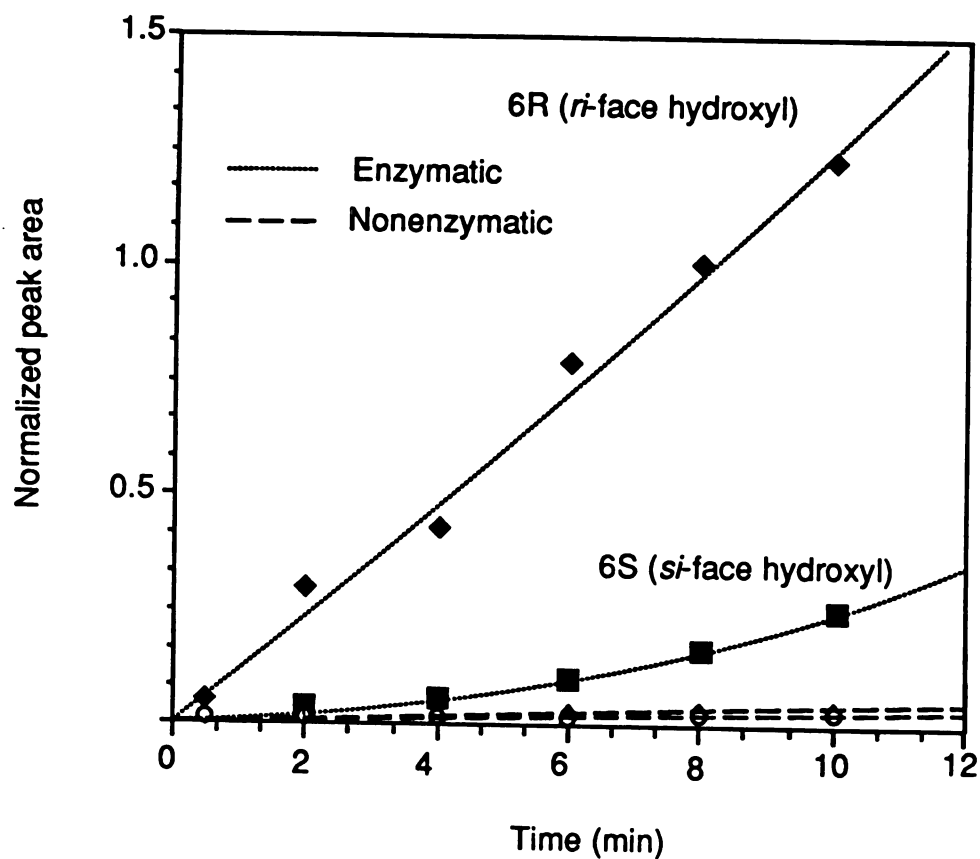
Figure I.18. Time course of the enzymatic and nonenzymatic hydroxylation reactions showing the stereoselective hydroxylation to the *si*-face of the nicotinamide ring for the enzymatic reaction. The products for the nonenzymatic reaction appear at equilibrium for the entire course of the reaction.
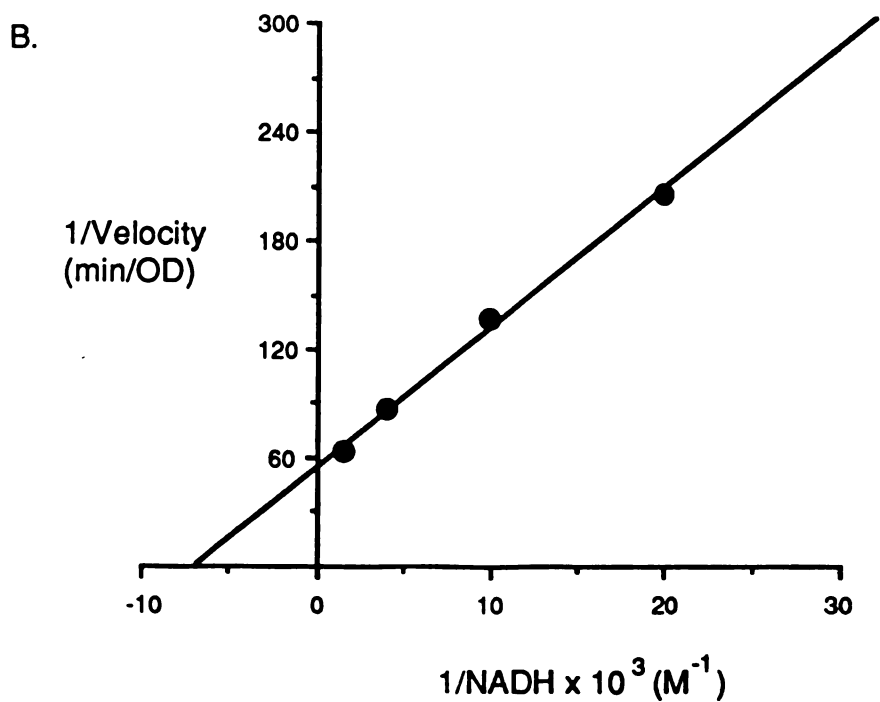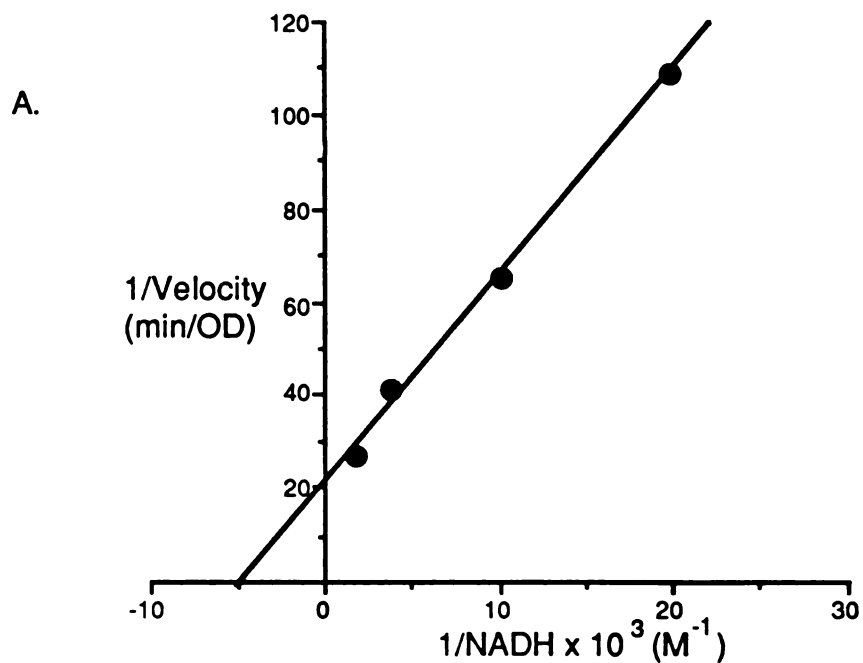
Figure I.19. (A). Lineweaver-Burk plot for native G3PDH-catalyzed hydration of β–NADH. (B). Lineweaver-Burk plot for thiomethylated G3PDH-catalyzed hydration of β-NADH. The anion used in both cases was 0.5 M phosphate.

This compares favorably to the equilibrium constant of 200 μM for β-NADH binding to yeast G3PDH (Ellenreider, et al., 1972).

NADH binding to thiomethylated G3PDH

Figure I.19b shows the Lineweaver-Burk plot for binding of β-NADH to G3PDH that was treated with MMTS resulting in the thiomethylation of Cys-149. This modified enzyme not only shows comparable activity in the hydration reaction but also gives a Michaelis constant for the dinucleotide that is similar to that of the native enzyme (170 μM). This shows that Cys-149 is not involved in catalysis and has no significant effect on dinucleotide binding.

Anion binding

Investigations into the binding of the polybasic anion to the enzyme resulted in the sigmoidal curves as illustrated in Figure I.20. Above 1.0 M citrate, the velocity begins to level off and approaches a maximum. The curves for phosphate and pyrophosphate do not level off, however, and there is no observable maximal rate below concentrations of 1.5 M and 1.0 M, respectively. Sigmoidal binding/velocity curves of this type are characteristic of positive cooperativity (Fersht, 1977). The data for the citrate velocity curve were therefore fit to a cooperative binding equation, and the data are shown in Figure I.21. A replot of the data is shown in Figure I.22. This is the usual 'Hill' plot done for analysis of cooperativity in binding. A slope greater than unity in a Hill plot indicates positive cooperativity in substrate binding. The fitted parameters for the citrate binding curve are listed in Table I.3. Table I.4 shows the relative rates of phosphate, pyrophosphate and citrate at a concentration of 0.5 M along with their relevant pK_a values. Figure I.20 also shows the effect of

49
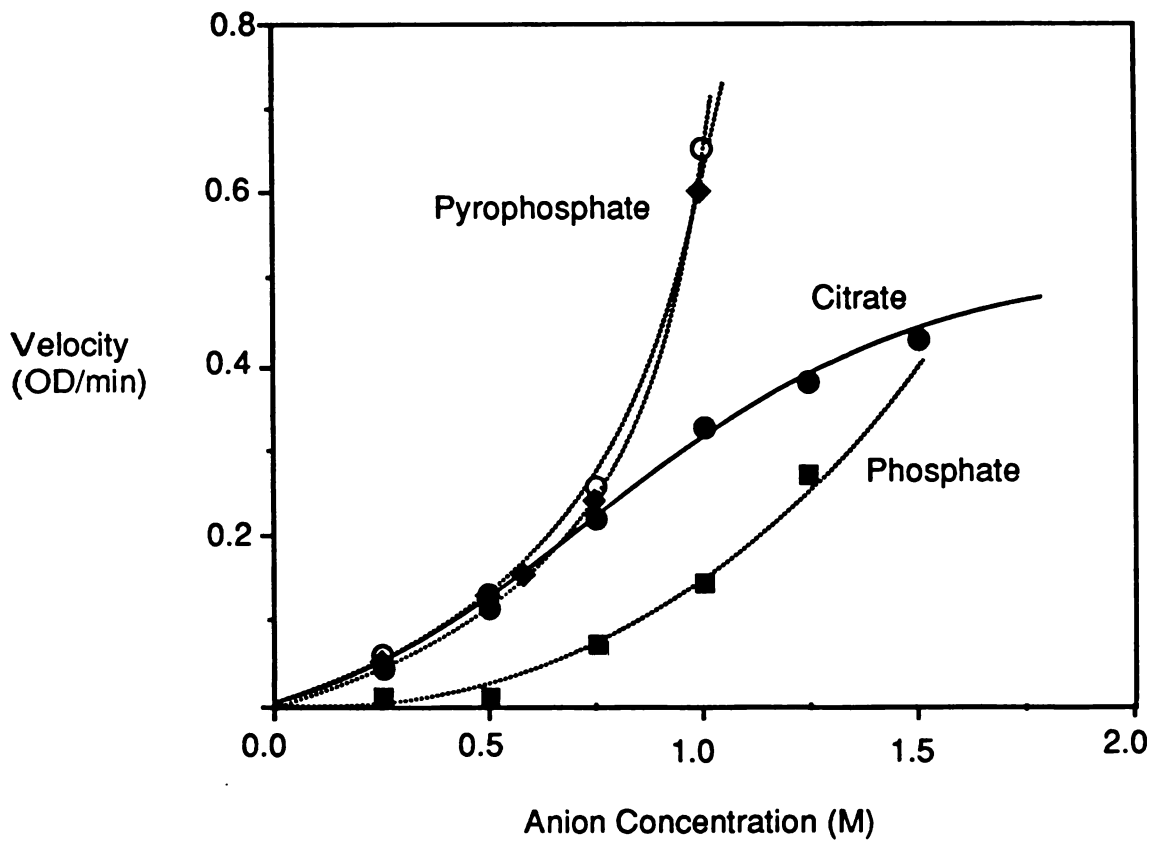
Figure I.20. Comparison of the hydration velocity for various concentrations of the polybasic anion. The open circles correspond to the profile for thiomethylated G3PDH with pyrophosphate. The β-NADH concentration was 0.25 mM.
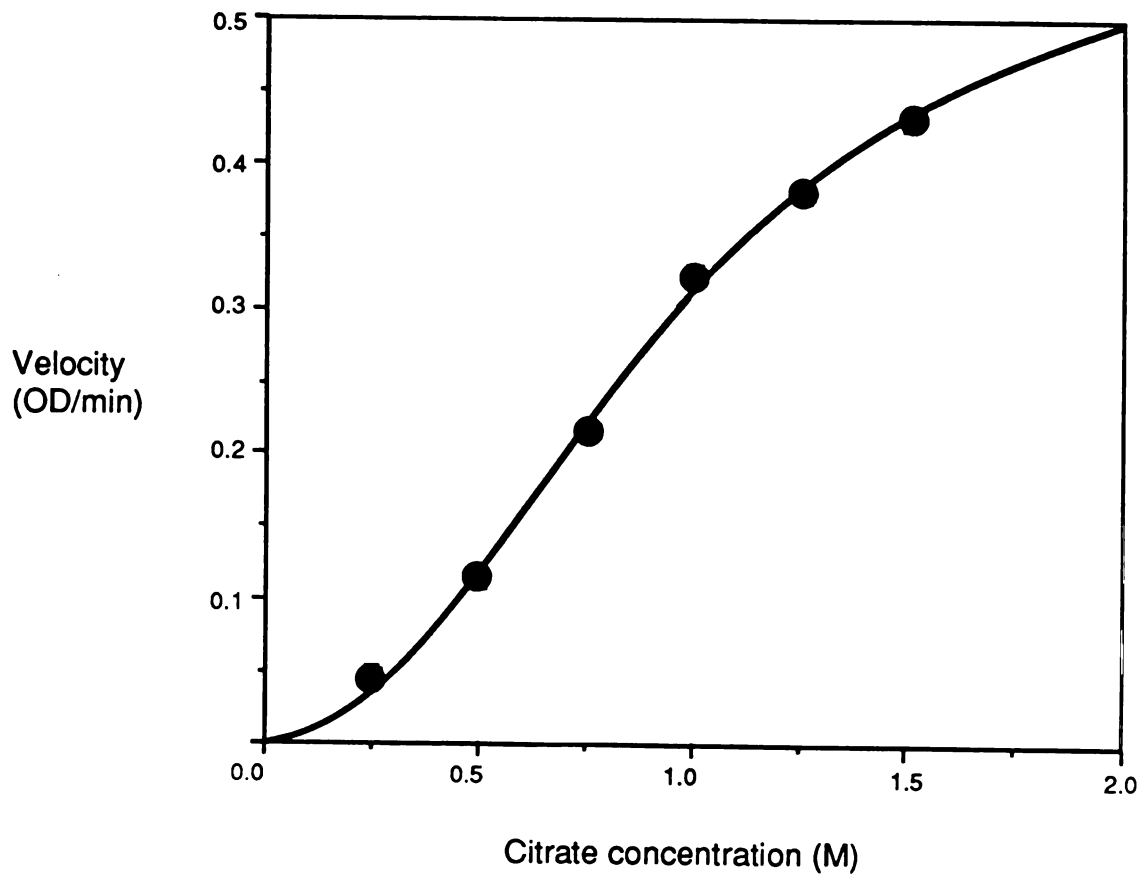
Figure I.21. The citrate velocity data fit to a cooperative binding equation. The fitted parameters are listed in Table I.3.
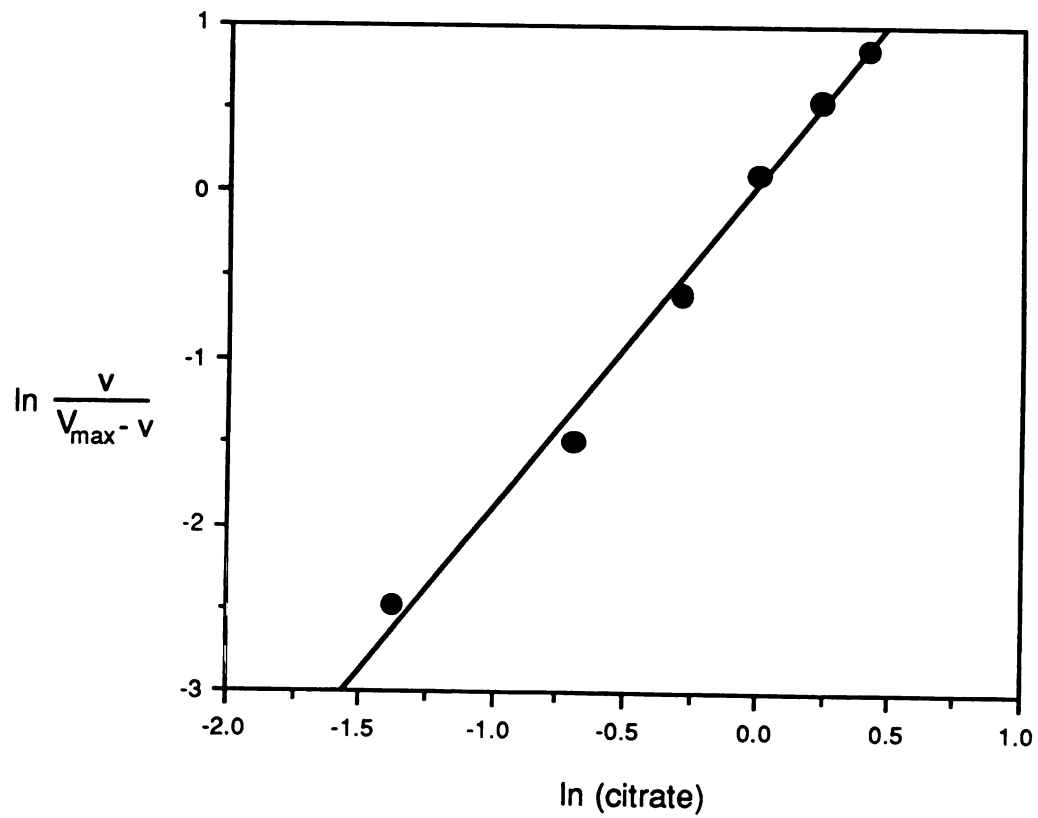
Figure I.22. The Hill plot for citrate binding to G3PDH. A slope of 2.1 indicates positive cooperativity.

thiomethylation of G3PDH on the anion binding and velocity of the hydration reaction using pyrophosphate as the anion. As with β-NADH binding, there appears to be little if any effect on anion binding or enzyme activity caused by the introduction of a thiomethyl group in the active site.

Table I.3 Fitted parameters for citrate binding assuming positive cooperativity.[a]

Parameter	Value
V_{max}	0.61OD/min
K'	0.96 M
n	2.1[b]

[a]The data were fit to the nonlinear form of the cooperative binding equation.
[b]A value of n > 1 indicates positive cooperativity.

Table I.4. Relative rates for the G3PDH-catalyzed hydration reaction using various anions.[a]

Anion	Relative rate	pK_a[b]
Pyrophosphate	1.0	6.6
Citrate	0.86	6.4[c]
Phosphate	0.08	7.2

[a]The anion concentrations were 0.5 M, a region of the curve where the concentration dependence for all the anions appears first order. This minimizes the K_M dependence of the rate.
[b]The pK_a values are for the relevant ionizations near pH 6.0. These do not necessarily reflect the pK_a of the ionization in the active site of the enzyme.
[c]The second ionization of citric acid has a pK_a of 4.8 but its concentration at pH 6.0 is < 1% of the total citrate concentration.

Discussion

Stereochemistry of G3PDH-catalyzed hydration

Protonation

The nonenzymatic hydration of β-NADH was shown by Johnson and Tuazon (1977) to involve general acid catalysis in the hydration of the 5,6 double bond of the dihydronicotinamide ring. They studied a wide range of buffers and found a linear dependence of the general acid rate constant on the pK_a of the general acid. The Brønsted coefficient α for the reaction was 0.46 ± 0.06, which reflects the sensitivity of the protonation step to the pK_a of the general acid. This value is also a measure of the degree of bond formation in the transition state. Solvent isotope effect experiments showed that the rate-limiting step was proton transfer from the general acid species to C5 of the dihydronicotinamide ring. The incorporation of a single deuterium at C5 in the nonenzymatic hydration reaction (Figure I.14) also suggests that the protonation step is rate limiting.

The G3PDH-catalyzed hydration reaction is similar in that it also shows a solvent deuterium isotope effect and the incorporation of only a single deuterium at C5 (Figure I.12). The requirement for a polybasic anion, the pH dependence and the dependence of the rate on the particular anion used suggest that general acid catalysis may also be involved in the enzymatic reaction. Acetylation of the enzyme was shown by Rafter and Colowick (1957) to increase the rate of (6HTN)AD formation. This observation suggests that the enzyme-catalyzed hydration of the 5,6 double bond of β-NADH results from the reaction of a ternary complex composed of acyl-enzyme, β-NADH and phosphate. Catalysis by the enzyme may therefore be the fortuitous

consequence of NADH and phosphate binding sites in the same active site thereby increasing the 'effective' concentration of the general acid (Fersht, 1977). Since anion binding sites on enzymes are generally known to involve cationic amino acid residues, the pK_a of the phosphate group may also be lowered in the active site resulting in a more activated phosphate and an additional increase in the rate of NADH hydration analogous to the pK_a dependence of the nonenzymatic hydration reaction rate.

Bound β-NAD(P)$^+$ and β-NAD(P)H exist in two main conformations in the active sites of dehydrogenases as shown by X-ray crystallography. These orientations are termed *syn* and *anti* and describe the orientation of the nicotinamide ring relative to the nicotinamide ribose (Figure I.23). In G3PDH, β–NADH is bound with the dihydronicotinamide in a *syn* orientation with the *si*-face of the ring exposed to solvent. The *re*-face of the ring faces inward toward the protein. Hydride transfer catalyzed by pyridine nucleotide dependent dehydrogenases has been shown to be a direct transfer from the substrate to NAD$^+$ with no evidence of reduced enzyme intermediates (Colowick et al., 1966; Walsh, 1979). Thus, the orientation of the nicotinamide ring alone is sufficient to explain the observed stereochemistry for hydride transfer in which transfer of hydride occurs stereospecifically to the *re*-face of the ring. The results for the protonation stereochemistry, in which protonation occurs stereospecifically to the *re*-face of the dihydronicotinamide ring, are consistent with this model. Assuming that the polybasic anion binds in the inorganic phosphate binding site on the enzyme, its proximity to the dihydronicotinamide ring in the active site makes it an ideal candidate for the species involved in the general acid catalysis of the protonation reaction. G3PDH has been crystallized with bound citrate and, as shown in Figure I.24, one of the terminal carboxylates lies directly over the *si*-face of the nicotinamide ring (Olsen et al., 1976). In this

55
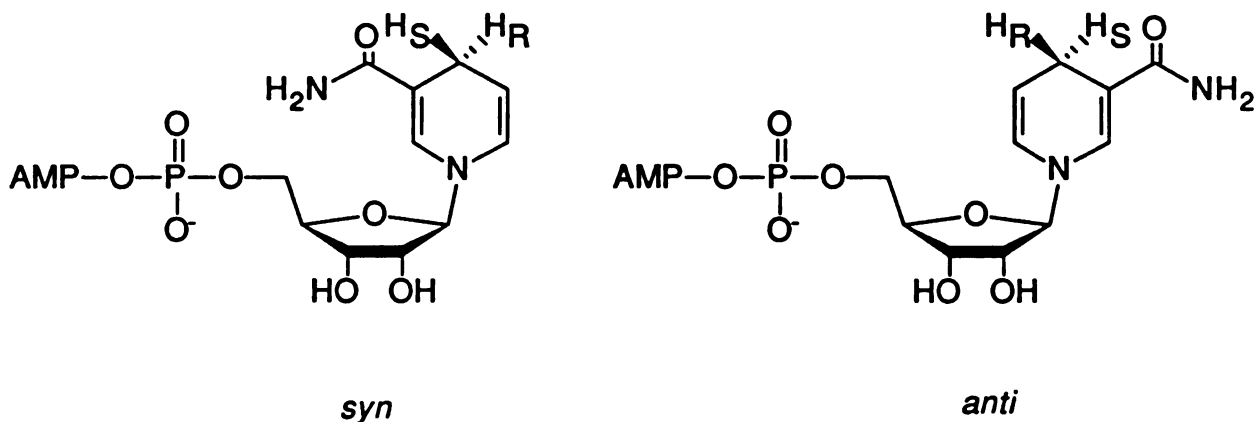
syn   anti

Figure I.23.   The *syn* and *anti* conformations of pyridine nucleotides found when bound in the active site of dehydrogenases.
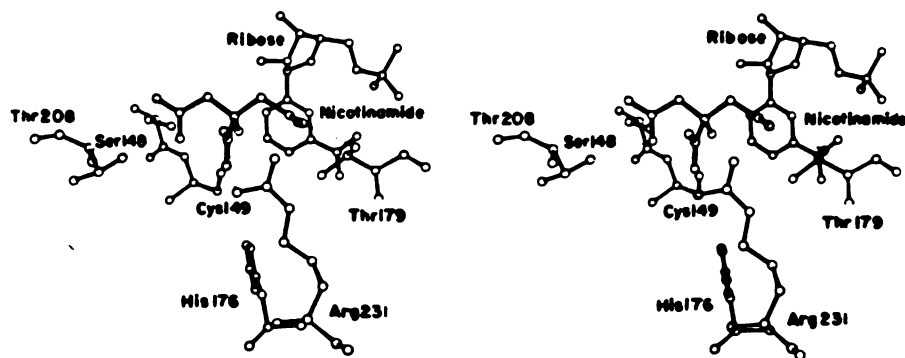
Figure I.24.   Stereo drawing of citrate bound in the active site of lobster muscle G3PDH showing the proximity of the terminal carboxyl group to the nicotinamide ring (from Olsen et al., 1976).

56

structure, the citrate bridges the inorganic phosphate binding site and the anion binding site for the natural substrate, D-glyceraldehyde-3-phosphate. The central carboxylate, with a pK_a of 3.13, forms a salt bridge with Arg-231 and the terminal carboxylates are liganded to Thr-179 in the GAP binding site and Ser-148 and Thr-208 in the inorganic phosphate binding site. Thus, the ability of citrate to promote the G3PDH-catalyzed hydration reaction can also be explained by this mechanism, i.e., general acid catalysis by a polybasic anion in the inorganic phosphate binding site. In the normal oxidative phosphorylation reaction, pyrophosphate has been shown to be a competitive inhibitor of G3PDH with respect to the phosphate analogue, molybdate (Byers et al., 1979). This suggests that pyrophosphate can also bind in the inorganic phosphate binding site and promote the enzymatic hydration reaction analogous to phosphate and citrate.

In the nonenzymatic reaction, the protonation step does not show such stereospecificity and deuterium incorporation occurs equally to either the *re*- or *si*-face of the dihydronicotinamide ring. The intramolecular association between the pyridine and adenine moieties in solution (Oppenheimer, 1982) could impart a stereoselective protonation at C5 as it does for nucleophilic attack of β-NAD+ by cyanide at C4. This stereoselectivity is not observed and its absence is most likely due to the rapid equilibrium (relative to the rate of protonation) between the folded and open forms of the dinucleotide. The equilibrium is also temperature dependent and at 37° C lies primarily toward the open form (Oppenheimer, 1982).

Hydroxylation stereochemistry

The stereoselectivity for the reaction in which hydroxylation occurs on the *si*-face of the dihydronicotinamide ring indicates that the attack by water on the

57

iminium ion intermediate occurs in the active site of the enzyme and not in solution. Since the *re*-face of the intermediate faces back toward the protein, solvent is not able to attack from that side. The *si*-face of the ring, however, is exposed to solvent and attack at C6 results in the formation of the 6S-epimer. After the product is released, it undergoes a facile acid-catalyzed, nonenzymatic epimerization (both general and specific acid catalysis) forming a diastereomeric equilibrium mixture of the product. In contrast, the nonenzymatic reaction does not show such stereoselectivity for the hydroxylation step and both epimers are produced at their equilibrium concentrations. Any inherent stereoselectivity in the nonenzymatic hydroxylation reaction due to conformational or electrostatic effects is masked by the rapid equilibration of the diastereomers relative to their rate of production. The observation by Oppenheimer and Kaplan (1974b) of the G3PDH-catalyzed formation of a mixture of epimers with the 6R epimer in excess over the 6S epimer gives the illusion of apparent stereoselectivity in the enzymatic reaction for hydroxylation. The data presented here shows that, in fact, hydroxylation occurs stereospecifically to the *si*-face of the dihydronicotinamide for a net *syn* hydration of the 5,6 double bond.

Most enzymatic hydration reactions occur via a concerted *anti* addition of water for steric and energetic reasons (Walsh, 1977). In this type of addition, the mechanism favors the pathway with less eclipsing of the groups compared to the corresponding *syn* addition. Model studies also show that *anti* addition of HX is favored energetically when the species H+ and X- are added in a concerted or near-concerted fashion (Cristol, 1947). In a less synchronous reaction, such as a carbonium ion or carbanion process, there would be less of a steric effect. Of the enzymatic reactions shown in Figure I.5 which catalyze the *syn* hydration of a double bond (or *syn* elimination of water), all appear to

catalyze their respective reactions by a two-step (carbanion) mechanism (Rose, 1970). The mechanism proposed for the hydration of β-NADH is in general agreement with this theory in that the reaction does indeed go through a two-step process with no strict energetic or steric requirements to do otherwise.

Enzyme kinetics

Dinucleotide binding

The binding of β-NADH to G3PDH for the hydration reaction shows normal saturation kinetics as shown in Figure I.19. The apparent K_M for β-NADH is calculated to be 270 μM at a phosphate concentration of 0.5 M compared to a dissociation constant of ~200 μM obtained for the yeast enzyme (von Ellenrieder et al., 1972). In a very qualitative sense, this suggests that the dinucleotide binds in the same binding site as in the normal oxidative phosphorylation reaction. Coupled with the stereochemistry results, with chemistry occurring to the *si*-face of the nicotinamide ring, the binding of β-NADH appears to be similar for both hydration and oxidative phosphorylation. Modification of the enzyme with methyl methanethiosulfonate does not affect enzymatic hydration activity even though the enzyme is completely inactive for oxidative phosphorylation. The K_M for the dinucleotide in the hydration reaction with thiomethylated G3PDH is comparable to that for the native enzyme indicating little interaction between the active site thiol and the dinucleotide in this complex.

Anion binding

The rate dependence on the anion concentration gave some surprising results as shown in Figure I.20. The data show that neither phosphate nor

59

pyrophosphate saturate the enzyme below concentrations of 1.0 M. Citrate, however, does appear to level off, and the data for citrate binding were fit to a cooperative binding equation giving a K' of 0.96 M. This suggests that the anion, although appearing to bind in the normal phosphate binding site, does so with much poorer affinity than in the normal redox reaction. The question of what form of the enzyme binds phosphate in the normal reaction must be addressed. It has been shown that the phosphate binding constant to the free enzyme is unmeasurably high (i.e. first order up to 0.1 M) (Harrigan and Trentham, 1974). At high glyceraldehyde-3-phosphate concentrations, where the enzyme exists predominantly as the thioester with GAP (Bloch et al., 1971), the K_M for phosphate is lowered to ~6 mM. It appears therefore that the acyl-enzyme is much better suited to bind phosphate than the free form of the enzyme. This could explain the increase in the rate of hydration observed by Rafter and Colowick (1957) upon acylation of the enzyme. Under their conditions, the binding constant of phosphate was presumably lowered in the acetylated enzyme resulting in an increased rate of hydration at a fixed level of anion. Therefore, the relative rates of catalysis for the different anions, as shown in Table I.4, reflects not only the different pK_a values of the individual anions but also, to some extent, their binding constants. Unfortunately, it is not possible to measure the Michaelis constants for phosphate and pyrophosphate for the native enzyme at reasonable ionic strengths.

Cooperative nature of anion binding

As shown in Figures I.20-21, there appears to be some degree of cooperativity in binding of the anion to G3PDH resulting in sigmoidal binding and velocity curves. A slope greater than unity (m = 2.1) in the Hill plot in Figure I.22 indicates that positive cooperativity is involved with the affinity of the

enzyme for the anion increasing as the anion binds. Cooperativity is a common phenomenon in substrate binding for multimeric enzymes and results from the direct interaction between subunits (Fersht, 1977). The binding of substrate to the first subunit of the multimer alters the protein conformation in the second subunit and, in the case of positive cooperativity, increases its affinity for the substrate. In hemoglobin, a well studied protein exhibiting positive cooperativity towards oxygen binding, this interaction involves the breaking of intersubunit salt bridges (Fersht, 1977).

G3PDH is also known to exhibit cooperativity in substrate binding for the normal oxidative phosphorylation reaction although there is some controversy as to its exact nature. The enzyme isolated from muscle (e.g., rabbit and lobster muscle) shows negative cooperativity in its binding of β-NAD$^+$ with the first molecule of NAD$^+$ binding with a dissociation constant of ~10^{-9} M (Conway and Koshland, 1968). The fourth molecule of β-NAD$^+$ binds to the enzyme with a binding constant of ~25 μM. The yeast enzyme appears to be different from the muscle enzymes in that it shows distinct positive cooperativity for dinucleotide binding (Kirschner et al., 1966). Binding of β-NAD$^+$ in this enzyme can be described by the concerted model of Monod, Wyman and Changeaux (1965) in which the enzyme exists in two symmetrical tetrahedral forms, R and T. The R form has a higher affinity for NAD$^+$ and the T form is enzymatically inactive. There is a relatively slow T to R conversion upon addition of NAD$^+$. In contrast, the binding of β-NADH is hyperbolic with equal affinity for both the R and T forms (K_d = 2 mM). The sources of cooperativity in G3PDH are conformational changes in the protein upon binding of substrate. The active site in G3PDH is located very close to the subunit interface with the most extensive intersubunit contacts involving an antiparallel β-pleated sheet defining a portion of the catalytic domain (Harris and Waters, 1975). Little attention has been paid to the

61

binding of phosphate to yeast G3PDH, however, and from the results presented here it appears that phosphate could also be involved in the metabolic control of enzyme activity, most likely through the acylated enzyme.

References

Alworth, W. L. *Stereochemistry and Its Application in Biochemistry;* Wiley: New York, 1972.

Bloch, W., MacQuarrie, R. A., Bernhard, S. A., (1971), *J. Biol. Chem., 246,* 780-790.

Byers, L. D. (1981) *Methods in Enzymology, 89,* 326.

Chaykin, S., Meinhart, J. O., Krebs, E. G. (1956) *J. Biol. Chem. 220,* 811.

Cleland, W. W. (1967) *Adv. Enzymology, 29,* 1-32.

Cohn, M.; Pearson, J.; O'Connell, E. L.; Rose, I. A. (1970) *J. Am. Chem. Soc., 92,* 4095.

Colowick, S. P., van Eys, J., Park, J. H. in "Comprehensive Biochemistry", Florkin, M. and Stotz, E., Eds., Elseveir, New York, 1966, pp. 1-98.

Conway, A., Koshland, D. E., Jr., (1968), *Biochemistry, 7,* 4011.

Cori, G. T.; Slein, M. W.; Cori, C. F. (1945) *J. Biol. Chem. , 159,* 565.

Cornforth, J. W.; Ryback, G.; Popjak, G.; Donninger, C.; Schroepfer, G. Jr. (1962) *Biochem. Biophys. Res. Commun., 9,* 371.

Cristol, S. J. (1947) *J. Am. Chem. Soc., 69,* 338.

Davidson, B. E.; Sajgó, M.; Noller, H. F.; Harris, J. I. (1967) *Nature (London), 216,* 1181.

Fersht, A. "Enzyme Structure and Mechanism", San Francisco, CA., W. H. Freeman and Company, 1977, pp. 42-48.

Gawron, O.; Fondy, T. (1954) *J. Am. Chem. Soc., 81,* 6333.

Glasoe, P. K. and Long, F. A. (1960) *J. Phys. Chem. 64,* 188.

Griffiths, D. E.; Chaplain, R. A. (1962) *Biochem. Biophys. Res. Commun., 8,* 501.

Hanson, K. and Rose, I. (1963) *Proc. Natl. Acad. Sci. U.S.A., 50,* 981.

Harrigan, P. J. and Trentham, D. R. (1974) *Biochem. J., 143,* 353-363.

Harrigan, P. J. and Trentham, D. R. (1974), *Biochem. J., 143,* 353-363.

Harris, J. I. and Waters, M. *The Enzymes.* Vol. 13, Academic Press: New York, 1975, pp. 1-49.

Harris, J. I.; Perham, J. I. (1965) *J. Mol. Biol., 13,* 876.

Harting, J. In "The Mechanism of Enzyme Action"; McElroy, W. E., Glass, B., Eds.; The Johns Hopkins Press: Baltimore; 1954, p. 536.

Harting, J.; Velick, S. F. (1954) *J. Biol. Chem., 207,* 867.

Hilvers, A. G.; Weenen, J. H. M.; van Dam, K. (1966) *Biochim. Biophys. Acta, 128,* 74-81.

Horecker, B. L.; Kornberg, A. (1948) *J. Biol. Chem., 175,* 385-390.

Jaenicke, R.; Schmid, D.; Knof, S. (1968) *Biochemistry, 7,* 919.

Johnson, S. L. and Tuazon, P. T. (1977) *Biochemistry, 16, 1175-1183.*

Jones, G. M. T.; Harris, J. I. (1972) *FEBS Lett., 22,* 185.

Kirschner, B. K.; Eigen, M.; Bittman, R.; Voigt, B. (1966) *Proc. Natl. Acad. Sci., 56,* 1661.

Kirschner, K., Eigen, M., Bittmann, R., Voigt, B. (1966), *Proc. Natl. Acad. Sci. U. S. A., 56,* 1661.

Krebs, E. G.; Rafter, G. W.; Junge, J. M. (1953) *J. Biol. Chem. , 200,* 479.

Levy, H. R.; Vennesland, B. (1957) *J. Biol. Chem. , 228,* 85.

Long, C., Ed. in *Biochemists' Handbook*; E. & F. N. Spon, Ltd.: London, 1961, pp782-783.

Messner, B., Eggerer, H., Cornforth, J. W., Mallaby, R. (1975) *Eur. J. Biochem., 53,* 255.

Miksik, J. R.; Brown, P. R. (1978) *Biochemistry, 11,* 2234-2238.

Monod, J., Wyman, J., Changeaux, J.-P., (1965), *J. Mol. Biol., 12,* 88.

Moras, D.; Olsen, K. W.; Sabesan, M. N.; Buehner; Ford, G. C.; Rossman, M. G. (1975) *J. Biol Chem., 250,* 9137-9162.

Oesper, P. (1954) *J. Biol. Chem., 421,* 421.

Oguchi, M.; Gerth, E.; Fitzgerald, B.; Park, J. H. (1973) *J. Biol Chem., 248,* 5571.

Olsen, K. W., Garavito, R. M., Sabesan, M. N., Rossmann, M. G. (1976), *J. Mol. Biol., 107,* 571-576.

Oppenheimer, N. J. and Kaplan, N. O. (1975) *Arch. Biochem. Biophys., 166,* 526.

Oppenheimer, N. J. In *Pyridine Nucleotide Coenzymes: Chemical, Biochemical, and Medical Aspects.* Vol. 2A. Dolphin, D.; Poulson, R.; Avramovic, O., Eds. John Wiley and Sons: New York, 1987, pp. 323-365.

Oppenheimer, N. J. In *The Pyridine Nucleotide Coenzymes;* Everse, J.; Anderson, B. M.; You, K.-S., Eds; Academic Press: New York, 1982, pp. 51-89.

Oppenheimer, N. J.; Kaplan, N. O. (1974a) *Biochemistry, 13,* 4675-4684.

Oppenheimer, N. J.; Kaplan, N. O. (1974b) *Biochemistry, 13,* 4685-4694.

Park, J. H.; Meriwether, P.; Clodfelder, P.; Cunninham, L. W. (1961) *J. Biol. Chem., 236,* 136.

Rafter, G. W.; Chaykin, S.; Krebs, E. G. (1954) *J. Biol. Chem., 208,* 799-811.

Rafter, G. W.; Colowick, S. P. (1957) *J. Biol. Chem., 244,* 373.

Rose, I. A. *Crit. Rev. Biochem.* (1972-1973), *1,* 33-57.

Rose, Z. B. (1970) *Arch. Biochem. Biophys., 140,* 508.

Segal, H. L.; Boyer, P. D. (1953) *J. Biol. Chem. , 204,* 265.

Segel, I. (1975) "Enzyme Kinetics", John Wiley and Sons: New York. pp. 72-77.

Smith, D. J., Maggio, E. T., Kenyon, G. L. (1975) *Biochemistry, 14,* 766.

Tiepel, J.; Hass, G.; Hill, R. (1968)*J. Biol. Chem., 243,* 5684.

Trentham, D. R. (1971) *Biochem. J., 122,* 59.

von Ellenrieder, G., Kirschner, K., Schuster, I. (1972), *Eur. J. Biochem., 26,* 220-236.

Walsh, C. (1979) "Enzymatic Reaction Mechanisms", W. H. Freeman, San Francisco. pp. 322-330.

Willadsen, P.; Eggerer, H. (1975) *Eur. J. Biochem., 54,* 247-252.

Williams, T. J.; Ellis, P. D.; Bryson, T. A.; Fisher, R. R.; Dunlap, R. B. (1976) *Arch.*

Biochem. Biophys., 176, 275-284.

Wolff, E. C.; Black, S. (1959) *Arch. Biochem. Biophys., 80,* 236.

Worthington Enzyme Manual, Worthington Biochemical Corporation, Freehold, New Jersy, 1972, pp. 27-29.

SECTION II. Synthesis, Characterization and Enzymatic Properties of α- and β-Nicotinamide Arabinoside Adenine Dinucleotides.

Introduction

Analogs of pyridine coenzymes have long been important in the study of the steric constraints and mechanism of dehydrogenases, ADP-ribosyltransferases and other coenzyme utilizing enzymes. Modifications have focused primarily on the pyridine ring, with special emphasis on the 3-substituent because of their ease of synthesis (Anderson et al., 1959), and to a lesser extent on the adenine moiety (see Anderson, 1982 and Woenckhaus and Jeck, 1987 for comprehensive reviews). There have been few investigations directed at synthesis of analogs containing modifications of the nicotinamide sugar moiety (Goebbeler and Woenckhaus, 1966; Woenckhaus et al., 1964; Woenckhaus and Jeck, 1970; Woenckhaus and Jeck, 1987). The lack of such analogs represents a significant omission since the sugar moiety can influence directly the chemical properties of the coenzyme, alter coenzyme binding to dehydrogenases and has been suggested to play an important mechanistic role (Oppenheimer, 1986a).

In this section the the synthesis and biochemical characterization of both the α- and β-anomers of a new NAD+ analog[1] containing a nicotinamide arabinoside moiety as shown in Figure II.1 are presented. The procedures

---

[1] Abbreviations used: araNMN+, oxidized nicotinamide arabinomononucleotide; araNAD+, oxidized nicotinamide arabinoside adenine dinucleotide; araNADH, reduced nicotinamide arabinoside adenine dinucleotide; ADH, alcohol dehydrogenase; TBA, tetrabutylammonium; Hepes buffer, N-2-hydroxy-ethylpiperazine-N'-2-ethanesulfonic acid; Pipes buffer, 1,4-piperazinediethanesulfonic acid. In the NMR spectra **A** is used to designate resonances of the adenine moiety and **N** is used to designate resonances of the nicotinamide moiety.

developed for this synthesis, which are based on the general properties of 5'-O-tritylpentofuranosylamine intermediates (Kam and Oppenheimer 1979a,b), represent a generalized approach to the synthesis of a wide range of NAD+ analogs. The structure-function questions to be addressed focus on the effects that alterations in configuration of the 2' hydroxyls will have upon: (1) the chemical and physical properties of ribo and arabino nucleotides, (2) the conformation of the sugar moieties, and (3) the binding and utilization of the analogs by two pyridine nucleotide-dependent enzymes, specifically, yeast and horse liver alcohol dehyrdrogenase.

β-araNAD+   α-araNAD+

Figure II.1. Structure of α- and β-araNAD+.

69

Experimental

Materials:

Yeast alcohol dehydrogenase, horse liver alcohol dehydrogenase, Hepes and Pipes buffers and semicarbazide hydrochloride were purchased from Sigma. β-NAD$^+$ and β-NADH were also from Sigma. Acetaldehyde and propanal were from Aldrich and were distilled before use. [U-^{2}H$_5$]-ethanol was purchased from KOR Isotopes. Solvents were either spectrograde or freshly distilled prior to use. All synthetic reagents were of the highest quality commercially available and used without further purification.

Synthesis:

The synthesis of α- and β-araNAD$^+$ was begun by Dr. Bernard Kam in this laboratory and completed in collaboration with Dr. Olaf Malver (Kam et al., 1987).

D-(-)-Nicotinamide-Arabinofuranoside (**4**). The synthesis of the nicotinamide arabinoside was conducted as outlined in Figure II.2. Tritylation of D-(-)-arabinose was conducted according to the procedure of Kam and Oppenheimer (1979a) with the following correction; the concentration of arabinose in the reaction mixture should be *0.7 mmol per mL of pyridine*. The crude product was purified by flash chromatography on silica gel. It was first eluted with chloroform to remove triphenylmethanol then ethyl acetate to recover the product. The trityl arabinose **1** was obtained as a pale yellow syrup which was dissolved in saturated methanolic ammonia at 0° C and incubated overnight to give the trityl arabinosylamine **2** (Kam and Oppenheimer, 1979b). The nicotinamide arabinoside was prepared according to the procedure of Kam and

70

Figure II.2. Synthesis of α,β-araNMN+.

71
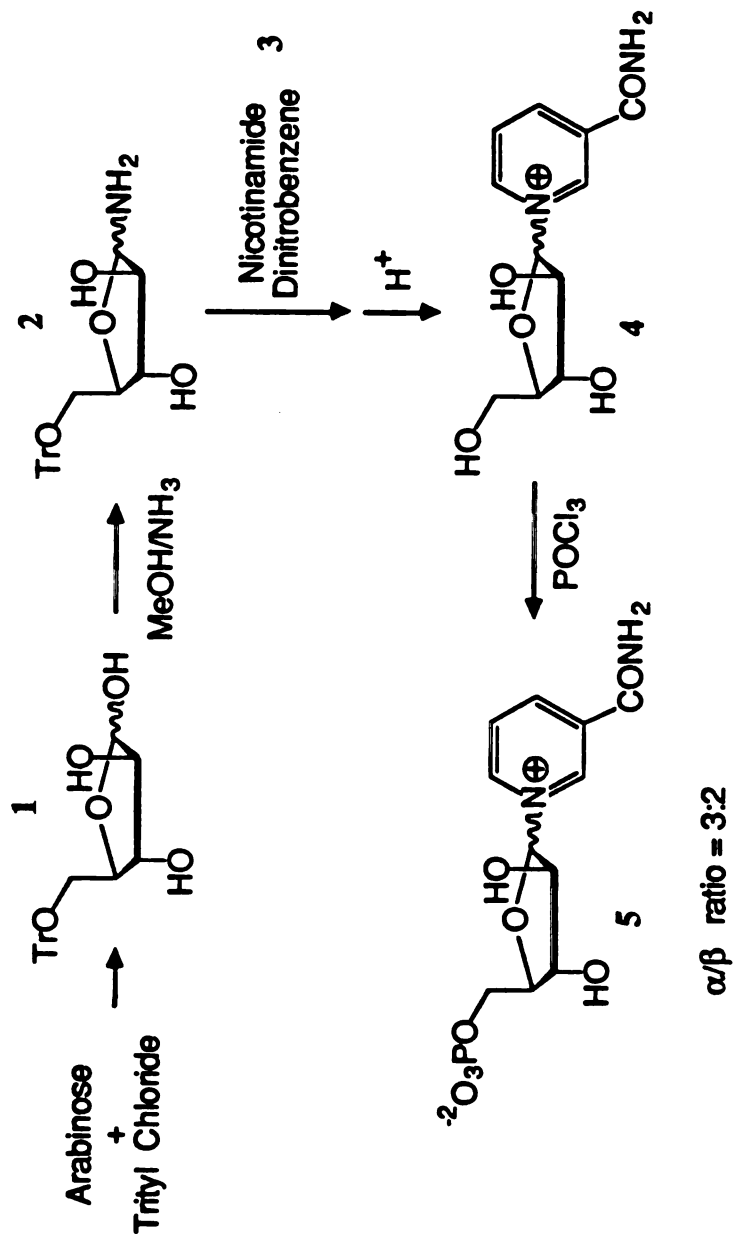
Oppenheimer (1979b) for the synthesis of nicotinamide riboside. Trityl-arabinosylamine was added to a methanolic solution of N-1-nicotinamide-2,4-dinitrobenzene, **3**, where it reacts to give the tritylnucleoside. After 4 hours ammonia was bubbled through the solution at 0° C to destroy excess **3** and the solvent was then removed by rotoevaporation (the bath temperature was maintained below 30° C). The 5'-trityl group was removed by incubating the residue in 0.1N HCl for fifteen minutes at room temperature and the triphenyl-methanol was then filtered off. The nicotinamide arabinoside, **4**, was precipitated with acetone/ether 1:1 by volume and was recovered as a 3:2 mixture of α:β anomers as determined by ^{1}H NMR.

α-, β-Nicotinamide Arabinonucleotide (**5**). The phosphorylation and coupling with AMP were conducted as outlined in Figure II.3. The arabinotide was prepared by phosphorylating **4** with $POCl_3/H_2O$ in triethyl phosphate according to the method of Yoshikawa et al., (1967). The reaction mixture was left overnight at 0°C and then quenched with ice water. Evaporation of the water and precipitation in cold acetone gave a white, hygroscopic precipitate. TLC and ^{1}H NMR spectroscopy showed quantitative conversion to mononucleotide.

α,β-araNAD+ (**7**). The nicotinamide arabinoside adenine dinucleotide was synthesized via the Michelson (1964) method for coupling of nucleotides to generate a pyrophosphate linkage. Because ara-NMN+ is insoluble under the reaction conditions, it is necessary to increase the solubility by acetylation of the 2' and 3' hydroxyls of the arabino moiety. A solution of α,β-araNMN+ (750 μmol) in 1.5 mL water was added to a rapidly stirred solution of 15 mL acetic anhydride in 27 mL pyridine. The reaction mixture was stirred at room
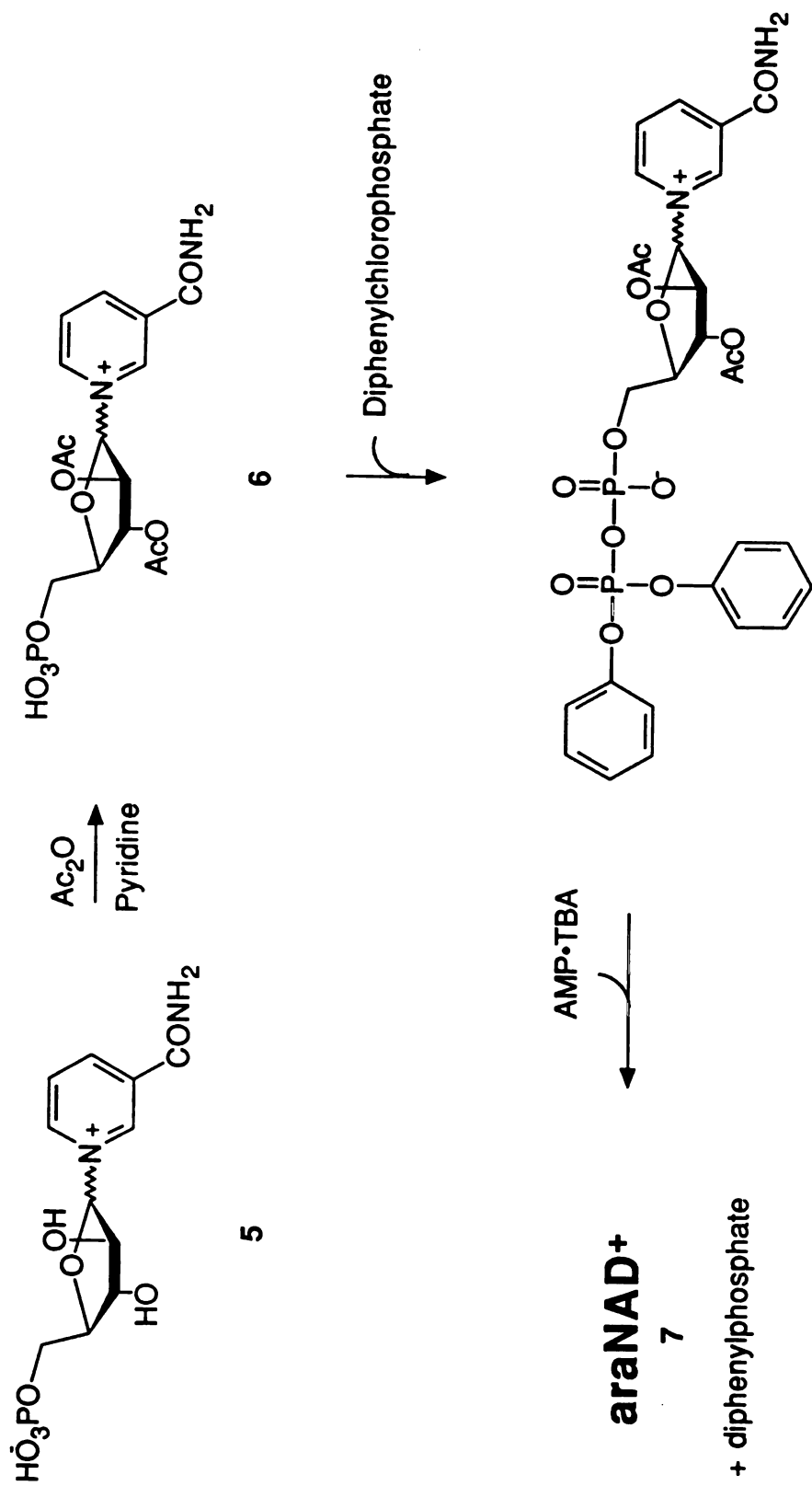
Figure II.3. Acetylation of α,β-araNMN+ and Michelson coupling with AMP forming α,β-araNAD+.

temperature for 2 hours and at 5° C for 10 hours. The solvent was removed *in vacuo* (0.2 mm Hg) with a bath temperature below 40° C. The product of the acetylation reaction was a mixture consisting of the 2',3'-acetylated araNMN+ and the mixed anhydride with acetate as observed by ^{31}P NMR. The residue was therefore treated with 50% aqueous pyridine for 30 minutes at 30° C to destroy the mixed anhydride (Saneyoshi, 1971), and after removal of solvent gave a yellow oil that was used directly in the coupling reaction. TLC and ^{1}H NMR spectroscopy showed complete conversion of araNMN+ (5) to the 2',3' diacetyl nucleotide (6).

Although we have accomplished coupling by activating either the AMP or the araNMN+, only the procedure for araNMN+ activation is presented. Diphenylchlorophosphate (250 µl) and tri-n-butylamine (250 µl) were added under N$_2$ to a solution of 750 µmol of 6 in 5 mL freshly distilled dioxane and 3 mL dry DMF. After stirring at room temperature for 2 hours the solvent was removed *in vacuo* with a bath temperature not exceeding 30° C. Addition of ethyl ether (100 mL) generated an oily precipitate. The mixture was stirred at 0° C for 30 minutes then the ether phase was decanted and residual ether was removed *in vacuo*. The tetrabutylammonium (TBA) salt of AMP (1.5 µmol) was dissolved in 5 mL DMF and then added, along with 5 mL of pyridine, to the yellow oil. The solution was stirred for ten hours at room temperature and then the solvent was removed *in vacuo*. Residual solvent was removed by coevaporation with dry methanol (3 x 15 mL). The residue was dissolved in 30 mL ammonia-saturated methanol and stirred for 4 hours at 0° C to deacetylate the arabinose moiety. After stripping off the solvent the residue was dissolved in water (200 mL), adjusted to pH 6.5 with dilute formic acid and applied to a Dowex AG-1 (formate) column (5 x 25 cm). The column was eluted with a 0 to 0.5 N formic acid linear gradient, 2 L total. The araNAD+ eluted as a single

peak at 0.07 N formic acid with no resolution of anomers. A total of 510 μmol of araNAD+, **7**, was obtained (yield 67%) and an additional 114 μmol of araNMN+ was recovered. Separation of the anomers was achieved by HPLC on a Whatman Partisil M9 strong anion exchange (SAX) column eluted isocratically with 7 mM ammonium phosphate, pH 3.5 at a flow rate of 5 mL/min. Fractions containing the individual anomers of araNAD+ were pooled and lyophilized. The individual anomers were >99% pure based on analytical HPLC (Figure II.4) and ^{1}H NMR.

α,β-araNADH. Reduction of either α- or β-araNAD+ was conducted enzymatically on a semi-preparative scale (typically 5-10 mg at a time) using yeast alcohol dehydrogenase. Reaction mixtures were incubated at 30° C and consisted of 50 mM Hepes buffer, pH 8.0, 1 M ethanol and 10 mM semicarbazide. The extent of reaction was monitored spectrophotometrically and sufficient enzyme was added to complete the reduction in less than 30 minutes. The reduced dinucleotides were purified by ion-exchange chromatography on a Pharmacia FPLC system using a Polyanion HR 5/5 column according to the method of Orr and Blanchard (1984) for the purification of β-NADH.

Redox potentials:

Redox potentials were determined from the eqilibrium constants for the following reaction at pH 9.0:

$$araNADH + CH_3CHO + H^+ \rightleftharpoons araNAD^+ + CH_3CH_2OH$$
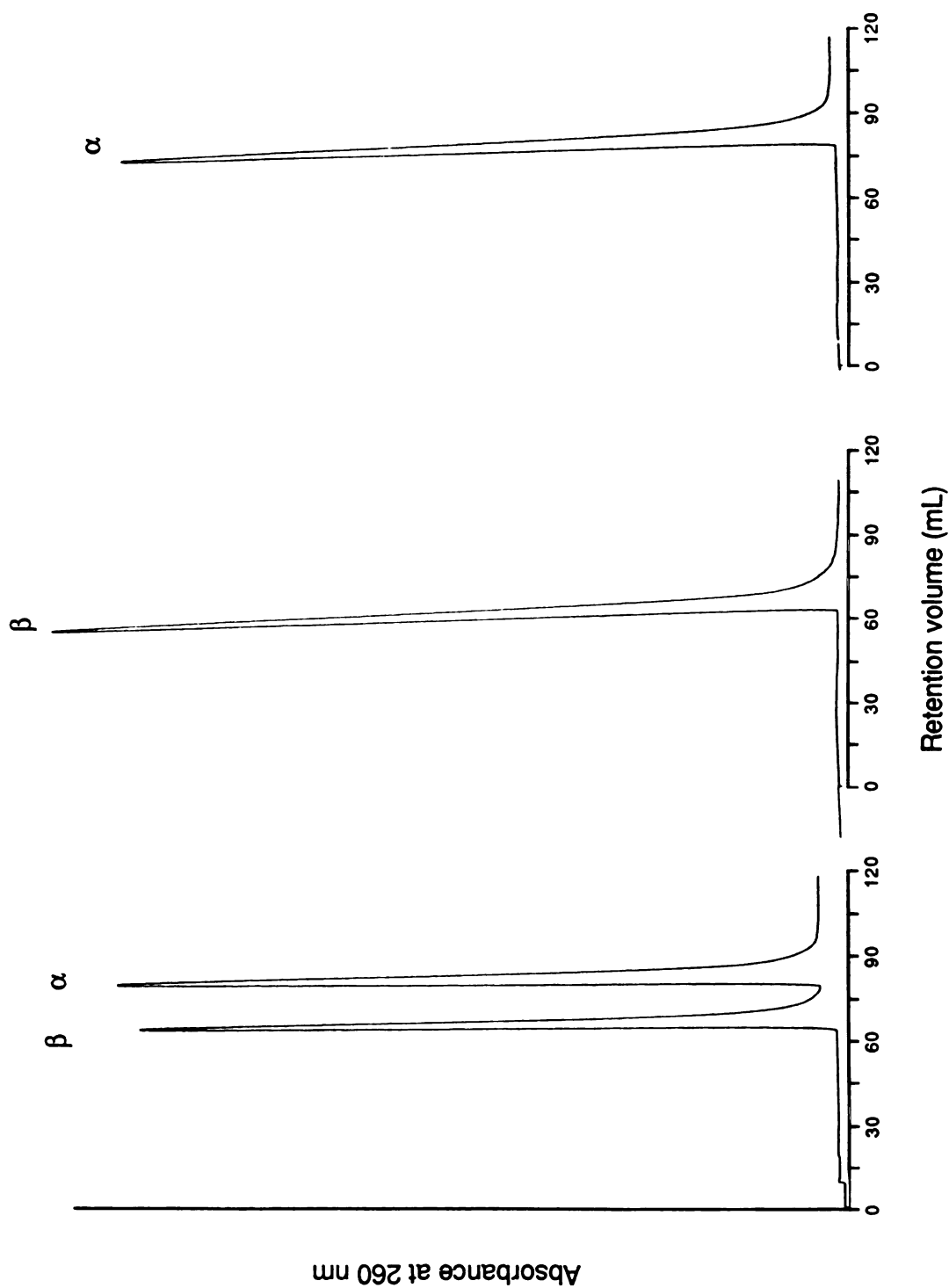
Figure II.4. HPLC separation of α- and β-araNAD$^+$

Absorbance at 260 nm

Retention volume (mL)

76

The equilibrium constant for this reaction is:

$$K_{eq} = \frac{[NAD^+]_{eq} \, [ethanol]}{[NADH]_{eq} \, [acetaldehyde] \, [H^+]}$$

If the acetaldehyde and ethanol concentrations are known along with the pH of the reaction mixture, K_{eq} can be calculated from the equilbrium concentrations of reduced and oxidized dinucleotide. The equilibrium constants for the above reaction for both α- and β-araNAD$^+$ were determined by incubating the reduced dinucleotide in a buffered solution containing ethanol and acetaldehyde and monitoring the reaction spectrophotometrically as it approached equilibrium. The total absorbance change was used to calculate the dinucleotide concentrations using:

$$[NADH]_{eq} = \frac{^{340}A_{eq}}{6220 \, M^{-1}cm^{-1}}$$

$$[NAD^+]_{eq} = [NADH]_0 - [NADH]_{eq}$$

The ethanol and acetaldehyde concentrations in the initial assay solution were adjusted so that the total absorbance change would be about -0.4 absorbance unit (64.3 μM). The inital reduced dinucleotide concentration was approximately 0.14 mM giving an initial absorbance of 0.9 OD. The ratio of the ethanol/acetaldehyde concentration needed to give an OD change of -0.4 was calculated assuming that the redox potential for the arabinose analogs would be similar to that of β-ribNADH (-340 mV corrected to pH 9.0). Their absolute

concentrations were calculated so that they both would be in large excess over dinucleotide. Therefore, as the reaction approached equilibrium there would be essentially no change in the concentrations of either ethanol or acetaldehyde, and their ratio would be fixed. The concentrations used in the assay were 10 mM acetaldehyde and 460 mM ethanol and the stock solutions were calibrated using a dinucleotide of known redox potential (β-ribNADH). Under these conditions, the acetaldehyde concentration would change by only a total of 0.6%. Yeast alcohol dehydrogenase was used to catalyze the reaction and the buffer was 50 mM pyrophosphate, pH 9.0. The equilibrium constants were calculated at pH 7.0 and the standard redox potentials were determined using:

$$e \text{ (volts)} = \frac{RT \ln K_{eq}}{n F}$$

where n = 2 (number of electrons transferred), F is the Faraday constant, R is the gas constant and T is the absolute temperature (298 K).

Enzyme kinetics:

The kinetic parameters were measured at 30° C in stoppered 1 mL cuvettes on a Hitachi 100-80 UV/Vis spectrophotometer interfaced to an Apple II computer. The wavelength was set to correspond to the λ_{max} for the particular dinucleotide used in the assay. Stock enzyme solutions were prepared in 50 mM Pipes buffer, pH 7.2. All reactant concentrations were determined using enzymatic end point assays as described by Cook et al. (1980). Reactions were conducted in 50 mM Hepes buffer, pH 8.0. Semicarbazide (10 mM) was included in those yeast alcohol dehydrogenase assays where acetaldehyde was being formed. The stock semicarbazide solution was adjusted to pH 8 with

KOH before use. The enzyme concentration used in the assay was adjusted to give rates of 0.01 to 0.1 OD/min at the λ_{max} of the reduced coenzyme. Initial rates were measured by linear regression. Kinetic parameters were measured by nonlinear regression using the programs of Cleland (1979). (See the Appendix for a description of the regression algorithm). Ethanol and acetaldehyde were used as substrates for yeast alcohol dehydrogenase at saturating concentrations of 75 mM and 250 mM, respectively. For studies with horse liver alcohol dehydrogenase (in the direction of oxidation of the reduced dinucleotide), saturating concentrations of propanal could not be reached without substantial substrate inhibition. The concentrations of propanal as well as the dinucleotide were therefore varied and the observed kinetic parameters ($^{app}K_M$ and $^{app}V_{max}$) were extrapolated up to saturating levels of both dinucleotide and aldehyde (Cleland, 1977).

NMR Spectroscopy:

Proton nuclear magnetic resonance spectra were acquired at 500 MHz on a General Electric GN-500 instrument interfaced to a Nicolet 1280 computer and at 360 MHz on a Bruker HXS-360 NMR spectrometer equipped with a Nicolet Technologies 1180 computer/Fourier transform system. Samples at 500 MHz were 1 mM in coenzyme and were prepared in 25 mM phosphate buffer, pD 7.8, with 50 μM EGTA to suppress paramagnetic broadening. Samples were lyophilized twice from 99.8% D_2O and then dissolved in 100.0% D_2O. The probe temperature was maintained at 20° C, unless otherwise noted, and 5 mm NMR tubes were used. Typically, 256 scans were acquired with a spectral width of ±3000 Hz, using 16K data points, for 500 MHz spectra and ±1805 Hz, using 16K data points, for 360 MHz spectra. The pulse width was set to correspond to a 45° tip angle and a 0.5 s post acquisition delay was used to

allow for relaxation. For measurement of the sugar coupling constants, the free induction decay was apodized with a double exponential to enhance resolution. Chemical shifts were measured relative to internal 3-(trimethylsilyl)propionic-[$2,2,3,3$-$^2H_4$] acid (TSP). Partially relaxed spectra were obtained using a (180°-τ-90°-acquisition)$_n$ pulse sequence. The delay τ was set to null the desired resonances (methines or methylenes).

^{31}P NMR spectra were acquired at 97.3 MHz on a homebuilt spectrometer interfaced to a Nicolet 1180 computer. The concentration of the analog was 1 mM and was prepared in 25 mM Hepes buffer, pH 7.8, containing 50 μM EGTA and 10% D_2O to provide a lock signal. The sample temperature was 25° C and 5 mm NMR tubes were used. A total of 512 acquisitions were obtained with a spectral width of ±2000 Hz using 16K data points. Broadband proton decoupling (180° square wave modulation) was applied during acquisition (~4 W). The free induction decay was apodized with a single exponential resulting in a line broadening of 1.0 Hz. Chemical shifts were measured relative to external 85% phosphoric acid.

RESULTS

Physical Properties.

Ultraviolet Spectral Properties: The UV absorption spectrum and redox properties of the dihydronicotinamide nucleotides are listed in Table II.1. The λ_{max} of the dihydronicotinamide chromophore is 338 nm in α-araNADH and 346 nm in β-araNADH. As can be seen in Table II.1, this pattern is opposite to that observed for the ribo coenzymes where for α-NADH the λ_{max} is 346 nm and for β-NADH it is 338 nm. The extinction coefficients of the dihydronicotinamide moiety are within 3% those of the corresponding ribonucleotides based on the ratio of $A_{340}:A_{259}$.

Table II.1. Physical Properties of Ribo- and Arabino-Coenzymes.

	λ_{max}	Redox Potential (mV)[a]
β-NADH	338	-320[b]
α-NADH	346	-340[c]
β-araNADH	346	-339
α-araNADH	338	-319

[a]Values from (Burton and Wilson, 1953; Rodkey 1955).

[b]Values from (Kaplan, 1960).

[c]Redox potentials were determined at 25° C.

Redox Potential: The redox potentials for α-araNAD+ and β-araNAD+ have been measured using yeast ADH and the ethanol/acetaldehyde couple (Kaplan

et al., 1956). The values of the redox potential obtained under standard conditions are listed in Table II.1 along with the literature values for α-NAD+ (Kaplan, 1960) and β-NAD+ (Burton and Wilson, 1953; Rodkey 1955). The redox potentials for the corresponding α- and β-anomers of the ribo- and arabino-analogs show an interesting correlation. The value for β-riboNAD+ corresponds to that of α-araNAD+, whereas α-riboNAD+ has the same potential as β-araNAD+.

Anomeric Stability. A unique feature of the dihydronicotinamide-ribonucleotides is the configurational instability of the dihydronicotinamide-ribosyl linkage (Woenckhaus and Zumpe, 1965; Oppenheimer et al., 1971). The linkage in NADH anomerizes at measurable rates under physiological conditions (Oppenheimer and Kaplan, 1975), and the reaction can be observed directly by UV spectroscopy (Oppenheimer, 1986a). We find that the dihydronicotinamide arabino nucleotides also anomerizes under similar conditions. Both the ribo- and arabino-coenzymes undergo acid-catalyzed anomerization. For araNADH at 90° C, a 5:1 ratio of α- to β-anomers, i.e., trans to cis configurations of the base and the 2' hydroxyl, is observed (see Figure II.7b). At 22° C the ratio of α:β is 7.5:1, similar to that for NADH (Oppenheimer, 1982). Note that in contrast to riboNADH, where the β-anomer predominates, the α-anomer is favored for araNADH.

NMR Spectral Parameters.

Assignments. The α- and β-anomers of araNAD+ give well resolved ^{1}H NMR spectra at 500 MHz as shown in Figure II.5. The assignments of the proton resonances have been made by comparison with the resonances of
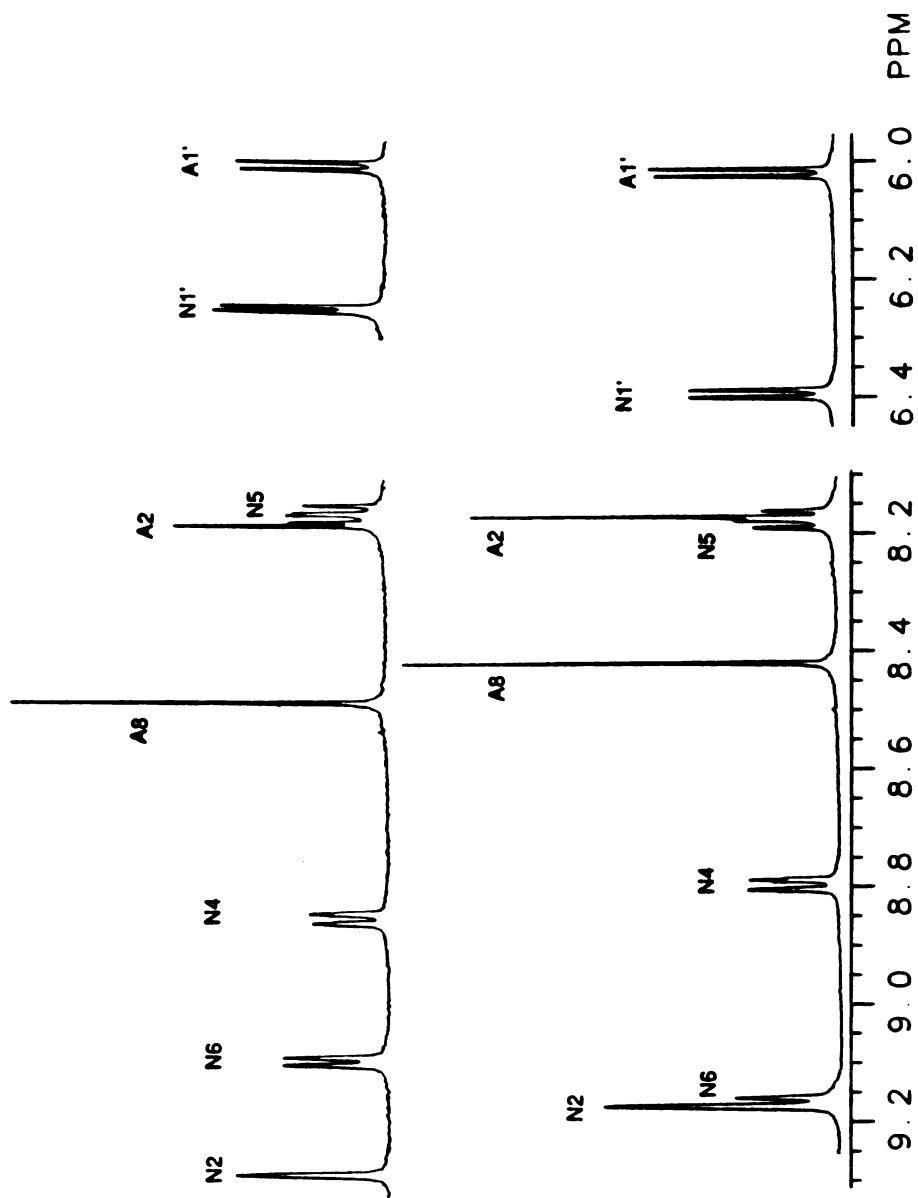
Figure II.5. Comparison of the downfield region of the 500 MHz 1H NMR spectra of 1 mM α–araNAD+ (top) and β–araNAD+ (bottom) obtained at 20° C, pD = 7.8

83

α-araNADH

Pro-S   Pro-R

2.85   2.80   2.75   2.70

β-araNADH

Pro-R   Pro-S

2.90   2.85   2.80   2.75   2.70

PPM
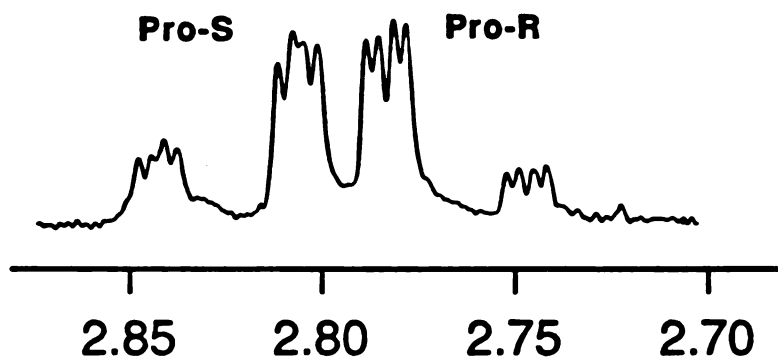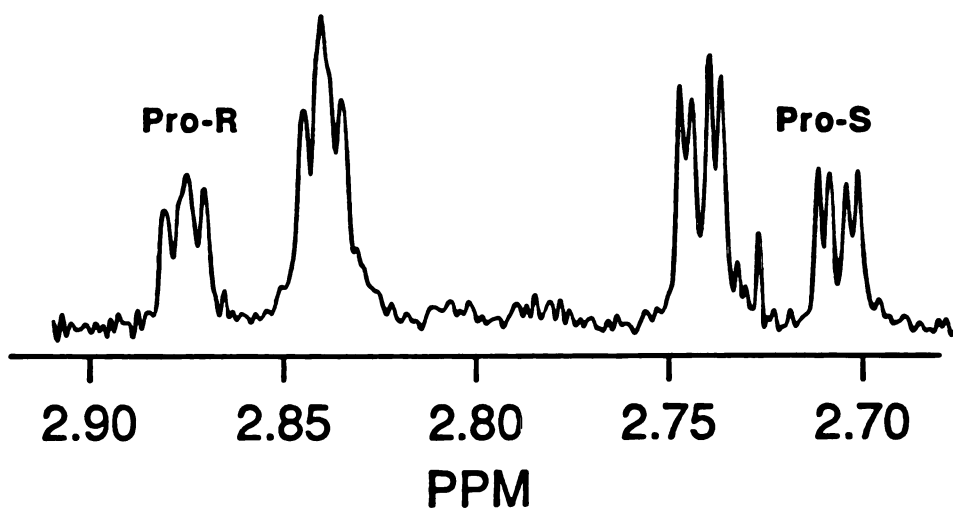
Figure II.6.   Comparison of the N4 methylene proton resonances in the 500 MHz ^{1}H NMR spectra of α- and β-araNADH obtained at 20° C. The absolute assignments of the protons are based on enzymatic deuterium labeling experiments

riboNAD+ and riboNADH (Oppenheimer, 1982) and confirmed, where necessary, by spin decoupling experiments. The stereochemical assignments of the N4 protons have been made by enzymatic deuterium labeling. The chemical shifts and coupling constants for the dihydronicotinamide protons are listed in Table II.2. Table II.3 lists the chemical shifts and coupling constantsfor the ribose and arabinose protons. The values of the chemical shifts and coupling constants have been refined by computer simulation using the program GEMSIM.

Chemical Shift Nonequivalence of the N4 Methylene Proton Resonances. The nonequivalence of the resonances for the N4 methylene protons is one of the most striking features of ^{1}H-NMR spectra of ribo-NAD(P)H (for a review see Oppenheimer, 1982). The N4 methylene protons of the α- and β-anomers of araNADH are also nonequivalent as can be seen in the spectra obtained at 20° C shown in Figure II.6. The values of the chemical shifts and the coupling constants for the dihydronicotinamide protons are listed in Table II.2. The individual N4 resonances in α- and β-araNADH have been assigned by the following method. A specific deuterium label has been incorporated using the pro-R specific enzyme, yeast ADH, and [U-^{2}H$_5$]-ethanol in analogy to the procedure outlined by Oppenheimer et al. (1971). A portion of the ^{1}H-NMR spectra of the resulting labeled analogs is shown in Figure II.7. Note that for β-araNADH, it is the downfield proton resonance that is eliminated by deuteration, whereas in the spectrum of labeled α-araNADH the upfield proton resonance is eliminated. Therefore the relative chemical shifts of the N4 protons for the α- and β-araNADH are opposite.

The stereochemistry of oxidation of α-NADH by yeast ADH has been shown to be identical to that for β-NADH through use of the anomerization

85

Table II.2. Chemical Shifts[a] and Coupling Constants[b] of the Base Protons

Chemical Shifts

	N2	N6	N4	N5	A8	A2	A1'
α-araNAD+	9.282	9.082	8.847	8.159	8.467	8.173	5.995
β-araNAD+	9.175	9.166	8.805	8.184	8.416	8.169	6.016

	N2	N6	N5	N4$_R$	N4$_S$	$\Delta\delta_{R,S}$[c]
β-araNADH	6.824	5.900	4.724	2.843	2.713	0.130
α-araNADH	6.877	5.913	4.801	2.749	2.793	-0.044

Coupling Constants

	$^3J_{5-6}$	$^3J_{4-5}$	$^4J_{4-2}$	$^4J_{4-6}$	$^4J_{6-2}$
β-araNAD+	6.2	8.2	1.5	1.5	<1.0
α-araNAD+	6.3	8.0	1.5	1.5	<1.0

	$^3J_{5-6}$	$^3J_{4R-5}$	$^3J_{4S-5}$	$^4J_{4-6}$	$^4J_{6-2}$	$^2J_{4-4}$
β-araNADH	8.2	3.1	3.8	1.4	1.6	-19.2
α-araNADH	7.2	3.6	3.3	2.2	1.6	-18.9

[a]Chemical shifts are reported in ppm from internal TSP and were obtained at 500 MHz at 20° C for 1 mM solutions.

[b]Coupling constants are in Hz and are reported to the nearest 0.1 Hz.

[c]$\Delta\delta_{R,S}$ is the chemical shift nonequivalence in ppm of the pro-R and pro-S N4 methylene protons.

Table II.3. Chemical Shifts[a] and Coupling Constants[b] for the Sugar Protons

Chemical Shifts[c]

		C1'	C2'	C3'	C4'	C5'	C5"
β-araNAD⁺	N	6.393	4.765	4.192	4.478	4.258	4.313
	A	6.016	4.739	4.507	4.385	4.313	4.253
β-araNADH	N	5.006	4.261	4.059	3.756	4.238	4.108
	A	6.135	4.676	4.520	4.385	4.277	4.248
α-araNAD⁺	N	6.237	4.382	4.424	4.714	4.308	4.227
	A	5.995	4.714	4.529	4.418	4.276	4.276
α-araNADH	N	4.699	4.092	4.172	4.092	4.156	4.040
	A	6.121	4.671	4.509	4.390	4.272	4.263

Coupling Constants

		1'-2'	2'-3'	3'-4'	4'-5'	4'-5"	5'-5"	5'-P	5"-P
β-araNAD⁺	N	6.1	7.8	7.8	2.5	2.5	-11.8	(5.5)	(5.5)
	A	6.1	5.4	3.3	2.5	2.5	-10.2	(5.5)	(5.5)
β-araNADH	N	6.6	7.0	8.1	2.9	2.8	-11.6	3.9	5.8
	A	5.2	5.2	4.0	3.3	3.0	-11.6	4.0	5.0
α-araNAD⁺	N	4.2	5.5	5.6	3.1	5.7	-11.8	5.4	5.7
	A	6.2	5.1	3.2	3.8	3.8	-[d]	3.8	3.8
α-araNADH	N	7.4	8.0	8.5	2.1	5.2	-11.2	4.8	5.2
	A	5.3	5.0	4.1	2.9	3.0	-11.1	4.7	5.7

[a]Chemical shifts are reported in ppm from internal TSP and were obtained at 500 MHz at 20° C for 1 mM solutions.

[b]The coupling constants are in Hz and are reported to the nearest 0.1 Hz. Coupling constants for which only the mean value can be determined because of the fortuitous chemical shift equivalence of the N5' methylene protons or the pyrophosphate ^{31}P resonances are enclosed in parentheses.

[c]The nicotinamide arabinose protons are labeled N and the adenine ribose protons are labeled A.

[d]The adenine ribose C5' and C5" protons of α-araNAD⁺ are chemical shift equivalent and their mutual coupling constant is not observed.
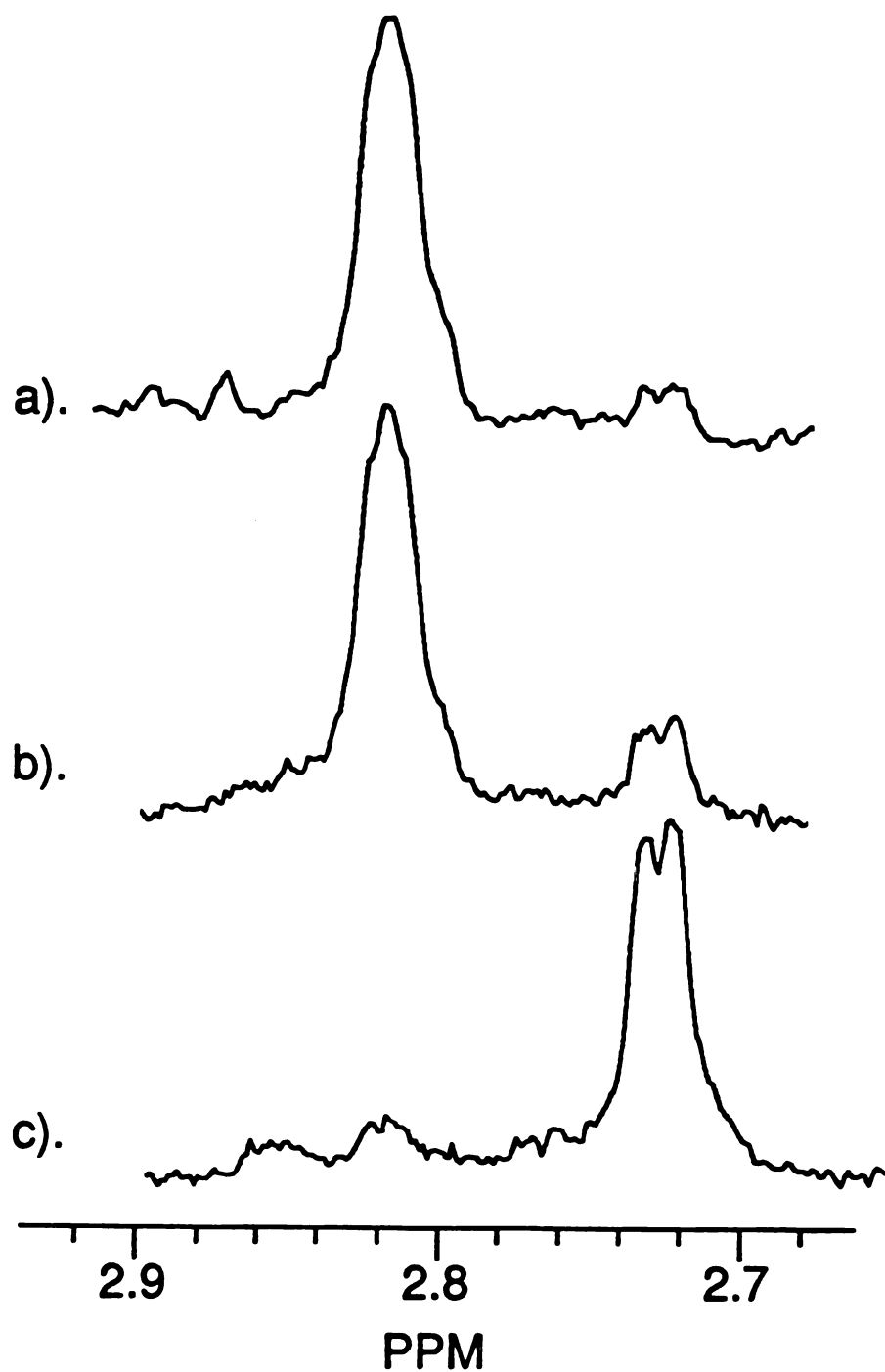
Figure II.7. Comparison of the N4 proton resonances in the 360 MHz 1H NMR spectrum of specifically labeled araNADH generated by yeast ADH reduction (a pro-R specific dehydrogenase) with [U-2H] ethanol. Spectrum a is the pro-S proton of α-[R-N4-2H]-araNADH, spectrum c is the pro-S proton of β-[R-N4-2H]-araNADH and spectrum b was obtained after incubating the sample of β-[R-N4-2H]-araNADH (shown in spectrum c) for five minutes at 90° C. Under these conditions the sample anomerizes to an equilibrium mixture of 5:1 α:β anomers (the S-proton for β-[R-N4-2H]araNADH can be seen as the upfield doublet). The coincidence of the chemical shifts and coupling constants in spectra b and a confirm that yeast ADH reduces both the α- and β-anomers with the identical stereochemistry.

88

reaction (Oppenheimer and Kaplan, 1975). The stereochemistry of the yeast ADH-catalyzed redox reactions with either the α- or β-anomers of araNAD+ can be established in a similar manner. Starting with the specific label at N4 for β-araNADH, anomerization interconverts the asymmetric center at the 1' carbon without any alteration in the stereochemistry at the N4 position. As shown in Figure II.7, incubation of an anaerobic sample of stereospecifically labeled β-[(R)^{2}H-N4]-araNADH at 90° C for five minutes affords the equilibrium mixture containing 5:1 α- to β-anomers of araNADH. The resulting ^{1}H-NMR spectrum of the labeled α-araNADH generated by anomerization of R-labeled β-araNADH is identical to the ^{1}H-NMR spectrum of the labeled α-araNADH obtained from the direct reduction of α-araNAD+. This result conclusively establishes that the stereospecificity of enzymatic reduction by yeast ADH is identical for both the α- and β-anomers of araNAD+. Therefore we can make the absolute stereochemical assignment of the methylene protons (see Figure II.7 and Table II.2). Note that by establishing the stereochemistry of yeast ADH we can generate specifically labeled arabino coenzymes and thus determine the stereochemistry of reduction of araNAD+ in reactions catalyzed by other dehydrogenases in analogy to the methodology for riboNAD+ (You et al. 1978).

Analysis of the ^{1}H NMR Spectra of the Sugar Protons: A portion of the ^{1}H NMR spectrum containing the sugar resonances of β-araNAD+ is shown in Figure II.8. The ^{1}H resonances of the arabinose protons for both α- and β-anomers of araNAD+ and araNADH have been assigned by homonuclear spin decoupling experiments and partially relaxed ^{1}H NMR spectra (Figure II.8). The chemical shifts and coupling constants are listed in Tables II.3. In general the chemical shift properties are similar to the corresponding protons in the ribo coenzymes, e.g., the N1' proton is shifted 1.387 ppm upfield upon reduction of
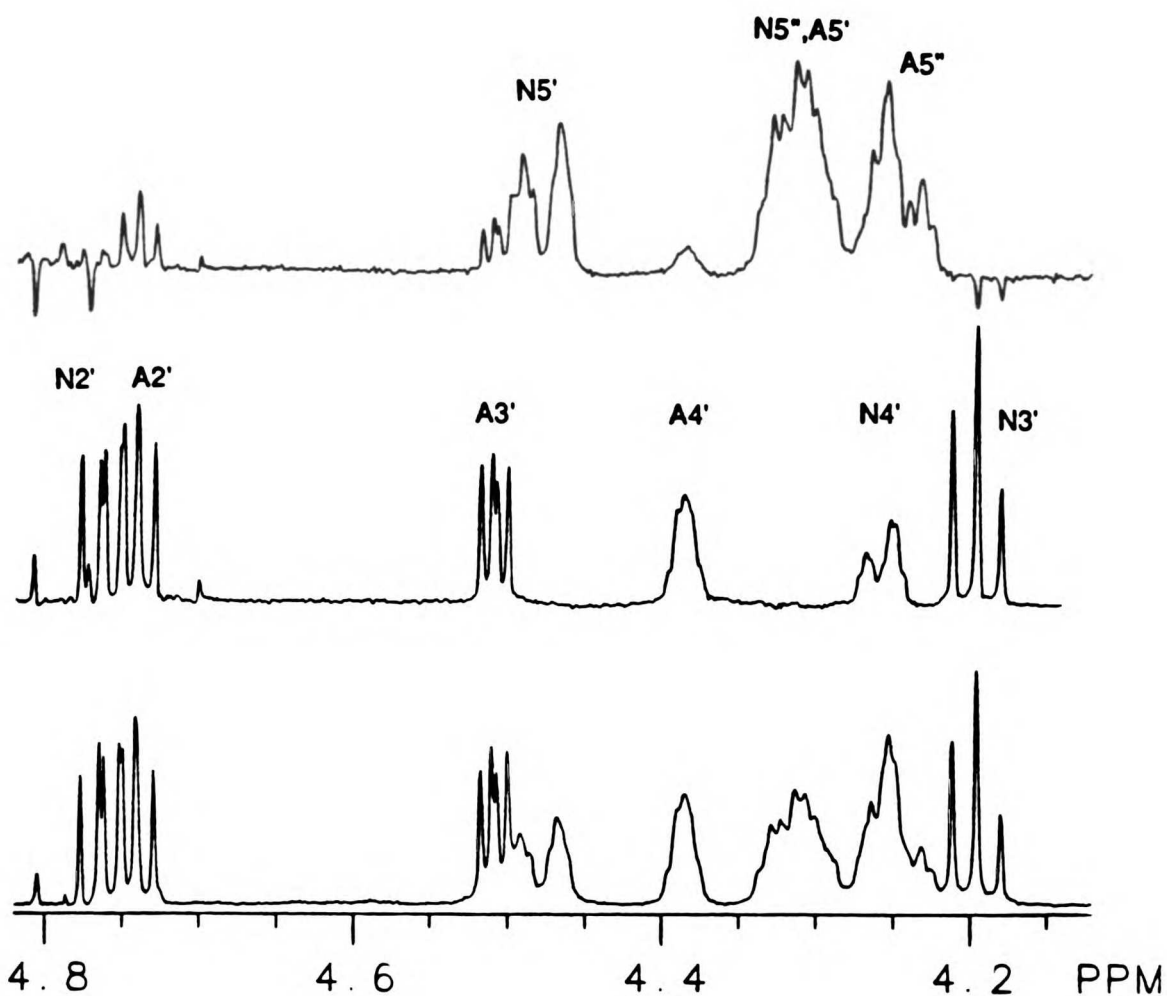
Figure II.8. A portion of the resolution enhanced 500 MHz ^{1}H NMR spectra of the sugar region of 1 mM β-araNAD+ obtained in D_2O at 20° C (bottom). The top spectrum is a partially relaxed FT spectrum in which the methine resonances have been nulled (τ = 1.00 s) and the middle spectrum is a partially relaxed FT spectrum in which the methylene resonances have been nulled (τ = 0.35 s).

90

the β-arabino coenzyme and 1.300 ppm for the β-ribo coenzyme (Oppenheimer, 1982). The spectral properties for the proton resonances of the adenosine moiety show negligible differences from the corresponding resonances in the ribo-coenzymes.

^{31}P NMR of the Pyrophosphate Backbone: The ^{31}P NMR spectra of the anomers of araNAD+ and araNADH have been obtained at 97.3 MHz and the spectra for the β-anomers are shown in Figure II.9. Note that the pyrophosphate resonances of β-araNAD+ appear as a singlet. The nonequivalence of the two phosphorus resonances has been calculated to be less than 0.004 ppm based on computer simulation of the ^{31}P NMR spectrum and the ^1H NMR spectrum of the sugar proton resonances. In contrast the ^{31}P chemical shifts for the pyrophosphate backbone of β-araNADH differ by 0.16 ppm. The ^{31}P resonances in the α-anomers are nonequivalent for both oxidized and reduced forms (Figure II.9). The ^{31}P chemical shifts for all four arabino analogs are listed in Table II.4.

Enzyme Properties: The α- and β-arabino analogs have been investigated as coenzymes with yeast and horse liver alcohol dehydrogenases and have been found to follow Michaelis Menten kinetics (Figures II.11-12). The kinetic parameters for araNAD+/NADH with yeast alcohol dehydrogenase are listed in Table II.6. The relative V_{max} for coenzyme oxidation of β-araNADH is 35% that of β-NADH whereas the relative V_{max} for reduction of β-araNAD+ is only 3% that for β-NAD+. As might be expected, the α-anomers are poorer coenzymes. The V_{max} for oxidation of α-araNADH is only 0.1% the rate for β-NADH and reduction of α-araNAD+ is only 0.07% the rate for β-NAD+. The results

Table II.4. ^{31}P Chemical Shifts of NAD+ and Related Nucleotides.[a]

Nucleotide	δ_1	δ_2	$\Delta\delta_{NA}$
β-araNADH	-11.72	-11.88	0.16
β-araNAD+	-11.80	-11.80	<0.004[b]
α-araNADH	-11.62	-11.89	0.27
α-araNAD+	-11.98	-12.14	0.16

---

[a]Spectra were obtained at 97.3 MHz and are reported in ppm from external 85% phosphoric acid. Specific assignments of the individual phosphorus resonances have not been made and $\Delta\delta_{NA}$ is the difference in chemical shift of the two phosphorus resonances.

[b]Maximum nonequivalence for the pyrophosphate resonances as calculated from the second order effects observed on the ^{1}H NMR spectrum at 500 MHz.
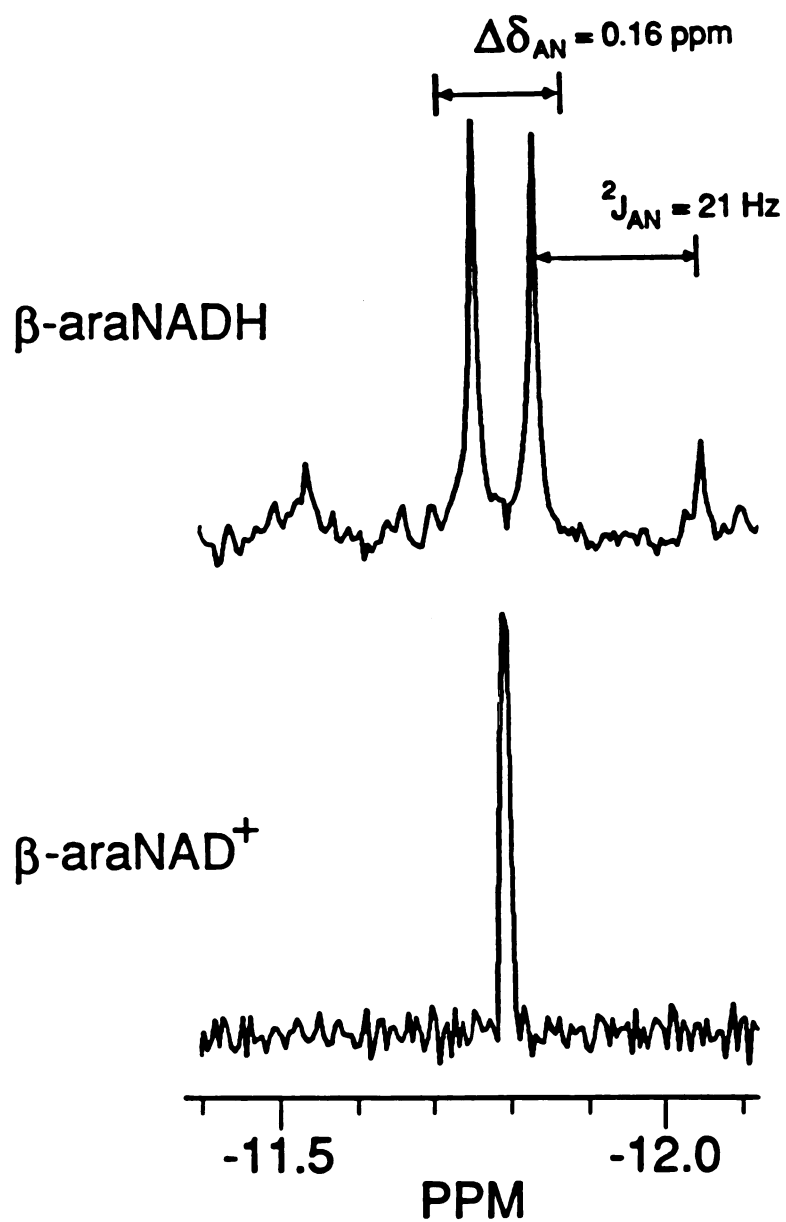
Figure II.9. The 200 MHz ^{31}P NMR spectra of 1 mM β-araNAD+ and β-araNADH obtained at 25° C, pH = 7.8. The chemical shifts are referenced to external 85% phosphoric acid.
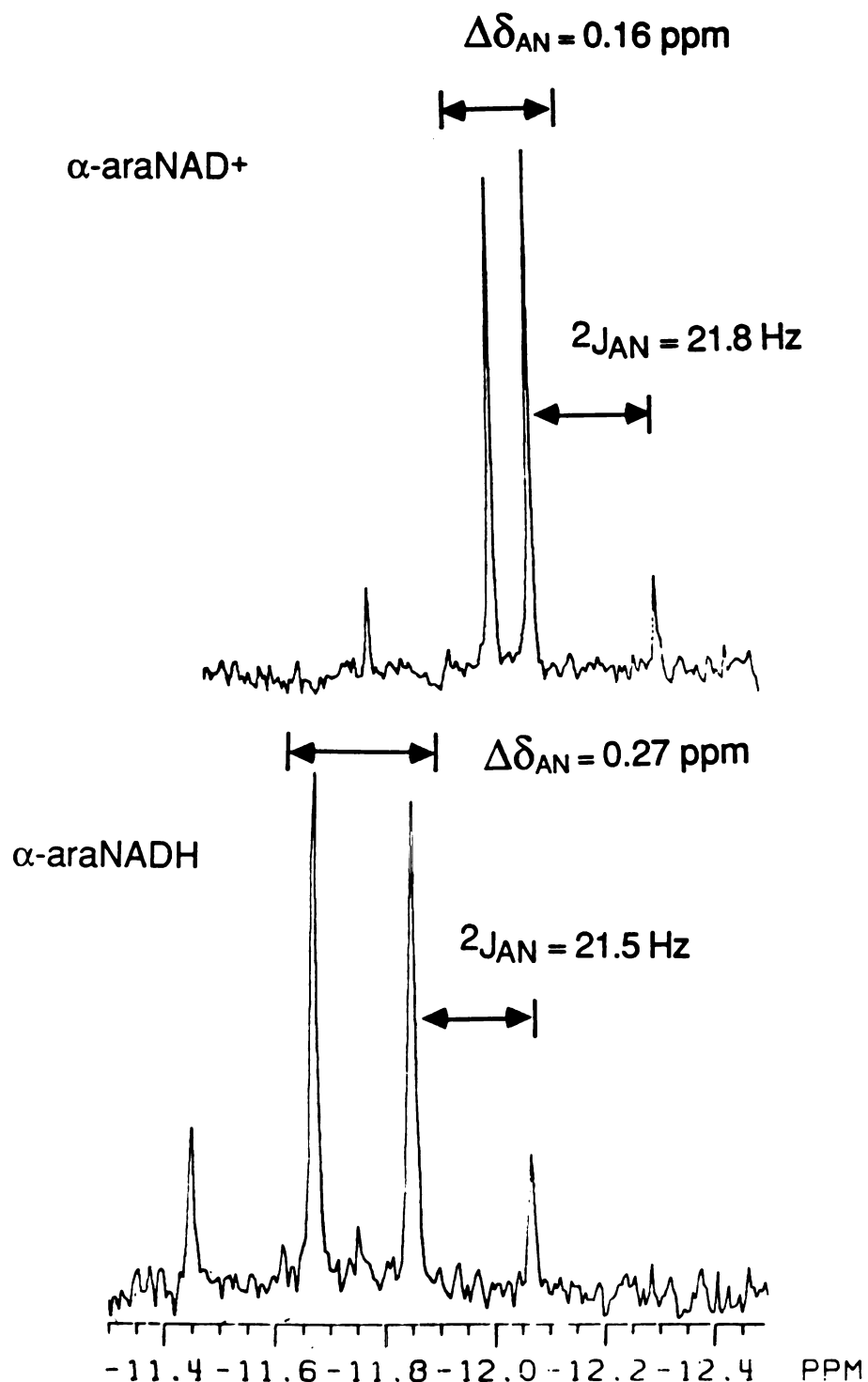
Figure II.10. The 200 MHz ^{31}P NMR spectra of 1 mM α-araNAD+ and α-araNADH obtained at 25° C, pH = 7.8. The chemical shifts are referenced to external 85% phosphoric acid.

94
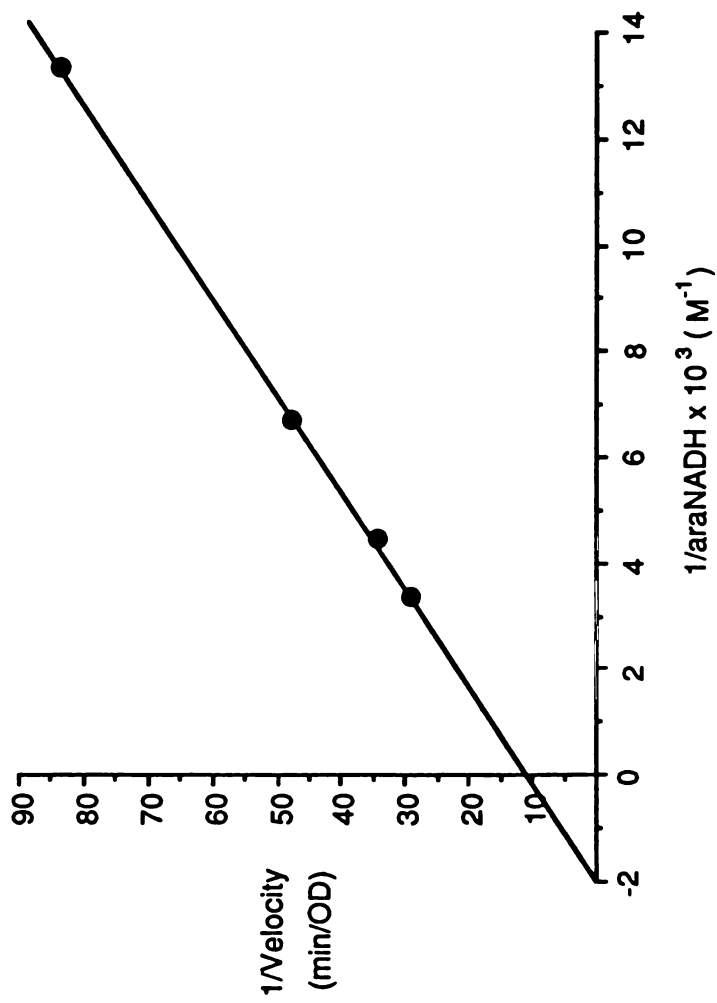
Figure II.11. Lineweaver-Burke plot for β-araNADH using ethanol and yeast alcohol dehydrogenase, pH 8.0.
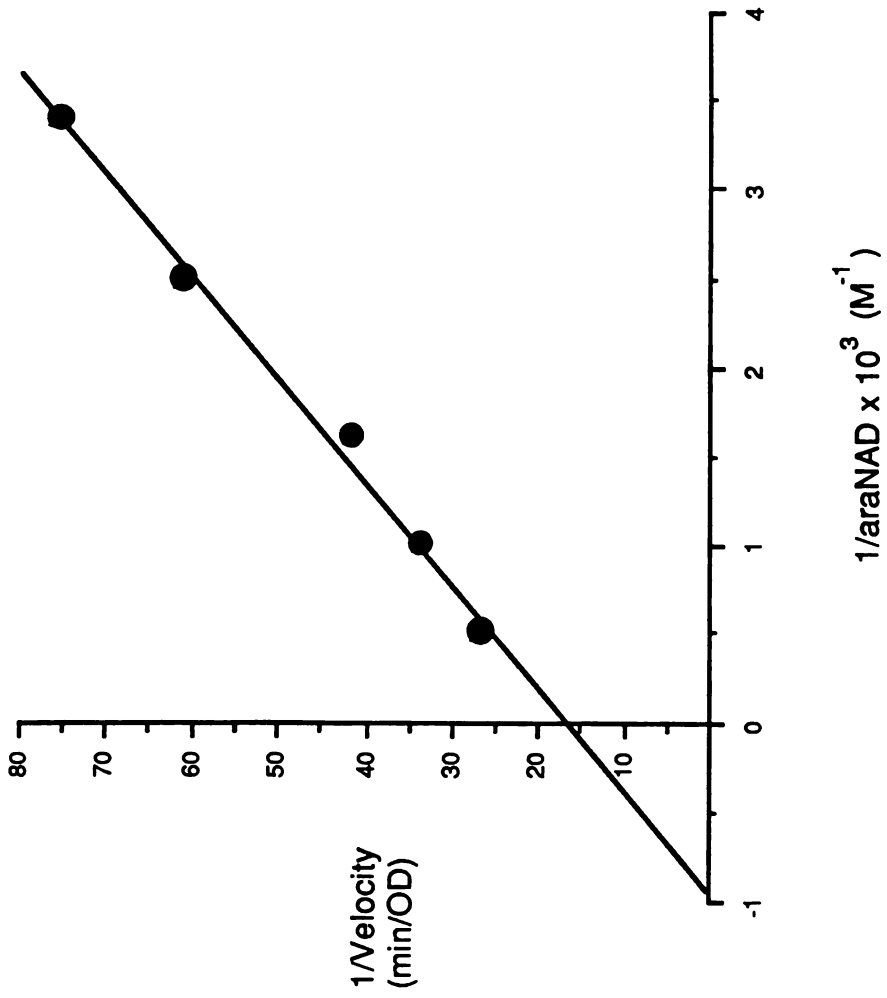
Figure II.12. Lineweaver-Burke plot for α-araNAD+ using n-propanol and horse liver alcohol dehydrogenase, pH 8.0.

demonstrate that under the assay conditions yeast ADH is better at catalyzing the oxidation of the coenzyme analogs than their reduction. Finally yeast ADH discriminates between the α- and β-anomers by a factor of 350 for coenzyme oxidation and 43 for coenzyme reduction.

Primary kinetic isotope effects for coenzyme reduction have been measured and the values listed in Table II.5. Yeast ADH already shows a primary isotope effect of V_{max} of 1.6 for the reduction of β-NAD+, indicating that hydride transfer is partially rate limiting. Reduction of the α- and β-anomers of araNAD+ shows kinetic isotope effects of 5.3 and 5.4, respectively. Therefore hydride transfer has become substantially more rate limiting for the analogs.

Table II.5. Primary Kinetic Isotope Effects for Yeast Alcohol Dehydrogenase[a]

	$^D V_{max}$
β-NAD+	1.6 ± 0.2
β-araNAD+	5.4 ± 0.7
α-araNAD+	5.3 ± 1.2

[a]Assays conducted at 30° C at pH 8.0 in 50 mM Hepes buffer using saturating [U-^{2}H$_5$]-Ethanol (0.1 M).

Enzymatic kinetic parameters have also been measured for horse liver alcohol dehydrogenase and the values for coenzyme oxidation are listed in Table II.6. The results are most dramatic. The relative V_{max} for both α- and β-araNADH with horse liver ADH are greater than for the natural coenzyme β-NADH. The V_{max} for β-araNADH oxidation is six times faster than for β-NADH and the V_{max} for α-araNADH oxidation is 1.7 times faster. The increase in V_{max} with β-araNADH is accompanied by a five fold decrease in the K_m relative to that for β-NADH, giving a V/K value for β-araNADH 20% greater than for β-NADH. The twenty fold decrease in K_m of α-araNADH still leads to a V/K value

that is 10% that for β-NADH.

Table II.6. Kinetic Parameters for Yeast Alcohol Dehydrogenase[a]

	V_{max}(rel)	K_M(mM)	V/K (mM^{-1})
β-NAD+	1.0	0.13	7.7
β-araNAD+	0.03	0.66	0.05
α-araNAD+	7.0×10^{-4}	1.05	6.7×10^{-4}
	V_{max}(rel)	K_M(mM)	V/K (mM^{-1})
β-NADH	1.0	0.18	5.5
β-araNADH	0.35	0.50	0.7
α-araNADH	0.001	0.34	2.9×10^{-3}

Kinetic Parameters for Horse Liver Alcohol Dehydrogenase[b]

	V_{max}(rel)	K_M(μM)	V/K (μM^{-1})
β-NADH	1.0	3.0	0.33
β-araNADH	6.1	15.0	0.41
α-araNADH	1.7	59.0	0.03

[a]Assays conducted at 30° C at pH 8.0 in 50 mM Hepes buffer using saturating ethanol or acetaldehyde (0.1M).

[b]Assays conducted at 30° C at pH 8.0 in 50 mM Hepes buffer using saturating n-propanol (0.1 M).

DISCUSSION

Physical Properties. The differences in the λ_{max} and redox potential listed in Table II.1 for the α- and β-forms of the ribo- and arabino-coenzymes are most striking. These results establish the sensitivity of the physical chemical properties of the dihydronicotinamide ring to alterations in the sugar moiety. We see that the redox potential and λ_{max} for the arabino- and ribo-coenzymes are correlated with the orientation of the 2' hydroxyl and not with the anomeric configuration of the glycosyl linkage. In dinucleotides where the 2' hydroxyl is trans to the base (both β-NAD$^+$ and α-araNAD$^+$), the redox potentials are comparable, -320 mV and -319 mV, respectively. In contrast, dinucleotides where the 2' hydroxyl is cis to the base (α-NAD$^+$ and β-araNAD$^+$) are stronger reductants with redox potentials of -340 mV and -339 mV, respectively. These effects can be explained by a combination of two factors: (i) destabilization of the electron-rich dihydronicotinamide ring through its juxtaposition with the 2'-hydroxyl and (ii) stabilization of the cationic nicotinamide moiety by the electron-rich 2'-hydroxyl. The results we observe for the ribose and arabinose nucleotides are in general accord with previous studies by Hajdu and Sigman (1977). In their investigations of neighboring group effects on the redox properties of model dihydronicotinamides, they found that the reactivity of the model compounds was best explained by stabilization of the cationic form. For the nicotinamide nucleotides, however, further experiments will be needed in order to determine the individual contributions from these two possibilities.

The K_{eq} for anomerization of dihydronicotinamide nucleotides also shows a correlation with the configuration at C2'. The observed anomeric preferences are consistent with our previous suggestion that steric hindrance and electrostatic interactions between the cis substituents on sugar carbons 1'

99

and 2' are the prime determinants of the preferred anomeric configuration (Oppenheimer and Kaplan, 1975). In the cis configuration the bulky, electron rich dihydronicotinamide ring is juxtaposed with the 2' hydroxyl. This configuration should be sterically crowded and thus disfavored relative to the less hindered trans orientation. The similarity of the ratio of the respective cis and trans anomers in the ribo- and arabino-analogs indicates a negligible influence on anomeric equilibria due to stereoelectronic effects between the furanose ring oxygen lone pairs and the C1' substituents.

Conformation of the Dihydronicotinamide Ring. The ^{1}H-NMR spectra of the N4 methylene protons in ribo-NAD(P)H have a number of important properties that are consistent with a specific puckering of the dihydronicotinamide ring in the dinucleotide when it is folded against the adenine moiety. The properties include chemical shift nonequivalence of the methylene protons and the dependence of this chemical shift nonequivalence on concentration, temperature and solvent. Differences in the values of the vicinal coupling constants for the N5 and N4 protons of the dihydronicotinamide ring also are consistent with a puckered geometry (Oppenheimer et al., 1971; 1978; Oppenheimer, 1982; 1986a).

The resonances of the dihydronicotinamide ring in araNADH also show large temperature and solvent-dependent chemical shifts (data not shown) that are similar to those of riboNADH (Oppenheimer et al., 1978). These results indicate that there are significant contributions from conformations in which the adenine and dihydronicotinamide moieties are base stacked in the arabino analogs. Important and sensitive indicators of the conformation of the dihydro-nicotinamide ring are the ^{1}H homonuclear coupling constants (see Table II.2). The values of the coupling constants of the dihydronicotinamide ring in β-

araNADH are similar to those obtained for the β-ribo-coenzyme (Oppenheimer et al., 1978). The coupling constant data, combined with the similar order of shielding of the N4 methylene protons of β-NADH and β-araNADH, argue strongly that both molecules adopt a similar folded form in solution as would be expected from the arguments given by Oppenheimer (1982, 1986a). The results are in accord with a single type of folded conformer being responsible for the preferential distortion of the dihydronicotinamide ring from planarity and such a form would be in fast exchange with an open, extended form. The similarity of the magnitude of the coupling constants also argues that the degree of distortion is comparable for both the β-ribo- and β-arabino-coenzymes.

The spectral properties of the dihydronicotinamide resonances for α-araNADH differ fundamentally. The chemical shifts of these resonances clearly indicate that there are major contributions from folded conformations to the solution structure of α-araNADH. Based on the coupling constansts listed in Table II.2, however, it is clear that the extent of preferential distortion of the dihydronicotinamide ring is smaller. The near equivalence of the $^3J_{4R-5}$ and $^3J_{4S-5}$ coupling constants indicates that the ring has a more nearly time-averaged planar conformation. These results, combined with the opposite order of the chemical shifts for the N4 protons of α-araNADH (the pro-S proton is downfield and the pro-R proton is upfield), suggest that there are major contributions from multiple folded forms. Furthermore, these interactions involve both faces of the dihydronicotinamide ring and may involve significantly different relative positioning of the two rings.

Sugar Conformation of Arabino Analogs of Pyridine Nucleotides   The sugar moieties of the α- and β-anomers of the ribonucleotides show distinct redox state-dependent conformational changes (Oppenheimer and Kaplan, 1976). In

101

the β-ribotide there is an intramolecular electrostatic attraction between the cationic nicotinamide moiety and the anionic 5' phosphate. In the α-ribotide the electrostatic interaction is between the base and the cis 2'-hydroxyl. Because of the altered stereochemistry of the 2' hydroxyl, the arabinotides provide an important system to investigate the relative contribution from these interactions in determining sugar conformations.

The value of $J_{3'-4'}$ alone can be used to obtain a qualitative estimate of the population distribution for both ribo- and arabinonucleotides. As discussed by Ekiel et al. (1979) and de Leeuw and Altona (1982), the value of $^3J_{3'-4'}$ should be equally sensitive to the population of sugar conformers for either ribo- or arabinonucleotides. For example, values of $^3J_{3'-4'}$ that are less than 3 Hz indicate a predominance of the an S type conformer (2'-endo) whereas values greater than 7 Hz reflect a predominance of the N type conformer (3'-endo). As shown in Table II.3 the value of $J_{3'-4'}$ (7.8 Hz) for the β-anomer of araNAD+ undergoes little change upon reduction to β-araNADH where the corresponding value is 8.1 Hz. Larger changes are observed in the values of $J_{3'-4'}$ in α-araNAD+ and α-araNADH, which are 5.6 Hz and 8.5 Hz, respectively. In all cases we see a predominance of the N-type conformers for the nicotinamide arabinonucleotides (Figure II.13) in contrast to the ribonucleotides which favor the S-type conformers (Altona and Sundaralingam,1973).

The favoring of the N-type conformer in the arabinotides is consistent with maintenance of a trans geometry for the 2' and 3' diol hydroxyls. Yet unlike the corresponding ribotides there are no simple redox-dependent conformational changes. This result is significant because in the β-arabinotides the base is cis to the 5' hydroxymethyl group, as found in the β-ribotides, as well as cis to the 2'-hydroxyl, as found in the α-ribotides, i.e., both cases where redox-dependent conformational changes are observed in the ribotides. The

reasons for these distinct differences between ribo and arabino nicotinamide nucleotides remain to be investigated.

2'-endo

S-type conformer

3'-endo
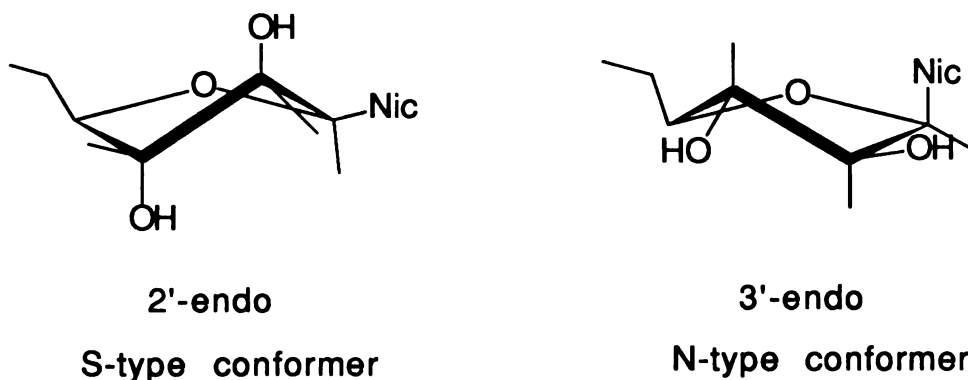
N-type conformer

Figure II.13. Conformations of the arabinose ring of β-araNAD+ and β-araNADH. The N-type conformer predominates in solution over the S-type conformer.

Conformation of the Pyrophosphate Backbone The chemical shifts of ^{31}P resonances are especially sensitive to two factors, electrostatic interactions and the conformation of vicinal substituents. The ^{31}P NMR spectrum of the ribo-coenzymes have been reported (Blumenstein and Raftery 1972; Sarma and Mynott, 1972) and their results demonstrate that the two ^{31}P resonances of the pyrophosphate of NAD+ are well resolved at 87 MHz. The spectrum of β-NAD+ appears as an AB pattern with a chemical shift difference of 0.29 ppm and a geminal coupling constant of -20 Hz. This coupling constant is typical of the [31]P-^{31}P geminal coupling constants found in pyrophosphates (see Section III). In contrast the ^{31}P NMR spectrum of β-NADH appears as a single peak in which the individual resonances can not be resolved. The nonequivalence of the ^{31}P resonances in β-NAD+ but not β-NADH has led to the proposal that the difference in chemical shift of the pyrophosphate resonances is due to an

103

electrostatic interaction between the pyridinium cation and the anionic pyrophosphate backbone (Blumenstein and Raftery 1972). By this reasoning, in the reduced form the absence of the charged pyridinium would lead to similar chemical environments for the two ^{31}P resonances. That is, the adenine and dihydronicotinamide rings are considered to have equivalent electrostatic properties, thus they should impart similar chemical shift environments on the ^{31}P resonances. The electrostatic model, however, is not consistent with the results for the β-arabino analogs of NAD$^+$. As can be seen in Figure II.9, the pyrophosphate resonances of β-araNAD$^+$ are less than 0.004 ppm nonequivalent whereas in β-araNADH they differ by 0.15 ppm. Clearly then, the arabinotides, unlike the ribotides, show an opposite correlation between the charge of the heterocyclic ring and the chemical shift nonequivalence of the two phosphorus resonances. Therefore electrostatic interactions are not the sole factor defining the magnetic environment of the pyrophosphate backbone. This is also shown in the ^{31}P spectra of the α-arabinotides (Figure II.10) where a similar nonequivalence of the phosphate resonances (0.16 and 0.27 ppm) is observed. The nonequivalence of the phosphorus atoms in the positively charged α-araNAD$^+$ is even less than that observed for the reduced dinucleotide.

Model studies by Gorenstein (1984) have shown that the chemical shifts of ^{31}P nuclei are as sensitive to the conformation of substituents as they are to electrostatic effects such as protonation of the phosphate. Comparison of the values of $J_{4'-5'R}$ and $J_{4'-5'S}$ listed in Table II.2 to the previously published data for the ribo-coenzymes (Oppenheimer, 1982) indicate that the rotamer populations around the 4'-5' and 5'-O bonds are similar for both the ribo and arabino coenzymes. Therefore significant differences in rotamer populations alone cannot account for the contrasting behavior of the ^{31}P resonances of the

pyrophosphate backbone for the two sets of compounds.

The sensitivity of the ^{31}P chemical shift to conformational changes may mean that the observed patterns of chemical shifts are in response to subtle differences in the rotamer populations. Note that the values of $\Delta\delta_{NA}$ are less than 0.2 ppm whereas the range of conformational-dependent shifts can be as large as 3 ppm, suggesting that differences of less than 10% in the rotamer populations could account for the effects. Alternatively there may be differences in the correlation of the rotamers around the 4'-5' and 5'-O bond. As discussed by Oppenheimer and Kaplan (1976), the populations of the overall orientations can change in response to alterations of the the total interaction potential even in the absence of any significant changes in the values of the individual rotamer populations. Such changes in correlation could easily account for the attendant changes in the chemical shifts of the ^{31}P resonances without any changes in the values of the observed vicinal coupling constants.

Enzyme Activity. The ability of both β-araNAD+ and α-araNAD+ to serve as coenzymes for yeast and horse liver ADH demonstrates conclusively that specific interactions between the enzyme and the 2'-OH, or for that matter the entire sugar moiety, is not *essential* in an absolute sense for their ability to function as coenzymes. The activity of the α-anomer is all the more remarkable if one considers the large differences in the spatial arrangement of the substituents around the anomeric carbon and the generally acknowledged high degree of stereoselectivity shown in most enzyme-substrate interactions and their resulting chemical reactions. The magnitude of the differences between α- and β-anomers is apparent in Figure II.1. Here we see explicitly the dissimilar disposition of substituents for the α-anomer of araNAD+ relative to either β-araNAD+ or NAD+. Note two important distinctions between the binding of α-

105

and β-anomers. First, in the β-anomers the sugar hydroxyls are directed toward the surface of the protein and the less crowded furanose ring oxygen is seated toward the protein. Second, the 5' hydroxymethyl group and its attached pyrophosphate linkage is cis to the base. In the α-anomers these arrangements have to be altered drastically in order for the nicotinamide ring to be seated for proper stereochemical function. The hydroxyls now must be directed toward the protein and the 5' phosphate is trans to the nicotinamide ring. Therefore our results suggest that the active site is designed to *accommodate* the sugar moiety sterically rather than to *bind* it via specific interactions.

The observed activity of both the α- and β-anomers of the ribo and arabino pyridine coenzymes also has a direct bearing on recent proposals regarding the mechanism of dehydrogenases. Benner (1982) and coworkers (Nambiar et al., 1983) have proposed a correlation between the stereochemistry of enzyme-catalyzed hydride transfer and the external redox potential of the substrates for a group of alcohol dehydrogenases meeting certain stringent criteria. The theoretical rationale for their correlation is a proposed stereoelectronic effect involving a specific interaction of the lone pair on the N1 nitrogen of the dihydronicotinamide ring and the antibonding orbital, σ*, of the C1'-O bond. Since both α-riboNADH (Oppenheimer and Kaplan, 1975; Oppenheimer 1986b) and α-araNADH transfer hydride with the identical stereochemistry as β-riboNADH, then the seating of the dihydronicotinamide ring with respect to the substrate in the active site must be the same in all cases. Given the importance of the adenosine moiety for coenzyme binding it is also reasonable that the ADP group of these analogs binds in its usual site. An antiperiplanar orientation between the O'–C1' bond and the lone pair on the ring nitrogen is readily achieved in the β-anomer as shown in Figure II.14. However, an α-anomer cannot achieve an antiperiplanar geometry without a

106

β-Nucleotides **α-Nucleotides**
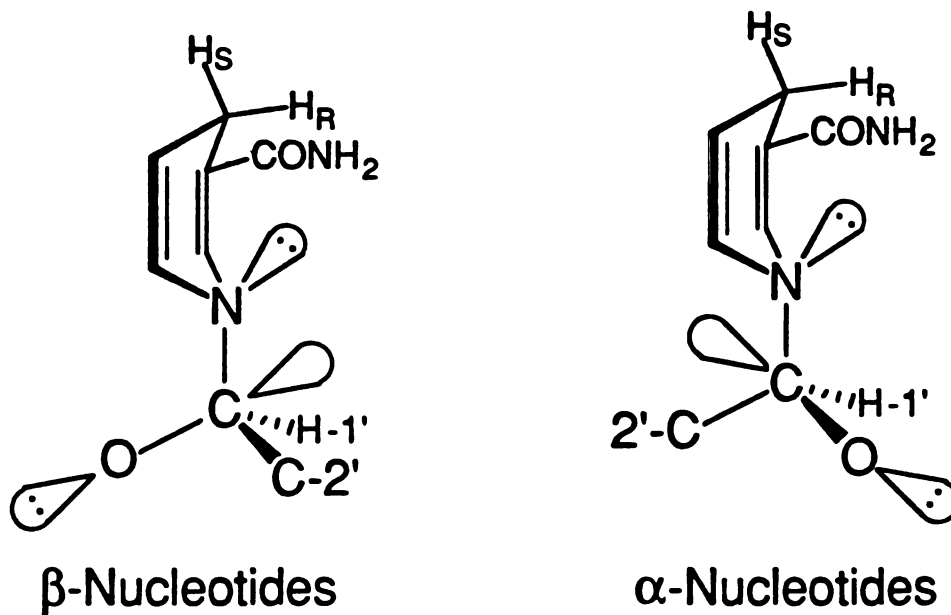
Figure II.14. Schematic representation showing the orientations of the lone pair of electrons on the ring nitrogen relative to the C1'–O antibonding orbital, σ*, for the α- and β- configurations of reduced pyridine coenzymes.

120° rotation around the N–C1' glycosyl bond. Such a rotation no longer permits the alignment of the dihydronicotinamide ring in the active site that is necessary to satisfy the observed stereospecificity of enzyme-catalyzed hydride transfer. As a consequence, any specific orbital interactions that occur for the β-anomers, even if not explicitly directed by the enzyme, must be either nearly eliminated or even reversed when the enzyme binds and utilizes an α-anomer. Since yeast ADH is an enzyme that fully meets the criteria as set forth in their paper, it is then apparent that a specific alignment of the designated electron orbitals is not *essential* for catalysis. These results raise additional questions regarding the general validity of their proposal (Oppenheimer, 1984).

Although the studies of the ability of the arabino analogs of NAD+ to function as a coenzyme analog have focused on yeast and horse liver ADH, preliminary results indicate that these properties are shared by a number of other common dehydrogenases. The ability of dehydrogenases to utilize coenzyme analogs with significant differences in substituents on the sugar moiety will have important consequences. This property should allow the design of other new analogs to investigate steric requirements for binding, specific mechanistic questions and substrate-coenzyme interactions for a wide range of dehydrogenases and other pyridine coenzyme-dependent enzymes.

References

Altona, C. and Sundaralingam, M. (1972), *J. Am. Chem. Soc. 94*, 8205-8212.

Altona, C. and Sundaralingam, M. (1973), *J. Am. Chem. Soc. 95*, 2333-2344.

Anderson, B. (1982) in "The Pyridine Nucleotide Coenzymes" Everse, J., Anderson, B. and You, K.-S., Eds., Academic Press Inc., New York. pp. 91-133.

Anderson, B.M., Ciotti, C.J. and Kaplan, N.O. (1959) *J. Biol. Chem. 234*, 1219-1225.

Benner, S.A. (1982) *Experientia 38*, 633-637.

Blumenstein, M and Raftery, M.A. (1972) *Biochemistry 11*, 1643-1648.

Burton, K. and Wilson, T.H. (1953) *Biochem. J. 54*, 86-94.

Cleland, W.W. (1977) *Adv. Enzymol. 45*, 273-387.

Cleland, W.W. (1979) *Meth. Enz. 63*, 103-138.

Cook, P.F., Blanchard, J.S. and Cleland, W.W. (1980) *Biochemistry 19*, 4853-4858.

Ekiel, I., Remin, M., Darzynkiewicz, E. and Shugar, D. (1979), *Biochim. Biophys. Acta 562*, 177-191.

Goebbeler, K.H. and Woenckhaus, C. (1966) Justus Liebigs Ann. Chem. 700, 180-186.

Gorenstein, D.G. (1984) in "Phosphorus-31 NMR Principles and Applications" Gorenstein, D.G. Ed.; Academic Press: New York, pp. 7-36.

Hajdu, J. and Sigman, D.S. (1977) *Biochem. 16*, 2841-2846.

Hoard, D.E. and Ott, D.G. (1965) *J. Am. Chem. Soc., 87*, 1785-1788.

Kam, B.L. and Oppenheimer, N.J. (1979a) *Carbohydrate Res., 69*, 308-310.

Kam, B.L. and Oppenheimer, N.J. (1979b) *Carbohydrate Res., 77*, 275-280.

Kam, B. L., Malver, O., Marschner, T., Oppenheimer, N. J. (1987) *Biochemistry, 26, 3453-3461.*

Kaplan, N.O. (1960) *The Enzymes 3B*, 105-169.

Kaplan, N.O., Ciotti, M.M. and Stolzenbach, F.E. (1956) *J. Biol. Chem. 221*, 833-844.

Kaplan, N.O., Ciotti, M.M., Stolzenbach, F.E. and Bachur, N.R. (1955) *J. Am. Chem. Soc. 77*, 815-816.

de Leeuw, F.A.A.M. and Altona, C. (1982) *J. Chem. Soc. Perkin II,* 375-384.

Michelson, A.M. (1964) *Biochim. Biophys. Acta 91*, 1-13.

Nambiar, K.P., Stauffer, D.M., Kolodkiej, P.A. and Benner, S.A. (1983) *J. Am. Chem. Soc. 105*, 5886-5890.

Oppenheimer, N.J. (1982) in "Pyridine Nucleotide Coenzymes" Everse, J., Anderson, B. and You, K.-S., Eds., Academic Press Inc., New York. pp. 51-89.

Oppenheimer, N.J. (1984) *J. Am. Chem. Soc. 106*, 3032-3033.

Oppenheimer, N.J. (1986a) in "Mechanisms of Enzymatic Reactions: Stereochemistry" Frey, P.A. Ed. Elsevier, New York. pp. 15-28.

Oppenheimer, N.J. (1986b) *J. Biol. Chem. 261*, 12209-12212.

Oppenheimer, N.J. and Kaplan, N.O. (1975) *Arch. Biochem. Biohys.166*, 526-535.

Oppenheimer, N.J. and Kaplan, N.O. (1976) *Biochemistry 15*, 3981-3989.

Oppenheimer, N.J., Arnold, L.J. and Kaplan, N.O. (1971), *Proc. Natl. Acad. Sci. U.S.A. 68*, 3200-3205.

Oppenheimer, N.J., Arnold, L.J., Jr. and Kaplan, N.O. (1978) *Biochemistry 17*, 2613-2619.

Orr, G.A. and Blanchard, J.S. (1984) *Anal. Biochem. 142*, 232-234.

Rodkey, F.L. (1955) *J. Biol. Chem. 213*, 777-786.

Saneyoshi, M. (1971) *Chem. Pharm. Bull. 19*, 493-498.

Sarma, R.H. and Mynott, R.J. (1972) *Org. Magn. Reson. 4*, 577-584.

Walt, D.R., Findeis, M.A., Rios-Mercadillo, V.M., Auge, J. and Whitesides, G.M. (1984) *J. Am. Chem. Soc. 106*, 234-239.

Woenckhaus, C. and Jeck, R. (1970) *Justus Liebigs Ann. Chem. 736*, 126-133.

Woenckhaus, C. and Jeck, R. (1987) in *"Pyridine Nucleotide Coenzymes",* Dolphin, D.; Poulson R., Avramovic, O. , Eds., John Wiley & Sons: New York. pp. 449-568.

Woenckhaus, C., Volz, M. and Pfleiderer, G. (1964) *Z. Naturforsch. 19b*, 467-470.

Woenckhaus, C. and Zumpe, P. (1965) *Biochem. Z. 343*, 326-328.

Yoshikawa, M., Kato, T. and Takenishi, T. (1967) *Tet. Lett., 50,* 5065-5068.

You, K.-S., Arnold, L.J., Jr., Allison, W.S. and Kaplan, N.O. (1978) *Trends Biochem. Sci., 3,* 265-268.

Section III. Isotope-induced Nonequivalence in a Symmetrical Molecule: Measurement of the ^{31}P-^{31}P Geminal Coupling Constant in Pyrophosphate

Introduction

^{18}O induces a small upfield shift in the ^{31}P NMR resonance frequency of phosphates (*ca.* 0.02 ppm/^{18}O bond), the magnitude of which is related to the P-O bond order (Cohn, 1982; Tsai, 1982; Cohn and Hu, 1982). Recent work in this laboratory involving the synthesis of ^{18}O-β,γ-bridge-labelled ATP for use in positional isotope exchange (PIX) experiments produces an interesting result while assigning resonances in the ^{31}P NMR spectra of ^{18}O-labelled pyrophosphate intermediates (Reynolds et al., 1983). The ^{31}P NMR spectrum at 97.3 MHz of pyrophosphate with one nonbridging ^{18}O appeared as a singlet 0.011 ppm upfield from ^{16}O-pyrophosphate and 0.008 ppm downfield from the ^{18}O-bridge-labelled pyrophosphate. A shift of approximately 0.007 ppm upfield from bridge-labelled ^{18}O-pyrophosphate was expected, however, due to the higher bond order of a nonbridging oxygen. Furthermore, at 202.5 MHz, the resonance appeared as a closely spaced doublet with a separation of 0.5 Hz. This splitting was presumed to be due to coupling between the nonequivalent phosphorus atoms with the observed doublet corresponding to the central doublet of an AB pattern. By selectively increasing the number of ^{18}O atoms attached to one of the two phosphorus atoms in the pyrophosphate molecule we can increase the nonequivalence of the phosphorus atoms sufficiently to allow observation of the outer resonances of the AB pattern. From this pattern the ^{31}P-^{31}P geminal coupling constant in pyrophosphate can be easily determined. The use of selective ^{18}O labelling of one phosphorus atom in pyrophosphate to induce chemical shift nonequivalence of the two phosphorus nuclei permits the observation of the individual resonances and measurement of an otherwise unobservable mutual coupling constant.

Experimental

$[\alpha\text{-}^{18}O_4]$Pyrophosphate was prepared from $[\gamma\text{-}^{18}O_4]$ATP using yeast acetyl coenzyme A synthetase (Berg, 1956; Boyer, et al., 1956). $[\gamma\text{-}^{18}O_4]$ATP was prepared by the method of Hoard and Ott (1965) from ADP and $[^{18}O_4]$phosphate [prepared, in turn from $H_2^{18}O$ (99%) and PCl_5] (Risley and Van Etten, 1978). The isotopic purity of the $[^{18}O_4]$phosphate was determined by mass spectral analysis of the trimethyl ester derivative, which was prepared by methylation of the free acid with diazomethane in diethyl ether (Midelfort and Rose, 1976; Wimmer and Rose, 1977; Eargle et al., 1977). Peaks occurring at m/e 140, 142, 144, 146 and 148, corresponding to the five possible $^{16}O/^{18}O$ isotopic species of trimethyl phosphate, were scanned and their relative intensities measured. The only detectable peaks in this region occurred at m/e 146 and 148 in relative intensities of 13% and 87%, respectively, for a total isotopic purity of 97.3%.

The isotopic composition of the $\alpha\text{-}^{18}O$-pyrophosphate was assumed to be the same as the starting $^{18}O_4$-phosphate since there should be no exchange of oxygen during the chemical and enzymatic steps of the synthesis. This has been confirmed by analysis of the ^{31}P NMR spectrum.

^{31}P NMR spectra were acquired at 202.5 MHz on a Bruker 500 MHz NMR spectrometer located at the Southern California Regional NMR Facility, California Institute of Technology. The NMR sample was prepared by dissolving $\alpha\text{-}^{18}O_4$-pyrophosphate (tetrasodium salt; 42 μmole) in 0.4 mL of 50% D_2O containing 0.5 mM EGTA to suppress paramagnetic broadening. A 5 mm NMR tube was used and the sample was spun at 17 Hz. The spectral width was $\pm$ 2000 Hz and the free induction decay was collected in 8192 data points and zero-filled to 16K before fourier transformation. A total of 128 acquisitions were

made. Simulations were done on a Nicolet 1180 computer using the Nicolet program NTCSIM. Linewidths in the simulations were set to 1.5 Hz and a coupling constant of 21.1 Hz was used. Chemical shifts were calculated as described below.

Results and Discussion

Figure III.1(b) shows the 202.5 MHz spectrum of α-$^{18}O_4$-labelled pyrophosphate. The ^{31}P-^{31}P geminal coupling constant in this AB pattern is simply the separation between either the two downfield or the two upfield peaks and was measured to be 21.1 Hz, a value comparable to the ^{31}P-^{31}P coupling constants found in ATP (Cohn and Hughes, 1960). The uncoupled chemical shift difference of the two resonances was calculated from Equation 1, where ϑ_1 - ϑ_4 are the resonances frequencies of the lines from low field to high field (Becker, 1980), respectively, and was calculated to be 13.3 Hz (at 202.5 MHz) for our labeled pyrophosphate.

$$| \nu_A - \nu_B | = [(\vartheta_1 - \vartheta_4) (\vartheta_2 - \vartheta_3)]^{1/2} \quad (1)$$

Based on a net difference of four P-^{18}O bonds, the observed chemical shift difference gives an upfield shift due to ^{18}O of 0.0164 ppm/bond, which is consistent with published values (Cohn, 1982). The unequal peak heights of the central doublet and the shoulder appearing on the downfield side of the central doublet were attributed to the presence of contaminating [α-$^{18}O_3$]pyrophosphate. Mass spectral results showed that this contaminating pyrophosphate amounted to 13% of the total pyrophosphate. Of the total pyrophosphate, 9.75% (75% of the contaminating pyrophosphate) contained a
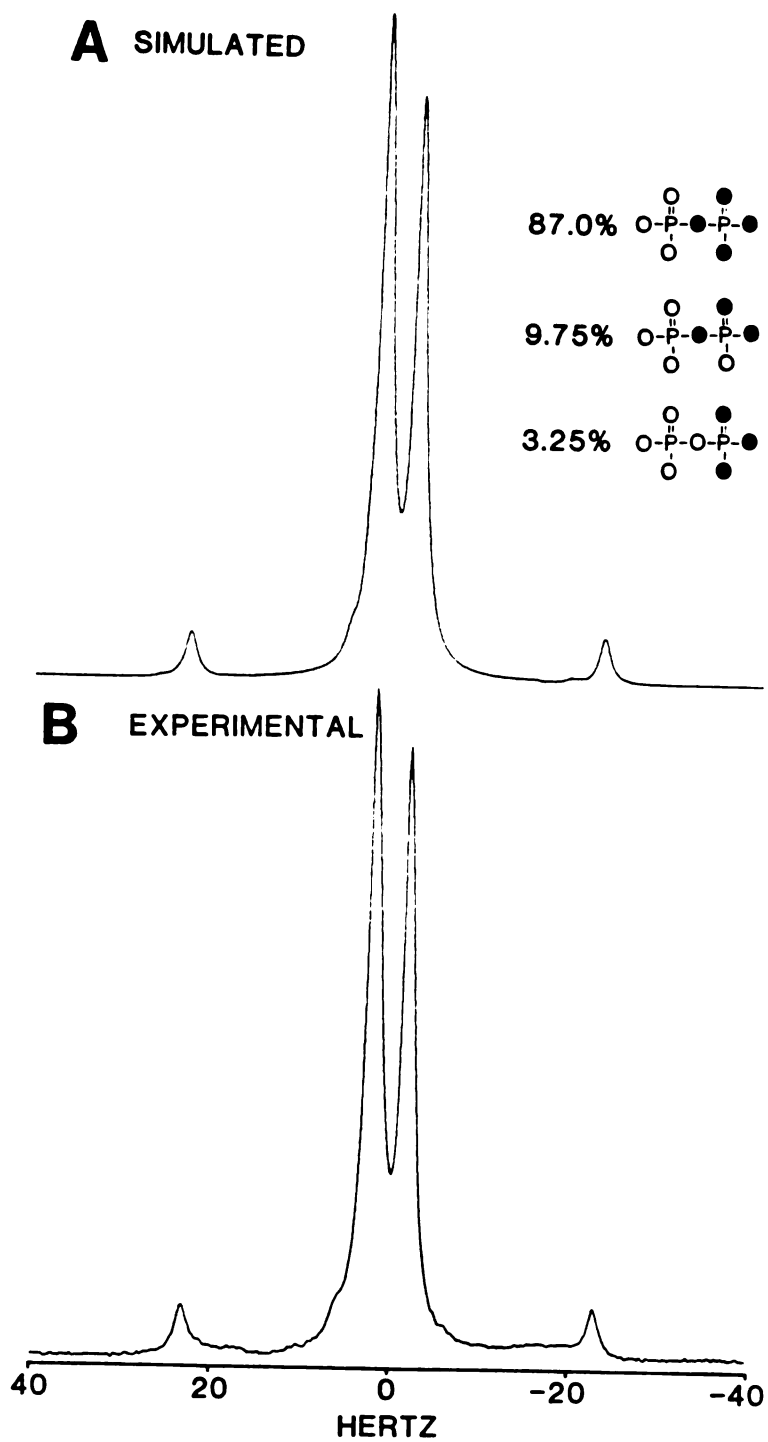
Figure III.1 Simulated (a) and experimental (b) spectra of ^{18}O labelled pyrophosphates showing the ^{31}P-^{31}P geminal coupling.

bridging ^{16}O atom. Figure III.1(a) shows the simulated spectrum generated from three separately simulated subspectra which were weighted appropriately and then summed. Chemical shifts of the pyrophosphates were calculated based on the experimentally determined upfield shift of 0.0164 ppm/^{18}O bond. In the case of ^{18}O-bridged [α-$^{18}O_3$]pyrophosphate the chemical shift difference used in the simulation was calculated using 3.67 ^{18}O bonds to the α-phosphorus (an average of the three resonance forms).

Since scalar coupling constants between equivalent nuclei cannot be determined using magnetic resonance experiments (Gutowsky et al., 1953; Abragam, 1961), the magnetic environment of one or more of the nuclei must be altered, usually by chemically modifying the molecule. The use of isotope-induced chemical shift perturbations as illustrated in this work permits the measurement of coupling constants between equivalent nuclei without modification of either structure or chemistry. Oxygen isotope-effects (specifically, ^{16}O and ^{18}O) are especially useful in this respect since the observed isotope-effect is due solely to a change in mass. Complications arising from changes in the spin quantum number (giving rise to additional coupling) can therefore be avoided.

References

Abragam, A. *The Principles of Nuclear Magnetism,* Oxford University Press: London, 1961; pp. 480-495.

Becker, E. D. *High Resolution NMR;* Academic Press: New York, 1980; pp. 135-139.

Berg, P. *J. Biol. Chem.* **1956,** *222,* 991.

Boyer, P. D.; Koeppe, O. J.; Luchsinger, W. W. *J. Am. Chem. Soc.* **1956,** *78,* 356.

Cohn, M. *Ann. Rev. Biophys, Bioeng.* **1982,** *11,* 23.

Cohn, M.; Hu, A. *J. Am Chem. Soc.* **1980,** *102,* 913.

Cohn, M.; Hughes, T. R. *J. Biol. Chem.* **1960,** *235,* 3250.

Eargle, D. H.; Licko, V.; Kenyon, G. L. *Anal. Biochem.* **1977,** *81,* 186.

Gutowsky, H. S.; McCall, D. W.; Slichter, C. P. *J. Chem. Phys.* **1953,** *21,* 279.

Hoard, D. E.; Ott, D. G. *J. Am. Chem. Soc.* **1965,** *87,* 1785.

Midelfort, C. F.; Rose, I. A. *J. Biol. Chem.* **1976,** *251,* 5881.

Reynolds, M. A.; Oppenheimer, N. J.; Kenyon, G. L. *J. Am. Chem. Soc.* **1983,** *105,* 6663.

Risley, J. M.; Van Etten, R. L. *J. Labelled Compd. Radiopharm.* **1978,** *15,* 533.

Tsai, M. *Methods Enzymol.* **1982,** *87,* 235.

Wimmer, M. J.; Rose, I. A. *J. Biol. Chem.* *1977,* *252,* 6769.

Appendix. Nonlinear Regression Analysis

Linear regression analysis is used routinely in the chemistry and biochemistry laboratory today and the functions to perform least squares are found on most scientific calculators. Common applications of least squares in the laboratory include the determination of rate constants in chemical kinetics, Michaelis constants in enzyme kinetics and standard curves for concentration measurements. Occasionally the need arises to fit experimental data to a nonlinear equation. Depending on the particular equation, it can sometimes be put in a linear form and solved by simple linear regression. This technique is done routinely for graphical analysis of Michaelis-Menten enzyme kinetics where data is fit to a linear double reciprocal Lineweaver-Burk plot. The major disadvantage of this technique, if it can be used at all, is that the fit suffers from the uneven weighting of the data points. Weighted linear regression can be used to overcome this problem but other techniques are available which eliminate it entirely.

Nonlinear regression allows the data to be fit to nonlinear equations with equal weighting (if desired) to all the data points. Also, the equations to be fit are not limited to only two unknown parameters as in a typical least squares analysis. Throughout the course of my graduate research, I made use of nonlinear regression for analysis of data ranging from pH titrations of NMR samples, pH rate profiles for pH-dependent reactions, Michaelis-Menten kinetics at high enzyme concentrations and the kinetics of first-order equilibration kinetics. The regression algorithm used for all these analyses was the same. The advent of the personal computer has allowed routine use of this method in the laboratory. For new equations, only slight modifications of the computer program source code are required and new equations can be fit almost as quickly as they can be surmised.

The algorithm used in the analyses was described by Cleland for the fit of

120

Michaelis Menten kinetic data to a rectangular hyperbola and included a source code listing for the FORTRAN program (Cleland, 1967). The basic technique is described here and applied in detail to the NMR pH titration curve. The BASIC source code is included at the end of this appendix for reference.

The best fit of any data to an equation minimizes the expression:

$$\sum_i [v_i - f(A_i; a,b,c...z)]^2 \qquad (1)$$

where v_i is the independent variable, A_i is the dependent variable, and a,b,c...z are the constants to be solved for. Equation 1 is merely the sum of the residuals between the best fit and the experimental data. If the equation to be fit, $f(A_i;$ a,b,c...z), is linear with respect *to* a,b,c...z, one can write:

$$v = aQ_1 + bQ_2 + ... + zQ_n \qquad (2)$$

where Q_1, Q_2, Q_3, ..., Q_n are different functions of the dependent variable A. The function to be minimized is therefore:

$$\sum_i [v_i - (aQ_1 + bQ_2 + ... + zQ_n)]^2 \qquad (3)$$

Now, one merely takes the derivative of Equation 3 with respect to each of a,b,c...z and sets these derivatives equal to zero (the first derivative set to zero finds the minimum of the function). This yields *n* equations in *n* unknown constants which can be solved simultaneously or by matrix methods. The set of *n* linear equations have the form :

$$a\sum (Q_{1,i})^2 + b\sum (Q_{1,i}Q_{2,i}) + \ldots + z\sum (Q_{1,i}Q_{n,i}) = \sum (Q_{1,i}v_i)$$

$$a\sum (Q_{1,i}Q_{2,i}) + b\sum (Q_{2,i})^2 + \ldots + z\sum (Q_{2,i}Q_{n,i}) = \sum (Q_{2,i}v_i)$$

$$\ldots \qquad \ldots \qquad \ldots$$

$$a\sum (Q_{1,i}Q_{n,i}) + b\sum (Q_{2,i}Q_{n,i}) + \ldots + z\sum (Q_{n,i})^2 = \sum (Q_{n,i}v_i) \qquad (4)$$

If the function to be fit is nonlinear, *i.e.*, one cannot separate and solve for the variables as in the above example, a linear form of the equation can be generated using the following procedure. For a function linear in *a* and nonlinear in *b* :

$$v_i = f(A_i; a,b) \qquad (5)$$

A new function can be written if an initial guess of b is made, b_0. If b_0 is a fairly good estimate of b the new function will have the form:

$$v_i = f(A_i; a, b_0) + (b - b_0) \times \text{Slope of tangent} \qquad (6)$$

The slope of the tangent is for the curve describing the dependence of v_i on b and is the first derivative of $f(A; a,b)$ with respect to b. The new function (6) now approximates Equation (2) and the two become identical when $(b - b_0) = 0$. Rewriting (6):

$$v_i = f(A_i; a, b_0) + (b - b_0)\left[\frac{\partial(f(A; a, b))}{\partial b}\right]_{b_0} \tag{7}$$

This equation is now linear in two constants, a and a(b - b_0), and can be written in the form of Equation 2, and minimized as described above (Equations 3 and 4). Q_1 and Q_2 from Equation 3 are now functions of A and b_0. Once a and a(b-b_0) are found they are easily combined to solve for b_0. This new value for b is substituted for b_0 and the solution is repeated. Several iterations are usually required and the values of the unknown parameters will converge on their best fit values. The presence of another unknown *nonlinear* parameter only adds another term to equation 7.

Now we will apply this technique to the NMR titration curve with an equation of the form:

$$\delta_{obs} = \frac{\delta_{HA}}{1 + K/H} + \frac{\delta_A}{1 + H/K} \tag{8}$$

In Equation 8 we must solve for δ_{HA}, δ_A and K. These correspond to the chemical shift of the protonated form, the chemical shift of the unprotonated form and the equilibrium constant, respectively. H is the independent variable and is the proton concentration calculated from the pH. This equation is linear in δ_{HA} and δ_A and nonlinear in K. First, we must determine Q_1, Q_2 and Q_3 (note that the number of Q's corresponds to the number of unknowns). Taking the first derivative with respect to the nonlinear unknown K:

123

$$\frac{\partial \delta_{obs}}{\partial K} = \frac{-\delta_{HA} \, K}{H^2 \, (1 + K/H)^2} + \frac{-\delta_A \, H}{K^2 \, (1 + H/K)^2}$$

$$= (\delta_A - \delta_{HA}) \left(\frac{H}{(H + K)^2} \right) \qquad (9)$$

The Q functions in Equation 2 can now be written:

$$Q_1 = \frac{1}{1 + K/H} = \frac{K}{K + H} \qquad (10)$$

$$Q_2 = \frac{1}{1 + H/K} = \frac{H}{K + H} \qquad (11)$$

$$Q_3 = \frac{H}{(H + K)^2} \qquad (12)$$

The values of the variables a,b and c in Equation 2 are then δ_{HA}, δ_A and (K - K_0)(δ_A - δ_{HA}) and the function to be minimized is:

$$\sum \left[\delta_{obs,i} - \left[\delta_{HA} \left(\frac{K_0}{K_0 + H_i} \right) + \delta_A \left(\frac{H_i}{K_0 + H_i} \right) + (\delta_A - \delta_{HA}) \, (K - K_0) \left(\frac{H_i}{(K_0 + H_i)^2} \right) \right] \right] \qquad (13)$$

Another Q function (Q_4) is used for the matrix solution of the equations and is simply the chemical shift values:

$$Q_4 = v_i = \delta_{obs,i} \qquad (14)$$

This Q_4 function is the v_i term in Equation 1. In all these Q functions, the H_i term is the one-dimensional matrix of the proton concentrations.

In the BASIC program included at the end of this appendix, the experimental data is first input from a text file containing pH vs. chemical shift (lines 10-110). The variables are h(i) and do(i) for proton concentration and chemical shift, respectively, and are in a single column in the text file. The first item in the list is the number of x,y pairs. The initial value of K_0 is entered as a pK which is then converted into an equilibrium constant (line 170). The number of unknown parameters is entered in line 180 and the iteration begins on line 200. The Q functions are entered in lines 270-300 and the iteration loop which solves the 3 linear equations is in lines 200-710. At the end of each iteration, the 2-dimensional array s contains the solved parameters a, b and c from Equation 2 in the first column i.e. s(1,1), s(2,1) and s(3,1). Again, these correspond to δ_{HA}, δ_A and $(\delta_A - \delta_{HA})(K - K_0)$ in Equation 13. From these, a new value of K_0 is obtained and the loop is repeated. If the initial guess is fairly accurate, the regression usually converges in about 5 iterations. The total number of iterations can be changed in line 200 if necessary. After 10 iterations, the error analysis is done (lines 720-850). The variance of the fit can be calculated by:

$$\sigma^2 = \frac{\sum [v_i - f(A_i; a,b,c)]^2}{P - n} \qquad (15)$$

where P is the number of experimental points and n is the number of unknown parameters (three for the titration curve). If the inverse matrix of s is taken and

125

multiplied by the variance of the fit (calculated in lines 720-760), the matrix will contain the variance and covariance terms of a,b and c:

$$
\begin{pmatrix} \text{Inverse} \\ \text{matrix} \end{pmatrix} \times \sigma^2 =
\begin{bmatrix}
\text{Var(a)} & \text{Cov(a,b)} & \ldots & \text{Cov(a,z)} \\
\text{Cov(a,b)} & \text{Var(b)} & \ldots & \text{Cov(b,z)} \\
\ldots & \ldots & \ldots & \ldots \\
\text{Cov(a,z)} & \text{Cov(b,z)} & \ldots & \text{Var(z)}
\end{bmatrix}
\tag{16}
$$

After each iteration the inverse matrix is found in the top n rows of matrix **s** in columns 2 to n+1, where n is the number of unknown parameters. From this matrix we can obtain the variances of δ_{HA} and δ_A directly (s(1,2) and s(2,3), respectively). The variance of K is more complicated, however, since the actual fitted parameter is a combination of δ_{HA}, δ_A and K. Element s(3,4) of the matrix contains the variance for $(\delta_A - \delta_{HA})K$. The variance of a combination of the fitted constant is given by:

$$
\text{Variance } [f(a,b,c)] = F_a^2 \, \text{Var(a)} + F_b^2 \, \text{Var(b)} + 2F_a F_b \, \text{Cov(a,b)}
\tag{17}
$$

In this equation, F_a is the derivative of $f(a,b)$ with respect to a and F_b is the first derivative with respect to b. In the specific example above, the combination of parameters that we wish to calculate the variance for is:

$$
f(a,b) = \frac{a}{b} = \frac{(\delta_A - \delta_{HA}) K}{(\delta_A - \delta_{HA})}
\tag{18}
$$

Note that this combination of the fitted parameters gives us K. We can calculate

the variance of K using Equation 17. Calculating the derivatives of 18:

$$\frac{\partial f(a,b)}{\partial a} = \frac{1}{(\delta_A - \delta_{HA})} \qquad (19)$$

$$\frac{\partial f(a,b)}{\partial b} = 0 \qquad (20)$$

Thus, from Equation 17 the variance of K is:

$$Var(\frac{a}{b}) = \left(\frac{1}{(\delta_A - \delta_{HA})^2} \right) \times Var\,((\delta_A - \delta_{HA})K) \qquad (21)$$

The second term on the right side of Equation 21 is element s(3,4) from the inverse matrix. Lines 820-840 calculate the variances and standard errors (square root of variance) for the fitted parameters using this method. Finally, the equilibrium constant is converted to a pKa and the final fitted values and their errors are printed.

References

Cleland, W. W. *Adv. Enzymology*, **1967**, *29*, 1-32.

```
REM     This program fits an nmr titration curve (one pKa)
REM     Obs Chem Shift = (∂HA/(1+H/K)) + (∂A/(1+K/H))
REM     Written by Tom Marschner
REM     Using algorithm of W.W. Cleland
REM     Max number of data points is 100.  Change here if necessary.
10  DIM h(100),do(100)
REM     Data input from a file with x data (pH) followed by y data (chemical
shift)
REM     all in one column
20  INPUT "Please enter the text filename ",n$
30  OPEN n$ FOR INPUT AS #1
REM     First item is number of data points
40  INPUT #1,np
50      FOR j = 1 TO np
60      INPUT #1,h(j)
REM     Convert from pH values to H+ concentrations
70      h(j)=10^-h(j)
80  NEXT j
REM     Now enter observed chemical shifts from file
90      FOR j = 1 TO np
100     INPUT #1,do(j)
110 NEXT j
REM     Print out values on screen to verify
120     FOR j = 1 TO np
130     PRINT h(j),do(j)
140     NEXT j
150 CLOSE #1
160 INPUT "Enter guess for pK ";pk
REM     Convert pKa to equilibrium constant ck

170 ck = 10^-pk
REM     n = number of unknown parameters
180 n=3
190 p=np-n:n1=n+1:n2=n+2
REM     This is the main interation loop
REM     Iterate 10 times; change if needed
200 FOR nt = 1 TO 10
210     FOR j=1 TO n2
220         FOR k=1 TO n1
230             s(k,j)=0
240         NEXT k
250     NEXT j
260     FOR i=1 TO np
REM     This is where the Q's are entered
270         q(1)=1/(1 + ck/h(i))
280         q(2)=1/(1+ h(i)/ck)
290         q(3)=h(i)/(h(i)+ck)^2
REM     q(4) is v(i) in Equation 2
300         q(4)=do(i)
310         FOR j=1 TO n1
320             FOR k=1 TO n
330                 s(k,j)=s(k,j)+q(k)*q(j)
340             NEXT k
350         NEXT j
360     NEXT i
370     FOR k=1 TO n
380         sm(k)=1/SQR(s(k,k))
390     NEXT k
400     sm(n1)=1
410     FOR j=1 TO n1
420         FOR k=1 TO n
```

```
430       s(k,j) = s(k,j) * sm(k) *sm(j)
440       NEXT k
450    NEXT j
460    ss(n1) = -1
470    s(1,n2) = -1
480    FOR l = 1 TO n
490       FOR k = 1 TO n
500          ss(k) = s(k,1)
510       NEXT k
520       FOR j = 1 TO n1
530          FOR k = 1 TO n
540             s(k,j) = s(k+1,j+1) - ss(k+1)*s(1,j+1)/ss(1)
550          NEXT k
560       NEXT j
570    NEXT l
580    FOR k=1 TO n
590       s(k,1) = s(k,1)*sm(k)
600    NEXT k

630    ck = ck - (s(3,1)/(s(2,1) - s(1,1)))
640    IF ck < 0 THEN PRINT "Equilibrium constant is negative":GOTO 160
650    PRINT "Iteration #";nt;":"
660    PRINT "Chemical shift of acid = ";s(2,1)
670    PRINT "Chemical shift of base =";s(1,1)

680    pk = -(LOG(ck))/2.303
690    PRINT "pK = ";pk
700    PRINT
710    NEXT nt

REM Calculate sum of residuals

720    sr = 0
730    FOR j = 1 TO np
740       sr = sr + (do(j) - ( (s(1,1)/(1+h(j)/ck)) + (s(2,1)/(1 + ck/h(j)))) )^2
750    NEXT j

REM Calculate variance

760    s2 = sr/p

REM Correct inverse matrix for scale factor used earlier

770    FOR j = 2 TO n1
780       FOR k = 1 TO n
790          s(k,j) = s(k,j)*sm(k)*sm(j-1)
800       NEXT k
810    NEXT j

REM Calculate standard errors from inverse matrix and sum of residuals

820    sedha = SQR ( s(2,3) * s2)
830    seda = SQR (s(1,2) * s2)
840    seck = SQR ( s(3,4)/((s(1,1)+s(2,1))^2) )
850    sepk = ((1/ck)*seck)/2.303

REM Print final values on printer

860    PRINT "Turn on printer and press return key..."
870    INPUT a$

880    LPRINT "Chemical shift of acid = ";s(2,1)
890    LPRINT "Standard error = ";sedha
900    LPRINT
910    LPRINT "Chemical shift of base = ";s(1,1)
920    LPRINT "Standard error =";seda
930    LPRINT
940    LPRINT "pK = ";pk
950    LPRINT "Standard error =";sepk

960    END
```